

**EXPERIMENTAL INVESTIGATIONS ON THE FLEXURE  
BEHAVIOUR OF REINFORCED GEOPOLYMER BEAMS  
PRODUCED FROM RECYCLED CONSTRUCTION  
MATERIALS**

**GERİ DÖNÜŞTÜRÜLMÜŞ YAPI MALZEMELERDEN  
ÜRETİLEN JEOPOLİMERİK KİRİŞLERİN EĞİLME  
DAVRANIŞI ÜZERİNE DENEYSEL ARAŞTIRMALAR**

**ŞABAN AKDUMAN**

**ASSOC. PROF. DR. ALPER ALDEMİR**  
**Supervisor**

Submitted to  
Graduate School of Science and Engineering of Hacettepe University  
as a Partial Fulfillment to the Requirements  
for be Award of the Degree of Master of Science  
in Civil Engineering

2021

## **ABSTRACT**

# **EXPERIMENTAL INVESTIGATIONS ON THE FLEXURE BEHAVIOUR OF REINFORCED GEOPOLYMER BEAMS PRODUCED FROM RECYCLED CONSTRUCTION MATERIALS**

**ŞABAN AKDUMAN**

**Master of Science, Department of Civil Engineering**

**Supervisor: Assoc. Prof. Dr. Alper ALDEMİR**

**June 2021, 100 pages**

Concrete requires a vast amount of aggregate and cement production. Although there are some efforts in the literature to reduce the amount of Portland cement in the concrete mixture to lessen the greenhouse gas release, a limited number of studies were conducted to investigate the possibility of using this geopolymer mixtures to serve as a structural component. Therefore, this study firstly aimed to produce geopolymer concrete from construction and demolition waste-based precursors, including masonry units (red clay brick, roof tile, hollow brick, etc.) and glass. In addition, recycled aggregates produced from the concrete waste portion of the CDW were used to obtain 100% recycled construction material on the scale of the binder and aggregate phase. Then, this study investigated the possible use of this proposed geopolymer concrete to produce structural components that perform similar to conventional concrete. Therefore, the structural properties of reinforced geopolymer concrete beams produced from the recycled construction demolition wastes were evaluated in this study by conducting laboratory experiments. To this end, bending tests were performed on reinforced conventional concrete beam specimens and reinforced geopolymer concrete beam specimens. The test observations clearly showed that

construction demolition waste could be recycled to produce new constructional components, considering its advantage of promoted sustainability.

**Keywords:** Geopolymer Beams, Construction and Demolition Waste, Shear and Flexural Tests, Concrete Beams, Sustainable Construction

## ÖZET

# GERİ DÖNÜŞTÜRÜLMÜŞ YAPI MALZEMELERDEN ÜRETİLEN JEOPOLİMERİK KİRİŞLERİN EĞİLME DAVRANIŞI ÜZERİNE DENEYSEL ARAŞTIRMALAR

**ŞABAN AKDUMAN**

**Yüksek Lisans, İnşaat Mühendisliği Bölümü**

**Tez Danışmanı: Doç. Dr. Alper ALDEMİR**

**Haziran 2021, 100 sayfa**

Beton, çok miktarda agrega ve çimento üretimi gerektirir. Literatürde sera gazı salınımını azaltmak için beton karışımındaki Portland çimentosu miktarını azaltmak için bazı çabalar olmasına rağmen, bu jeopolimer karışımlarının yapısal bir bileşen olarak kullanılma olasılığını araştırmak için sınırlı sayıda çalışma yapılmıştır. Bu nedenle, bu çalışmada öncelikle, duvar elemanları (kırmızı kil tuğla, kiremit, boşluklu tuğla vb.) ve cam dahil olmak üzere inşaat ve yıkım atıkları bazlı öncül maddelerden jeopolimer beton üretilmesi hedeflenmiştir. Ek olarak, İYA'nın beton atık kısmından üretilen geri dönüştürülmüş agregalar, bağlayıcı ve agrega aşamasında %100 geri dönüştürülmüş yapı malzemesi elde etmek için kullanılmıştır. Daha sonra, bu çalışmada, geleneksel betona benzer performans gösteren yapısal bileşenlerin üretilmesi için önerilen bu jeopolimer betonun olası kullanımı araştırıldı. Bu nedenle bu çalışmada, geri kazanılan inşaat yıkım atıklarından üretilen betonarme jeopolimer kirişlerin yapısal özellikleri laboratuvar deneyleri yapılarak değerlendirilmiştir. Bu amaçla konvansiyonel beton kiriş numuneleri ve jeopolimer kiriş numuneleri üzerinde eğilme testleri yapılmıştır. Test gözlemlerine göre, teşvik edilen

sürdürülebilirlik avantajı göz önüne alındığında, inşaat yıkım atıklarının yeni inşaat bileşenleri üretmek için geri dönüştürülebileceğini açıkça gösterdi.

**Anahtar Kelimeler:** Jeopolimer Kirişler, İnşaat ve Yıkıntı Atıkları, Kesme ve Eğilme Testleri, Beton Kirişler, Sürdürülebilir İnşaat

# TABLE OF CONTENTS

ABSTRACT .....	i
ÖZET .....	iii
TABLE OF CONTENTS .....	v
LIST OF FIGURES .....	viii
SYMBOLS AND ABBREVIATIONS .....	xi
1. Introduction .....	1
1.1. General.....	1
1.2. Research Objectives and Scope .....	4
2. Literature Review.....	6
2.1. Geopolymer Binders .....	6
2.2. Alkali Activators.....	9
2.3. Construction and Demolition Waste-based Geopolymers.....	10
2.4. Reinforced Geopolymer Concretes.....	12
2.5. Structural Tests of Reinforced Geopolymer Concretes .....	14
2.5.1. Geopolymer Beam Tests .....	15
3. Materials and Methodology .....	19
3.1. Introduction.....	19
3.2. Mixture Compositions .....	23
3.3. Alkali Activators.....	24
3.4. Aggregates .....	26
3.5. Reinforcing Bars Detail .....	27
3.6. Methodology .....	31
3.6.1. Preparation of Mixtures .....	31
3.6.2. Casting and Placing .....	33
3.6.3. Curing Conditions .....	34
3.6.4. Testing of Beams.....	35
3.6.5. Test setup and procedure .....	36
4. Experimental Results and Discussion.....	39
4.1. Introduction.....	39
4.2. Compressive and Splitting-Tensile Strength of Geopolymer .....	39

4.3. Geopolymer Concrete Beams .....	44
4.4. Conventional Concrete Beams.....	62
4.5. Summary of Beam Specimen Results.....	81
4.5.1. Test Results Summary of Beam Specimens with $a/d = 0.50$ .....	81
4.5.2. Test Results of Beam Specimens with $a/d = 1.00$ .....	83
4.5.3. Test Results of Beam Specimens with $a/d = 1.65$ .....	86
4.6. Analysis and Discussion .....	87
4.6.1. Effect of Material Type .....	87
4.6.2. Effect of Shear-span-to-depth Ratio .....	88
5. Conclusion.....	92
6. References .....	94

## LIST OF TABLES

Table 3.1. Chemical compositions of CDW-based precursors.....	22
Table 3.2. The content of the GPC .....	23
Table 3.3. The content of the CVC mixtures.....	24
Table 3.4. Chemical Properties of NaOH.....	25
Table 3.5. Chemical Properties of Na <sub>2</sub> SiO <sub>3</sub> .....	25
Table 3.6. Chemical Properties of Ca(OH) <sub>2</sub> .....	26
Table 3.7. Properties of reinforcing bar.....	28
Table 4.1. Test Specimens of GPC_NA.....	42
Table 4.2. Test Specimens of GPC_RA .....	42
Table 4.3. Test Specimens of CVC_NA.....	43
Table 4.4. Test Specimens of CVC_RA.....	43
Table 4.5. Summary of Test Results .....	83
Table 4.6. Estimation Performance of Code Proposed Equations.....	91



## LIST OF FIGURES

Figure 2.1. Geopolymerization process .....	6
Figure 2.2. Three-fold diagram of fly ash and slag .....	8
Figure 2.3. The process from CDW-based precursor to CDW-based concrete .....	11
Figure 2.4. First public structure built with structural Geopolymer Concrete .....	13
Figure 3.1. Visuals of CDW-based precursors .....	20
Figure 3.2. XRD Analysis of CDW-based precursors.....	21
Figure 3.3. Particle size distribution of CDW-based precursors .....	22
Figure 3.4. Alkali Activators pictures .....	25
Figure 3.5. The gradation curve of the normal and recycle aggregate .....	27
Figure 3.6. Rebar test machine .....	28
Figure 3.7. Beam cross-section.....	29
Figure 3.8. Beam reinforcing details .....	29
Figure 3.9. Stirrup dimensions .....	30
Figure 3.10. Cover and stirrup detail.....	30
Figure 3.11. Preparation of NaOH Solution .....	31
Figure 3.12. Preparation of GPC mixture.....	32
Figure 3.13. Preparation of CVC mixture .....	32
Figure 3.14. Casting and placing procedure of CVC .....	33
Figure 3.15. Casting and placing procedure of GPC.....	34
Figure 3.16. Curing of the specimens, (a) geopolymer samples, (b) concrete samples .....	35
Figure 3.17. Schematic of Variables, Curing Procedures, and Mechanical Tests.....	36
Figure 3.18. Test setup example.....	37
Figure 3.19. Details on Instrumentation .....	38
Figure 3.20. Details on Instrumentation .....	38
Figure 4.1. Compressive Strength Test Setup and Experiment.....	40
Figure 4.2. Splitting-Tensile Strength Test Setup and Experiment.....	41
Figure 4.3. GPC – NA – 0.50 beam, (a) first cracks, (b) failure .....	44
Figure 4.4. GPC – NA – 0.50 shear crack detail .....	44
Figure 4.5. GPC – NA – 0.50 moment-curvature graph .....	46
Figure 4.6. GPC – NA – 0.50 load-displacement graph.....	46

Figure 4.7. GPC – NA – 1.00 beam, (a) first cracks, (b) failure .....	47
Figure 4.8. GPC – NA – 1.00 failure crack propagation .....	48
Figure 4.9. GPC – NA – 1.00 moment-curvature graphs .....	49
Figure 4.10. GPC – NA – 1.00 load-displacement graph.....	50
Figure 4.11. GPC – NA – 1.65 beam, (a) first cracks, (b) failure .....	51
Figure 4.12. GPC – NA – 1.65 beam crushing.....	51
Figure 4.13. GPC – NA – 1.65 moment-curvature graphs(continued) .....	52
Figure 4.14. GPC – NA – 1.65 load-displacement graph.....	53
Figure 4.15. GPC – RA – 0.50 beam, (a) first cracks, (b) failure.....	54
Figure 4.16. GPC – RA – 0.50 shear crack .....	54
Figure 4.17. GPC – RA – 0.50 moment-curvature graphs .....	56
Figure 4.18. GPC – RA – 0.50 load-displacement graph .....	56
Figure 4.19. GPC – RA – 1.00 beam, (a) first cracks, (b) failure.....	57
Figure 4.20. GPC – RA – 1.00 moment-curvature graphs .....	58
Figure 4.21. GPC – RA – 1.00 load-displacement graph .....	59
Figure 4.22. GPC – RA – 1.65 beam, (a) first cracks, (b) failure.....	59
Figure 4.23. GPC – RA – 1.65 buckling of reinforcement bar.....	60
Figure 4.24. GPC – RA – 1.65 moment-curvature graphs .....	61
Figure 4.25. GPC – RA – 1.65 load-displacement graph .....	62
Figure 4.26. CVC – NA – 0.50 beam, (a) first cracks, (b) failure.....	63
Figure 4.27. CVC – NA – 0.50 failure crack propagation.....	63
Figure 4.28. CVC – NA – 0.50 moment-curvature graphs .....	65
Figure 4.29. CVC – NA – 0.50 load-displacement graph .....	65
Figure 4.30. CVC – NA – 1.00 beam, (a) first cracks, (b) failure.....	66
Figure 4.31. CVC – NA – 1.00 shear dominant failure detailed picture .....	66
Figure 4.32. CVC – NA – 1.00 moment-curvature graphs .....	68
Figure 4.33. CVC – NA – 1.00 load-displacement graph .....	68
Figure 4.34. CVC – NA – 1.65 beam, (a) first cracks, (b) failure.....	69
Figure 4.35. CVC – NA – 1.65 flexure dominant failure detailed picture .....	69
Figure 4.36. CVC – NA – 1.65 moment-curvature graphs .....	71
Figure 4.37. CVC – NA – 1.65 load-displacement graph .....	71
Figure 4.38. CVC – RA – 0.50 beam, (a) first cracks, (b) failure .....	72
Figure 4.39. CVC – RA – 0.50 shear dominant failure .....	72
Figure 4.40. CVC – RA – 0.50 moment-curvature graphs.....	74

Figure 4.41. CVC – RA – 0.50 load-displacement graph .....	74
Figure 4.42. CVC – RA – 1.00 beam, (a) first cracks, (b) failure .....	75
Figure 4.43. CVC – RA – 1.00 shear dominant failure deatiled picture .....	75
Figure 4.44. CVC – RA – 1.00 moment-curvature graphs.....	77
Figure 4.45. CVC – RA – 1.00 load-displacement graph .....	77
Figure 4.46. CVC – RA – 1.65 beam, (a) first cracks, (b) failure .....	78
Figure 4.47. CVC – RA – 1.65 flexure dominant failure picture .....	78
Figure 4.48. CVC – RA – 1.65 moment-curvature graphs.....	80
Figure 4.49. CVC – RA – 1.65 load-displacement graph .....	80
Figure 4.50. Test Results of Beam Specimens with $a/d=0.50$ .....	81
Figure 4.51. Observed Crack Patterns of Beam Specimens with $a/d=0.50$ .....	82
Figure 4.52. FEMA Idealization Method .....	83
Figure 4.53. Test Results of Beam Specimens with $a/d=1.00$ .....	84
Figure 4.54. Observed Crack Patterns of Beam Specimens with $a/d=1.00$ .....	85
Figure 4.55. Test Results of Beam Specimens with $a/d=1.65$ .....	86
Figure 4.56. Observed Crack Patterns of Beam Specimens with $a/d=1.65$ .....	87

## SYMBOLS AND ABBREVIATIONS

### Abbreviations

BA	Bottom Ash
BFS	Blast Furnace Slag
Ca(OH) <sub>2</sub>	Calcium Hydroxide
CDW	Construction Demolition Wastes
CW	Concrete Waste
EDX	Energy Dispersive X-Ray Analysis
FA	Fly Ash
GBFS	Ground Granulated Blast Furnace Slag
GW	Glass Waste
HB	Hollow Brick
Na <sub>2</sub> SiO <sub>3</sub>	Sodium Silicate
NaOH	Sodium Hydroxide
RCB	Red Clay Brick
RT	Roof Tile
SEM	Scanning Electron Microscopy
XRD	X-ray Diffraction Analysis

# INTRODUCTION

## 1.1. General

The excess of waste generated in the industry is a concern for environmental health. In this respect, utilizing the wastes in concrete is of great importance. By replacing a predetermined amount of cement and aggregate with waste products, it is aimed to increase the sustainability of the concrete and reduce the damage to the environment [1]. Although conventional concrete is one of the most extensively used construction materials in the world, there exist some environmental and structural disadvantages related to its sustainability. The main component of concrete is the Portland cement, whose production reaches billions of tons each year and responsible for 7% of human-induced carbon dioxide emissions [11-19]. For instance, approximately 1.5 tons of source materials are required to produce 1 ton of cement, emitting nearly 1 ton of carbon dioxide [1-12]. In addition, the production stages of the Portland cement require a high level of input energy. Considering the growth levels of emerging economies from day to day and the exponential increase in construction/renovation demand for infrastructures, the expectation is that the greenhouse gas emission and energy demand arising from the cement production will reach 105 Gt (gigatonne) and 505 TJ (terajoule) in 30 years, respectively [20]. Besides, increasing aggregate output in proportion to the demand for concrete is another concern to overcome due to adverse environmental impact. The carbon dioxide emissions derived by aggregate production are responsible for 20% of the emitted carbon dioxide by concrete [21]. Therefore, it is apparent that the extensive use of conventional concrete is not sustainable with all its components. For this reason, the development of eco-friendly, cost-effective, and low-carbon-footprint construction materials should become a forefront priority worldwide.

In addition to the environmental impacts created by conventional building materials, the repair and/or demolition and reconstruction of the infrastructure systems before completing

their service life, due to the weakness of these materials in terms of sustainability, causes harmful consequences for the national economies. All the operations carried out to extend the infrastructure systems' service life or reconstruction result in vast construction and demolition waste. While the amount of CDW reached 569.4 million tons in the USA in 2017 [22], it is expected that the annual increase rate of CDW for China will reach millions in the coming years [23]. Besides the detrimental financial impact of CDW, concerns including the use of agricultural lands as waste storage areas and the toxic waste components of CDW posing a danger to the environment and human health have compelled CDW regulation.

In this context, geopolymer binders produced by activating aluminosilicate sourced raw materials using alkali activators are in a promising position in terms of being an option to ordinary Portland cement (OPC) in recent decades. Geopolymer binders stand out by making possible lower carbon emissions levels, at least 50% lower than conventional cement-based binders, also ensures superior mechanical and durability properties [10, 20, 24]. Life Cycle Assessments on geopolymer binders produced using CDW or recycling of CDW to replace raw materials in different phases indicate that environmental impacts have remained relatively lower against conventional cementitious binders [25-28]. Cement-based materials generally have low tensile strength, limited ductility, and brittle behavior in the absence of proper reinforcement detailing. However, their high compressive strength, temperature and acid resistance and durability and, low cost could be considered the main reasons for the domination of conventional concrete in the construction market [6-16]. Geopolymers come from the inorganic polymer family. They show fast chemical reactions on Si-Al minerals under alkalic conditions with a three-dimensional polymeric chain and ring formation consisting of Si-O-Al-O bonds [18, 19]. Materials containing silicon and aluminum in their activator structure (e.g., fly ash, slag, rice ash, etc.) react with additives such as brass ash and produce binders [13-15]. The primary difference between the geopolymer concrete (GPC) and conventional concrete (CVC) is the used binder in their mixture (i.e., alkali active aluminosilicate) [6]. Geopolymer concrete is obtained by using activated pozzolanic

materials and aggregate instead of cement [10]. Besides, the enhanced alkalinity of the obtained geopolymer concrete provides corrosion resistance. With its resistance to sulfate and chloride carbonation environments, geopolymer concrete shows superior properties to conventional concrete [18-19, 29-30].

To the best of the authors' knowledge, earlier studies focused mainly on the structural properties of components made of the geopolymer concrete produced from fly ash with no or a limited amount of recycled materials in the concrete mixture. Therefore, in this study, geopolymer concrete was produced from construction and demolition waste-based materials, involving masonry units (red clay brick, roof tile, hollow brick, etc.) and glass. As a result of the research team's extensive preliminary studies on optimizing the physical and chemical properties of CDW-based raw materials from separate sources, a general mixture ratio for binder and activator combinations/concentrations was determined to produce geopolymer concrete with the targeted mechanical performance.

In addition, recycled aggregates produced from the concrete waste portion of the CDW were used to obtain 100% recycled construction material on the scale of the binder and aggregate phase. The result of the inclusion of recycled aggregate in the concrete mixture is also examined, to the best of the authors' knowledge, for the first time in the publicity. Besides, recycling aggregates obtained from CDW were not subjected to any treatment to improve their mechanical properties.

All the geopolymer concrete beam samples were cured at the room temperature. For each geopolymer concrete mixture, the flexural behavior was determined by conducting the four-point-bending test under displacement-controlled loading protocol. To this end,  $150 \times 250 \times 1100$  mm beam specimens (i.e.,  $\frac{1}{2}$  scaled beams) were produced with code-conforming lateral reinforcement detailing. In each test, the load midspan displacement curve, moment-curvature curve, and observed crack patterns were obtained. To find the effect of shear-span-to-depth ratio ( $a/d$ ) on the flexural behavior, three different shear span values for each

material type were used, which corresponds to a total number of 12 tests. Therefore, the flexural behavior of CDW-based recycled geopolymer concrete was obtained.

## **1.2. Research Objectives and Scope**

The goal of the study strategy is to help the public by producing high-performance new building materials made from CDW. Keeping the CDW useable in the manufacture of building materials through basic and easy procedures such as separating, crushing, and grinding without demanding any pre-treatment adds a unique value to the evaluation of CDW and new generation high-performance building materials. The main contribution of this thesis is to make and test environmentally friendly green geopolymer beams with adequate mechanical properties.

The study's initial stage is to determine the compressive strength of CDWs in order to assess their binding capacity. This is done by reusing roof tiles, hollow bricks, red clay bricks, glass, and concrete wastes, all of which are key components of CDWs. Understanding CDW's mechanical properties in this manner will be crucial in order to create the best mixture for manufacturing geopolymer beams.

Following the creation of the geopolymer binder, a study was conducted to determine the mechanical properties of CDW-based geopolymer and concrete compositions by integrating graded fine and coarse aggregates in the mixture, with the highest performing geopolymer mixes being chosen for the manufacture of geopolymer beams. Following this part, conventional Portland cement concrete beam samples were prepared in order to measure the differences between geopolymer and concrete beams in terms of structural performance. As a result, structural comparisons of manufactured beam samples of geopolymer and concrete mixtures that demonstrate similar mechanical properties are being made to determine the applicability of geopolymers in the building construction industry.



Geopolymer and conventional concrete compositions with identical mechanical behavior are generated in the study's final step. Flexural-critical beam samples were prepared in this respect. In the trials, three distinct  $a/d$  ratios (0.49, 1.00, and 1.65) were chosen for flexural-critical beams to investigate alternative failure modes. Load-displacement and moment-curvature graphs of beam samples are created within this study. Also, their characteristics such as stiffness, yielding load, and yielding displacement are compared.

# LITERATURE REVIEW

## 2.1. Geopolymer Binders

Geopolymers, also known as alkali-activated binders, are materials made by reacting with high aluminosilicate material and alkaline solution. Joseph Davidovits [31] used the word geopolymer to characterize the substance formed when an aluminosilicate precursor reacts with alkaline activators in the 1970s. Geopolymers are made up of silico-aluminates, which are made up of  $\text{Si}^{4+}$  and  $\text{Al}^{3+}$  bonding with oxygen. Ring polymers and basic chains are the most common materials, and their structure varies from semicrystalline to amorphous. Polymerization is defined as chemical reactions of aluminosilicate-based materials that build polymeric SiO-AlO bonding under alkaline solutions, with the formula  $\text{Mn-SiO}_2\text{z-AlO}_2\text{n}\cdot\text{wH}_2\text{O}$  [32].

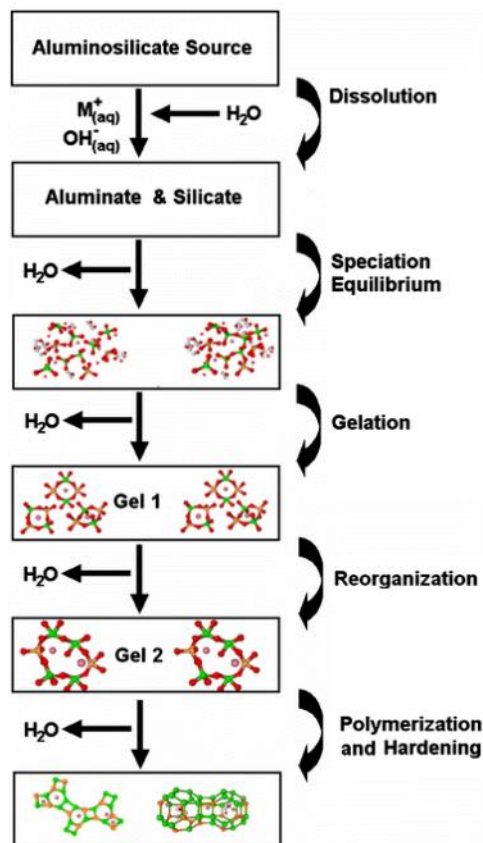


Figure 2.1. Geopolymerization process (adapted from Davidovits [33])

Geopolymers were first created as a type of fire-resistant material. Due to its mechanical and physical advantages such as high fire resistance, early compressive strength, chemical and

physical stability, and dense structure, geopolymer research and development studies started to grow internationally after a short time period. As a result, the construction sector took over the development and manufacture of geopolymer. As a result of alkaline activation usage, numerous aluminosilicate-based materials have begun to be used in the manufacturing of geopolymers with good mechanical and durability qualities, according to Wastiels et al. [34] findings.

Within the context of the development of geopolymer and alkali-activated materials, metakaolin was used widely in the construction applications. The simplest and most easy precursor material is metakaolin, according to the chemistry of geopolymer and alkali-activated materials. Metakaolin is alkaline activated to make zeolite forms before the geopolymer process is developed [35]. These activities were restricted by the high energy consumption of the process of calcination and the high cost of producing the metakaolin. The results of metakaolin's alkali activation have also provided insight into geopolymer systems that new precursor components can be produced. The first publication on alkali-activated binder (geopolymer) materials employing fly ash generated as a coal-fired power by-product was published in 1993 [36]. Because of the environmental benefits of fly ash-based geopolymers, research has risen significantly after these years. Many researchers have highlighted that geopolymers created from fly ash emit much less CO<sub>2</sub> than cementitious binders [37].

In the literature, fly ash has been separated into two categories: Class F, which has low calcium content but high silicate and aluminate content, and Class C, which has high calcium content low ignition loss. The chemical compositions of various classes of fly ash used for the research and the strength classes of the geopolymers created with these precursors are shown in Figure 2.2. When looking at the ternary diagram of fly ash chemical content and strength classes, it is obvious that chemical composition significantly impacts geopolymer binders' mechanical performance. In the consequence of fly ash-based geopolymer production, the usage of other aluminosilicate-based by product materials such as ground granulated blast furnace slag (GGBFS) and silica fume (SF) as a precursor material for geopolymerization has sparked a new wave of research in geopolymer manufacturing using various materials.

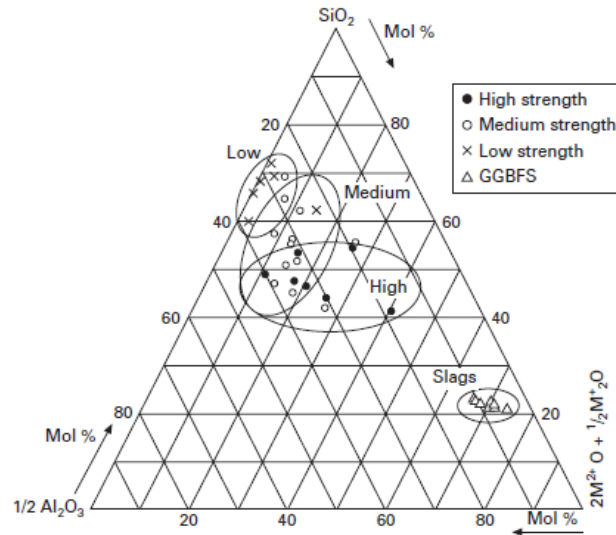


Figure 2.2. Three-fold diagram of fly ash and slag (adapted from Provis and van Deventer [38])

Another source material utilized in the manufacturing of geopolymer and alkali-activated solutions is GGBFS. Blast furnace slag can have hydraulic binding qualities similar to Portland cement, based on chemical content. Nevertheless, it takes a very long time to obtain binding properties because it is not reactive like Portland cement due to its composition. Therefore, it has been demonstrated in the literature that when it is activated using alkaline activators rather than water, or when it is replaced into Portland cement in certain quantities, the chemical gel reaction can increase rapidly [39]. In addition, gel formation of CASH begins early in the geopolymerization processes of blast furnace slag. The amount of alkali required in the development of this type of gel is estimated to be more than that necessary in the development of gels created following Portland cement hydration. Therefore, it was discovered that increasing the amount of Ca in the system decreases reaction processes [40].

Gruskovnjak et al. [41] compared alkali-activated slag hydration to that of a traditional Portland cement system. Multiple microstructural analyses such as scanning electron microscope and X-ray diffraction were used to examine the hydration products of slag and cement by the authors. The generation of C-S-H in the slag hydration occurs quickly relative to cement systems, which is a result of the rapid dissolving of Na-metasilicate in alkali-activated systems. The kinetics of the slag has been discovered to change as a result of its

quick consumption during the continuing hydration of the slag, and it has gained a lower late strength than cement systems.

Li and Liu [42] examined the impact of slag addition to fly-ash-based geopolymers in terms of compressive strength. Two different 0-and 4-per-cent slag content mixtures were designed by the authors, and the samples were subject to two different 30 °C and 70 °C cure temperatures. The results showed that 4% slag addition had a positive impact on the compressive strength values up to 70 MPa. The results reveal this situation through the enhanced reaction rate and the adding of slag to raise the gel formation in the matrix. Moreover, thanks to the addition of slag, the pores of the geopolymers were reported to be improved, especially during curing conditions at 70°C.

## **2.2. Alkali Activators**

When producing geopolymer binders, the type and ratio of the alkaline activator play a great important role apart from the nature of the precursor material. The activators in the research are used to activate aluminosilicate precursors by the alkali hydroxide and alkali silicate groups. Sodium and potassium are typically the best performing alkalis in both types of activator groups. The high solubility of sodium and potassium hydroxides up to 20 moles allows absolute flexibility in geopolymer preparation [43]. For alkaline silicates with pH values similar to other alkaline hydroxides, the alkalinity of alkaline silicates is higher. Although alkaline hydroxides have a high pH in the early reaction period, the silica provided by alkaline silicates will increase the pH level of the solution in the future [44].

Jimenez and Puertas [45] studied alkaline-activated slag cement hydration and mechanical strength behavior with the combination of alkali activators. Three combinations of the activators were designed by the authors: sodium hydroxide, sodium silicate, and sodium carbonate include Na<sub>2</sub>O ingredients being 4% of the binder ratio. Their results pointed out that the rate of slag dissolution was dependent on the pH value of the environment and that pH exceeding 12 had a positive effect. The authors noted that when pH is higher than 12, the setting time and compression strength are primarily affected by the anions from the activator, which react to Ca ions released by slag dissolution to form stable hydration products.

The factors affecting the strength of active alkali slags were examined by Wang et al. [46]. According to the authors' findings, the curing conditions were the most essential parameters to determine the strength properties of alkali-activating slag in the study, such as the liquid/slag ratio, silicate module, activator type, and the combination. The authors pointed out that sodium silicate is the most effective sodium activator in all situations, the optimum Na<sub>2</sub>O ratio ranges from 3.0 to 5.5%, the optimum solution/slag ratio ranges from 0.38 to 0.45, and the optimum slag fineness range from 4000 to 5500 cm<sup>2</sup>/g.

The impact of calcium content on the fly ash-based geopolymers was investigated by Dombrowski et al. [47]. By adding hydroxide calcium in different proportions, they analyzed the structural performance of the mixtures, the time, and gel mechanism. According to their results, the authors stated that the increase of calcium content boosted the reaction rate and improved mechanical performance, and showed the greatest performance of calcium hydroxide mixture with 8%. The addition of 8% hydroxide calcium was also noted to be successful under environmental conditions and high temperatures of healing.

### **2.3. Construction and Demolition Waste-based Geopolymers**

In recent decades, CDW has become a subject of researchers in the application of geopolymerization methods worldwide. Similar to some industrial sub-products, the high silica and alumina content of CDW allows these materials to be used again in the construction industry. Although several CDWs have successfully been used in the literature in recent years as sustainable geopolymer-based products, their performance differs. This section fundamentally mentions prior research and development studies on CDW-based geopolymers.

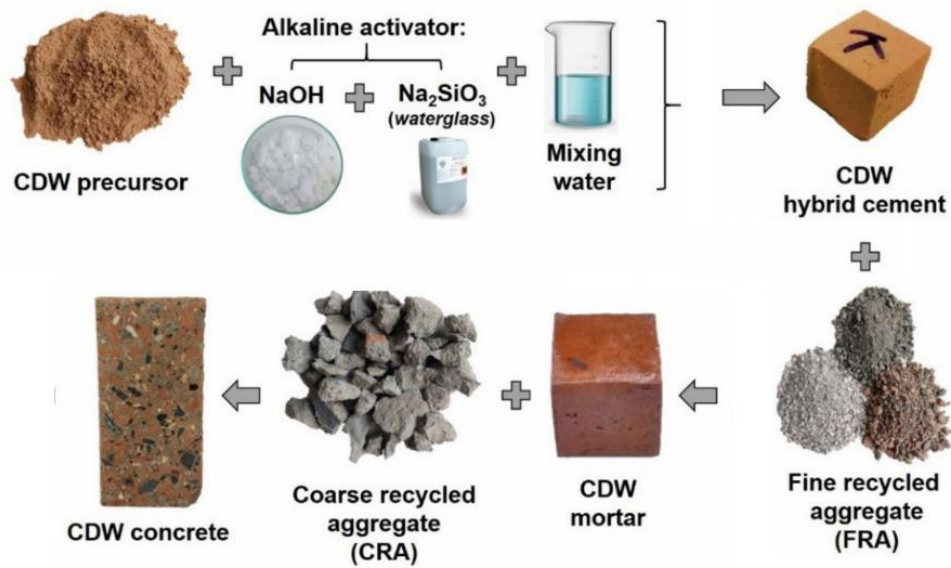


Figure 2.3. The process from CDW-based precursor to CDW-based concrete (adapted from Robayo-Salazar et al. [48])

The newly used geopolymerization technology for industrial wastes like fly ash and slag has been recognized as an important choice for the reutilization of inorganic material found in demolition waste construction. Puertas et al. [49] used a 6M NaOH and  $\text{Na}_2\text{SiO}_3$  mixture of alkaline-activated ceramic waste and reported eight-day compressive strength of 13 MPa. The authors attribute these low results to their half-crystalline nature. Khater [50] used NaOH and  $\text{Na}_2\text{SiO}_3$  to activate waste concrete, cement-based waste, and slaked lime in the study. During the investigation, he obtained compressive strengths ranging from 3 to 55 MPa with geopolymer paste and reported a significant effect of  $\text{SiO}_2/\text{Al}_2\text{O}_3$  ratio within the range 3.0-3.8 on final product performance.

In their study, Allahverdi and Hani [51] mixed concrete waste with brick waste. They achieved 50 MPa compressive strength using 8%  $\text{Na}_2\text{O}$  and 1.4 silica module  $\text{Na}_2\text{SiO}_3$  at the end of the experiment.

Vásquez et al. [52] accomplished a study with a result of 3-55 MPa compressive strength on the mechanical properties of ordinary Portland cement, concrete waste and methacholine mixtures. They emphasized that the alkaline activator percentage is significant.

Adding metakaolin and portland cement improves mechanical performance by dissolving the crystal phases into concrete waste.

In recent decades, many researches have gained much importance to manufacturing building materials through recycled CDW by geopolymerization. After 28 days of normal curing at room temperature, Mahmoodi et al. [53] created a high-compressive strength geopolymer binder of about 80 MPa with concrete waste and blast furnace slag. Similarly, in oven cure with CDW precursors, Ulugöl et al. [54] developed a geopolymer binder exceeding 45 MPa. On the other hand, Yıldırım et al. [5] used CDW-based materials and activated them with sodium hydroxide, then after curing the samples 48 hours at 115°C, compressive strength of 80 MPa was achieved.

Moreover, Robayo-Salazar et al. [48] activated CDW-based materials with NaOH and Na<sub>2</sub>SiO<sub>3</sub> and subjected the samples to environmental treatment. At the end of 90 days of ambient curing, the study has obtained a high compressive strength of up to 43.9 MPa. Studies have shown that waste materials based on CDW can be efficiently recycled, and high-performance and environmentally sustainable construction materials can be created as an option for Portland cement.

The hardened and fresh characteristics of the particle gradation change of CDW in fly ash-based geopolymers were surveyed by Rossi et al. [55]. In their studies, sodium hydroxide and silicate had been utilized as alkaline activators, and fine construction waste materials were used as aggregates. The results displayed that the compressive and bending strength of geopolymers based on CDW was 40 MPa and 8.5 MPa, respectively. Furthermore, sand-based geopolymers had compressive and bending strengths of 23 MPa and 3.1 MPa.

#### **2.4. Reinforced Geopolymer Concretes**

Geopolymer research in the literature has been conducted on mechanical properties such as compression strength and microstructural characterization of the product. Nevertheless, while the geopolymer products were successfully created both in mechanical and durable terms, large-scale structural element testing is also necessary. In this perspective, there has been a lot of research on structural elements of reinforced geopolymer concrete nowadays. Structural members like beams and columns made of geopolymer reinforced concrete must be produced, and the structural analysis and modeling of these elements should be examined.





Figure 2.4. First public structure built with structural Geopolymer Concrete: The University of Queensland, Australia, 2014

Although limited studies, some research and outputs on reinforced geopolymer concretes are available in the literature. The mechanical characteristics of reinforced geopolymer based fly-ash beams and traditional Portland cement concrete beams were compared by Sumajouw et al. [56]. The authors achieved that geopolymer concrete's compressive strength was between 46 MPa and 34 MPa, and failure load was between 112,6 kN and 326,00 kN. They reported that the geopolymer beams demonstrated similar mechanical characteristics compared to traditional cement beams.

PU Kumar and BSC Kumar [57] manufactured geopolymer beams with blast furnace slag and metakaolin, and assessing their bending behaviour. In consideration of the load-deflection and crack patterns aspect, the results pointed out that the geopolymer and Portland cement beams show almost identical behavior according to their results. The cracking moment of the geopolymer beam is still below that for Portland cement systems.

Jeyasehar et al. [58] have created precast elements for fly ash-based geopolymer and tested for the feasibility of geopolymers in the application. The geopolymer beams were

manufactured with a solution/fly ash ratio between 0.4 and 0.55, and traditional concrete beams were also manufactured as a reference. The result of the study showed that, in terms of first cracking load, yield strength and ultimate load, and average crack width, geopolymer beams were superior to the reference beams.

Kumaravel and Thirugnanasambandam [59] made a test on the bending behavior of a F class fly ash-based reinforced geopolymer beam. At nearly the same compressive strength, the authors compared the mechanical characteristics of the geopolymer concrete and cement concrete. Geopolymer concrete was 7.9 percent better in terms of service load than cemented concrete. They also revealed that the geopolymer beam is 5,68 percent stronger than the cement concrete beam in terms of average load-carrying capacities.

## **2.5. Structural Tests of Reinforced Geopolymer Concretes**

It is essential to use ecofriendly materials, which have been developed at a structural level as a replacement to Portland cement. Even if the durability and compressive strength of the developed construction materials are to be tested and defined prior to their development, it is also necessary to test the structural elements manufactured with these materials. Within this context, the strength of structural elements under various loading condition and structural analysis and characterization is also essential requirements. Therefore, determining the bearing capacities of these structural elements and behavior against lateral and vertical loads give rise to long-term reliable construction applications.

The adhesion between geopolymer and reinforcement bar is so crucial elements for assessing the structural performance of geopolymer concrete elements. The bond strength directly influences many characteristics such as carrying capacity, crack propagation geopolymer building elements. Although mechanical and physical characteristics of traditional concrete were have been standardized, the mechanisms of the geopolymeric structural elements, matrix chemistry, and adherence properties among reinforcements can be quite different from those of current standards and characteristics. Therefore, there are many surveys in the literature that analyze adhesion for structural geopolymers. A comprehensive overview of the structural features of geopolymer such as bond strength, load-bearing capacity, bending, and deformations of structural elements will be listed in the following section.

### **2.5.1. Geopolymer Beam Tests**

In recent studies [2-7], the mechanical characteristics of geopolymer concrete, its durability, and the effects of different by-products used were evaluated. It was stated that GPC was a promising candidate for conventional concrete in terms of both strength and durability [60-63]. Moreover, the carbon footprint of geopolymer concrete can be reduced up to 80-90%, by optimizing the alkali activators and binder content, compared to conventional concrete as it comprises by product materials such as fly ash, slag, glass powder, etc. [9, 10, 30, 60]. However, studies on the use of the geopolymer concrete in structural components are restricted [10, 63-66]. Raj et al. [67] determined the behavior of geopolymer concrete joints and compared the performance of the geopolymer joints with the conventional concrete joints. They concluded that the geopolymer joints with proper steel of fiber reinforcements could behave better under cyclic loading.

Sofi et al. [68] studied their adhesion by producing beam elements based on fly-ash. According to experiment results, splitting type failure of beam element was observed. They concluded that the bond strength of the beam end specimens was lesser than the pullout tests. According to correlating test methods, the direct pullout test could be more capable of evaluating the bond strength.

To evaluate the bending behavior of the geopolymer beams based on fly ash and slag, a four-point bending test of 1200 mm effective length was studied by Aslam and Khadiranaikar [69]. The geopolymer beam was compared to conventional cemented beams with about load deflection, initial crack loading, and ultimate load. According to the crack propagation, the geopolymer beam showed a ductile failure due to crushing in the compression zone. According to findings, the tensile reinforcement percentage and the geopolymer's compression strength were two important parameters in the beam's flexural capacity. In addition, the moment and the crack load were also proportional to the tensile steel percentage and the compression strength of the geopolymer. The authors approved that the geopolymer could be an option to Portland cement concrete in structural applications.

In a study of Visintin et al [70], F class fly ash-based geopolymer was used in production in shear dominant beams without stirrup. They analyzed geopolymer beam shear behavior under four direct shear tests and compared the outcome with reference cemented

beams. The author emphasized that shear dominant beam outcomes in terms of mechanical properties were similar to reference ones, but more research and modeling was essential. Also, they concluded that methodology of the test was successful, results were reliable. The geopolymer could be an option binder material to conventional Portland cement in the future.

Yost et al. [71] manufactured alkaline-active geopolymer beams produced with fly ash and tested under a four-point bending test and compared the geopolymer beams with reference cemented beams in terms of over-reinforced, under-reinforced and shear dominant conditions. The authors concluded that geopolymer beams and cemented beams showed similar behavior under the same testing criteria and methods. They also noted that geopolymer beams and cemented beams had similar elasticity failure mode in the under-reinforced testing. They found that the load-displacement curve of geopolymer was more linear than cemented ones; namely, cemented beams' load-displacement curve was nonlinear. They also mentioned that in the bending tests, geopolymer beams showed more brittle behavior than cemented ones. Consequently, they concluded that the geopolymer beams showed similar structural behavior under the same aggregate properties and compressive strength values in the flexural four-point test.

Darmawan et al. [72] studied shear dominant class C-based geopolymer beams. The compressive strengths was between 22-46 MPa, and the splitting strength between 2.38-3.12. They exposure the beams to two different curing conditions, marine water and normal condition. At the end of 28 days, the crack formation and the crack propagation of the samples were reported to be similar. However, the cracking load in the marina water cure raised more. Moreover, they reported that geopolymer beams cured normal condition showed lower porosity and higher toughness.

Ambily et al. [73] studied on shear behavior of various compositions of slag and fly ash in geopolymer beams. Two different a/d ratios were taken as 1.5 and 2 in testing beams. The authors found that when comparing middle span curves, the load-deflection, and the peak load values of the traditional Portland cementing beams and geopolymer beams were quite similar. Moreover, they emphasized that initial crack formation with 2 a/d ratio was shown earlier in geopolymer beams. Other results were that the compressive strength of geopolymer samples was 20% more than cemented ones, and ultimate load-

carrying capacity was 15% higher, too. However, they pointed out that geopolymer beams had similar crack pattern to Portland cement-based beams in two different a/d ratios.

Madheswaran et al. [74] also studied geopolymer beams with the a/d ratio 1.5 and 2. They produced 12 geopolymer beams and reference cemented beams. The results indicated that geopolymer beams showed more deflection and the maximum curvature graph was similar. Therefore, geopolymer could be an excellent alternative to Portland cement in structural applications.

Umniati et al. [75] compared the behavior of flexural dominant fly ash-based geopolymer and Portland cement beams. They designed beams with a/d as 1.11 and 2.24. Compressive strength, maximum load-carrying capacity, and bending shear strength were important measurements to compare the behavior of the beams. According to the outcomes of the experiment, the flexure performance of the geopolymer was weaker than cemented beams because geopolymer beams showed flexure dominant failure and cemented beam showed shear dominant failure.

Yacob et al. [76] produced fly-ash-based geopolymer and reference Portland cement beams to compare them. In this test, the shear characteristic of beams was evaluated. Fly ash was activated with a variety of sodium hydroxide and sodium silicate compositions. Also, water reducer additives and more water were inserted to the mixture to minimize workability problems. Then, geopolymer beams were cured at 65 ° C to attain compressive strength of 40 MPa at 28 days. In the test, the crack pattern of geopolymer and reference beams differed from each other. They further observed that the shear strength was apparently affected by the a / d ratio, compressive strength, and reinforcement amount. On that basis, as a result of the increase in the a/d ratio between 2.0 and 2.4, they saw a mode of failure change from shear dominant failure to shear-flexure dominant failure.

Ahmed et al. [77] examined the effects of glass fiber-reinforced polymer (GFRP) bars on behavior of geopolymer beams. In this study, it was shown that the stiffness of geopolymer beams was detected to be slightly less than the conventional concrete beams, but both types of beams had approximately the same value of the ultimate load. In another study conducted by Sumajouw et al. [78], the experimental researches and numerical analysis on the mechanical behavior and the strength of the geopolymer concrete slender columns was

evaluated. They tested twelve columns with different longitudinal reinforcement ratios under different axial load ratios. They concluded that heat-cured F-class fly ash geopolymer concrete had outstanding capability to produce in the pre-cast industry as the tests indicated similar behavior with the conventional concrete counterpart. Wu et al. [79] concluded that the shear strength and failure modes of GPC beams were comparable to those of RC beams.

Mathew and Joseph [80] examined the effect of elevated temperatures on the bending performance of geopolymer beams produced from low calcium fly ash. They perceived that the deformation characteristics of reinforced geopolymer concrete beams showed similar deformation behavior under loading at the room temperature to the reinforced cement concrete beams. However, when the geopolymer beams exposed more temperature curing, their ductility decreased rapidly.

Unlike these researches, in this study, the flexural behavior of beams produced from geopolymer concrete with 100% recycled construction material was determined in order to unveil the possibility to eliminate the CO<sub>2</sub>-gas emission due to aggregate and cement production and to enhance the recycling rate in the construction practice.

## MATERIALS AND METHODOLOGY

### 3.1. Introduction

GPC mixtures were designed based on extensive preliminary studies conducted to develop the geopolymer phase. In this context, the precursor phase of the geopolymer binders was obtained by applying the selective demolition procedure of the inert concrete (CW), clay originated brick elements as hollow brick (HB), red clay brick (RCB), roof tile (RT), and glass (GW) part of construction and demolition waste (CDW). All these CDW materials are clay-based except for inert concrete materials and glass. Visuals of CDW-based precursors taken by using a digital camera and by scanning electron microscopy (SEM) are presented in Figure 3.1. The chemical compositions of CDW elements were obtained via X-ray fluorescence (XRF) analysis and are summarized in Table 3.2. These precursors were exposed to a non-complex pre-crushing and subsequent grinding, making them suitable for polymerization reactions and reducing their particle size to cement fineness (i.e., maximum size less than 100 $\mu$ m). The primary objective of the simple procedure for processing precursors is to decrease the amount of energy consumption and labor. Given the variability of CDW elements and the fact that all CDW elements can be collected at a construction/demolition site in a batch, a consistent milling period is critical to ensure that separated and non-separated CDW elements have similar particle sizes. As a result of the preliminary studies carried out in this context, the materials were reduced to their final particle size during the 1-hour grinding period determined for the binder phase to reach a particle size of fewer than 100  $\mu$ m. Particle gradation of CDW-based precursors are given in Figure 3.3.

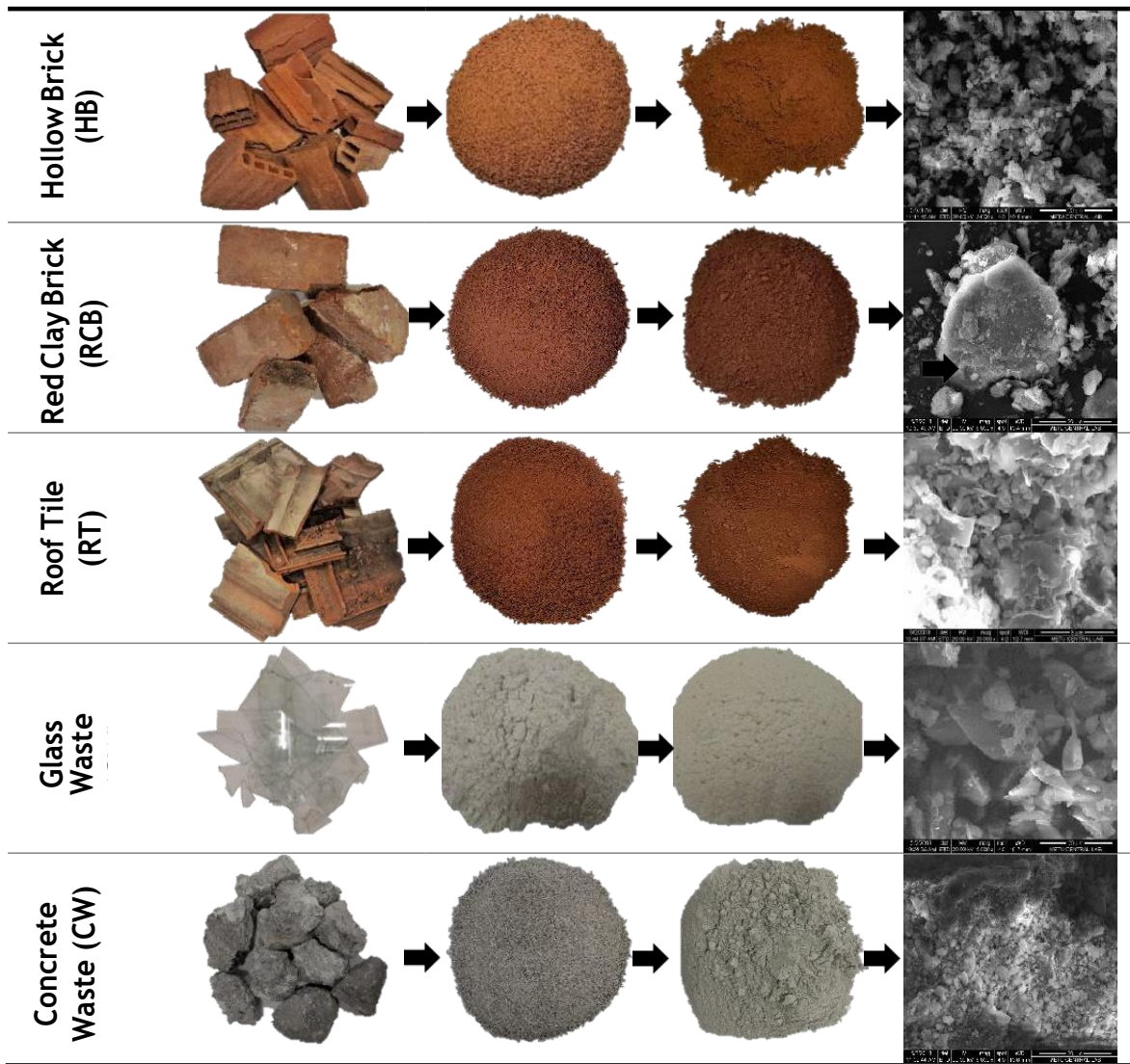
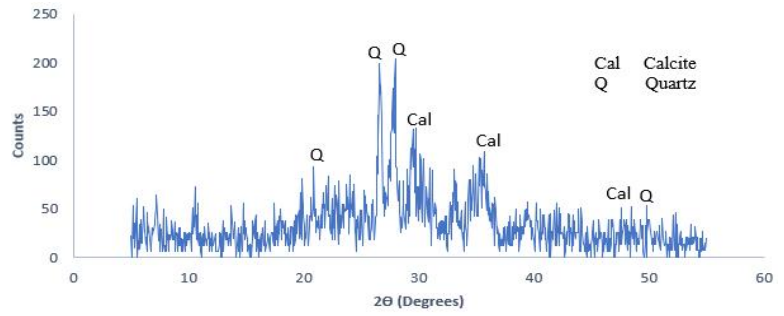


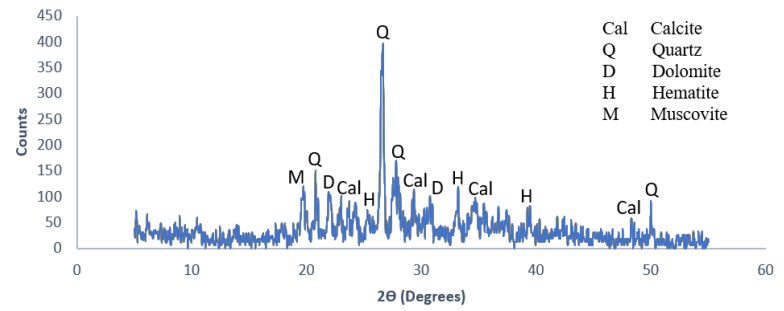
Figure 3.1. Visuals of CDW-based precursors  
 (from left to right; raw state, crushed state, ground state, SEM micrograph)



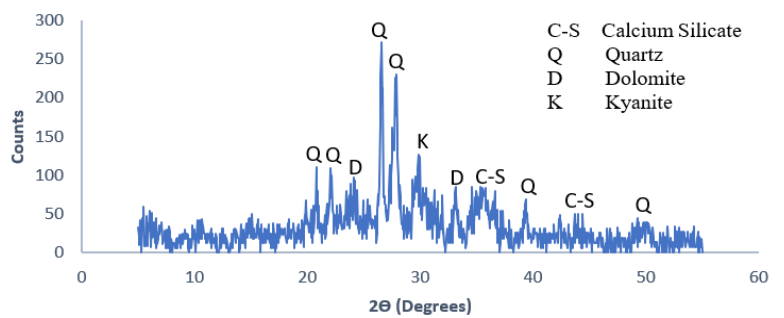
Hallow Brick  
(HB)



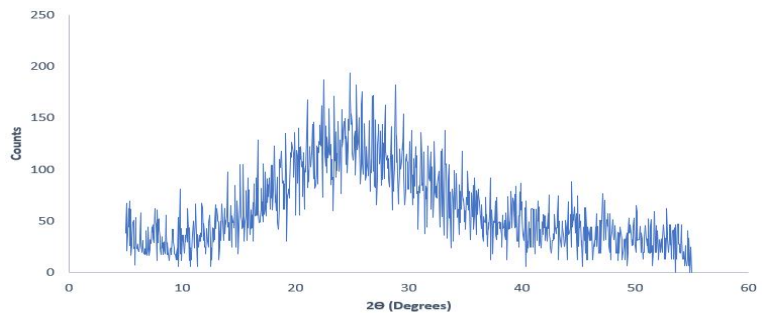
Red Clay Brick  
(RCB)



Roof Tile (RT)



Glass Waste  
(GW)



Concrete Waste  
(CW)

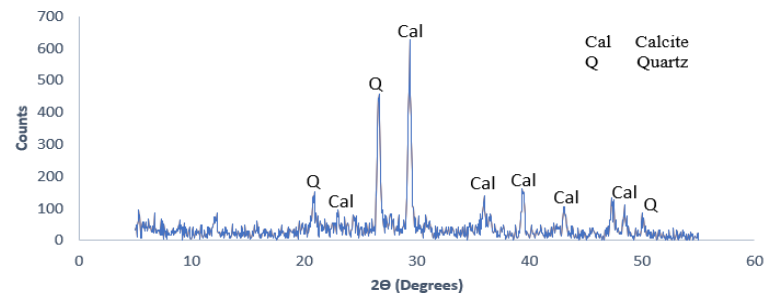


Figure 3.2. XRD Analysis of CDW-based precursors

Table 3.1. Chemical compositions of CDW-based precursors

Oxides, %	Hollow Brick (HB)	Red Clay Brick (RCB)	Roof Tile (RT)	Glass Waste (GW)	Concrete Waste (CW)
<b>SiO<sub>2</sub></b>	39.7	41.7	42.6	66.5	31.6
<b>Al<sub>2</sub>O<sub>3</sub></b>	13.8	17.3	15.0	0.9	4.8
<b>Fe<sub>2</sub>O<sub>3</sub></b>	11.8	11.3	11.6	0.3	3.5
<b>CaO</b>	11.6	7.7	10.7	10.0	31.3
<b>Na<sub>2</sub>O</b>	1.5	1.2	1.6	13.6	5.1
<b>MgO</b>	6.5	6.5	6.3	3.9	0.9
<b>SO<sub>3</sub></b>	3.4	1.4	0.7	0.2	0.5
<b>K<sub>2</sub>O</b>	1.6	2.7	1.6	0.2	0.7
<b>TiO<sub>2</sub></b>	1.7	1.6	1.8	0.1	0.2
<b>P<sub>2</sub>O<sub>5</sub></b>	0.3	0.3	0.3	0.0	0.1
<b>Cr<sub>2</sub>O<sub>3</sub></b>	0.1	0.1	0.1	0.0	0.1
<b>Mn<sub>2</sub>O<sub>3</sub></b>	0.2	0.2	0.2	0.0	0.1

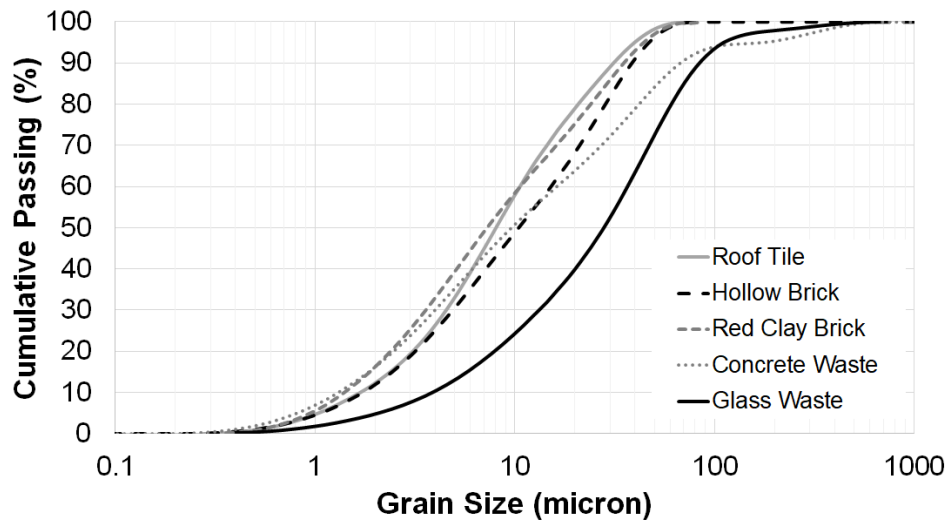


Figure 3.3. Particle gradation of CDW-based precursors

### 3.2. Mixture Compositions

In this study, control specimens were also produced to compare the performance of the GPC (GPC-NA) and GPC with recycled aggregates (GPC-RA). Thus, four different mixtures were prepared: GPC-NA, GPC-RA, conventional concrete with normal aggregates (CVC-NA), and conventional concrete with recycled aggregates (CVC-RA). The only difference between GPC-NA (CVC-NA) and GPC-RA (CVC-RA) is the inclusion of normal aggregates instead of recycled aggregates. The other components of the mixtures are kept the same. The details of mixtures GPC and CVC specimens are tabulated in Table 3.2 and Table 3.3, respectively.

Table 3.2. The content of the GPC

<b>Ingredients</b>	<b>Masses in Geopolymer Concrete (kg/m<sup>3</sup>)</b>
<b>Red Clay Brick</b>	150
<b>Hollow Brick</b>	200
<b>Roof Tile</b>	250
<b>Glass</b>	100
<b>Recycled Concrete</b>	100
<b>Slag</b>	200
<b>Fly Ash</b>	50
<b>Ca(OH)<sub>2</sub></b>	50
<b>NaOH</b>	112
<b>Na<sub>2</sub>SiO<sub>3</sub></b>	224
<b>Fine Aggregate</b>	250
<b>Coarse Aggregate</b>	750
<b>Water</b>	200
<b>Water/Binder</b>	0.19

Table 3.3. The content of the CVC mixtures

Ingredients	Masses in Conventional Concrete (kg/m <sup>3</sup> )
Cement	316
Fine Aggregate	917
Coarse Aggregate	917
Water	211
Water/Binder	0.67

### 3.3. Alkali Activators

Another essential element for the preparation of GPC mixtures is the type and concentration of alkaline activators. Three different activators were tested by activating the binding phase at different concentrations and in various combinations to determine the activator's types and phases in question. The mixtures with the highest mechanical performance formed the basis of the GPC mixtures. Calcium hydroxide( $\text{Ca}(\text{OH})_2$ ), sodium hydroxide( $\text{NaOH}$ ), and sodium silicate( $\text{Na}_2\text{SiO}_3$ ) have been used as activators in mixtures as their alkaline properties and capability to ensure a high power of hydrogen (pH) medium to provide the geopolymerization reactions. As it is well known, sodium hydroxide offers high alkalinity and prepares alkali-activated and geopolymer materials for geopolymerization reactions by breaking bonds such as  $\text{SiO}_2$ ,  $\text{Al}_2\text{O}_3$ , and  $\text{CaO}$  in the materials' structure. Sodium silicate releases a huge amount of reactive  $\text{SiO}_2$  and  $\text{Na}_2\text{O}$  into the mixtures during the gel-forming processing. Also, it accelerates the reaction of geopolymerization. Calcium hydroxide also increase the strength of geopolymer by adding the system extra C-S-H and C-A-S-H gel.

As a result of extensive studies carried out to determine the alkali activator combination, the molar concentration of sodium hydroxide was selected as 8M. In contrast, the sodium silicate was chosen to be two times the sodium hydroxide amount by weight. Calcium hydroxide was added to the mixtures as 5% of the total binder amount. Considering the properties such as water absorption, porosity, adherent cement particle content of the existing fine aggregates in the scope of CDW-based recycling aggregates that form the aggregate phase of GPC concrete mixtures, different gradations and different binder/aggregate ratios are tested at a 1/1 binder/aggregate ratio determined as a result of extensive preliminary studies [5, 6]. The summary of the geopolymer concrete compositions could be found in Table 3.2. Also, The

details of it could be found in the recent studies conducted by Yildirim et al. [5] and Ulugol et al. [6].

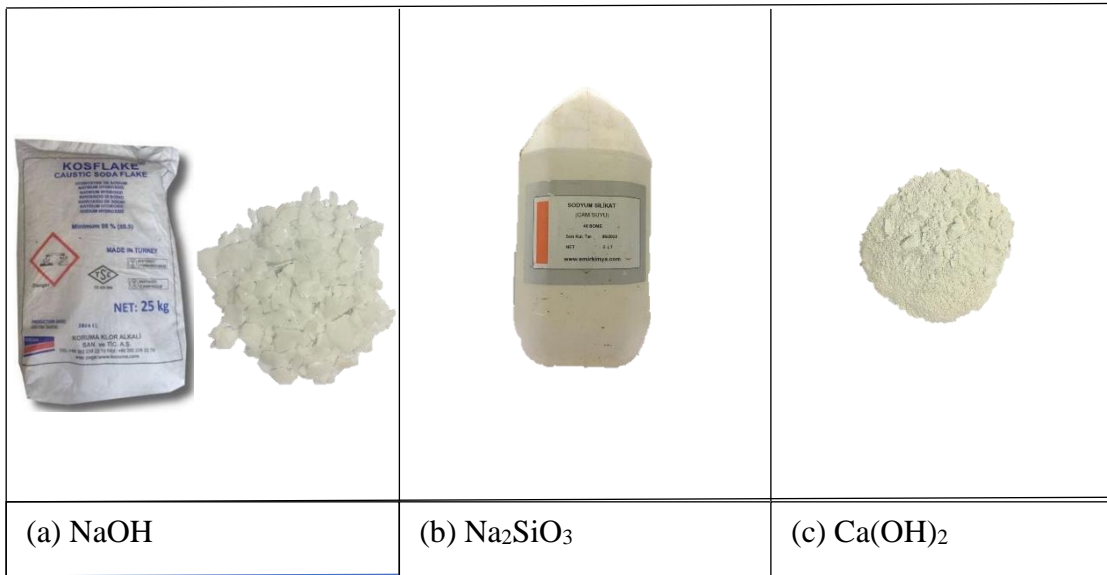


Figure 3.4. Alkali Activators pictures

Tables 3.4- 3.6 show the chemical characteristics of sodium hydroxide, sodium silicate, and calcium hydroxide, respectively.

Table 3.4. Chemical Properties of NaOH

Analyzes	Specifications	Unit	Results
Appearance	White flake		White flake
Sodium Hydroxide	min. 98	%	98.26
Sodium Chloride	max. 0.11	%	0.03
Sodium Carbonate	max. 0.41	%	0.34
Iron (Fe)	max. 16	ppm	13.18

Table 3.5. Chemical Properties of Na<sub>2</sub>SiO<sub>3</sub>

Parameter	Value
SiO <sub>2</sub> (%)	23
Na <sub>2</sub> O (%)	11
Module (SiO <sub>2</sub> /Na <sub>2</sub> O)	2.09
Baume (20 °C, Be <sup>1</sup> )	40
Density (20°C, gr/cm <sup>3</sup> )	1.40
H <sub>2</sub> O (%)	66

Table 3.6. Chemical Properties of Ca(OH)<sub>2</sub>

Analyzes	Results
Molecular Weight	74.1 g/mol
Melting Point	550 °C
Purity (%)	min. 88
MgO (%)	max. 1
Acid-insoluble (%)	max. 1
Loss of ignition (%)	max. 4
Particle size (<90 mm) (%)	min. 91

### 3.4. Aggregates

The aggregate phase of GPC mixtures was pulverized by using a jaw crusher. The recycled aggregates were obtained from construction and demolition waste (CDW) only to the pre-crushing process and separating the different particle size ranges by using sieves with various openings. In the production of geopolymer concrete, the maximum recycling aggregate size is determined to be  $D_{max} = 16$  mm in line with the particle size distribution Fuller-Thompson ideal gradation curve (Figure 3.5). Recycling aggregates obtained from CDW were not subjected to any procedures for their improvements.

To be able to compare GPC and CVC, the gradation of aggregate was selected similarly. Also, the effect of normal aggregate and recycle aggregate could be compared precisely.

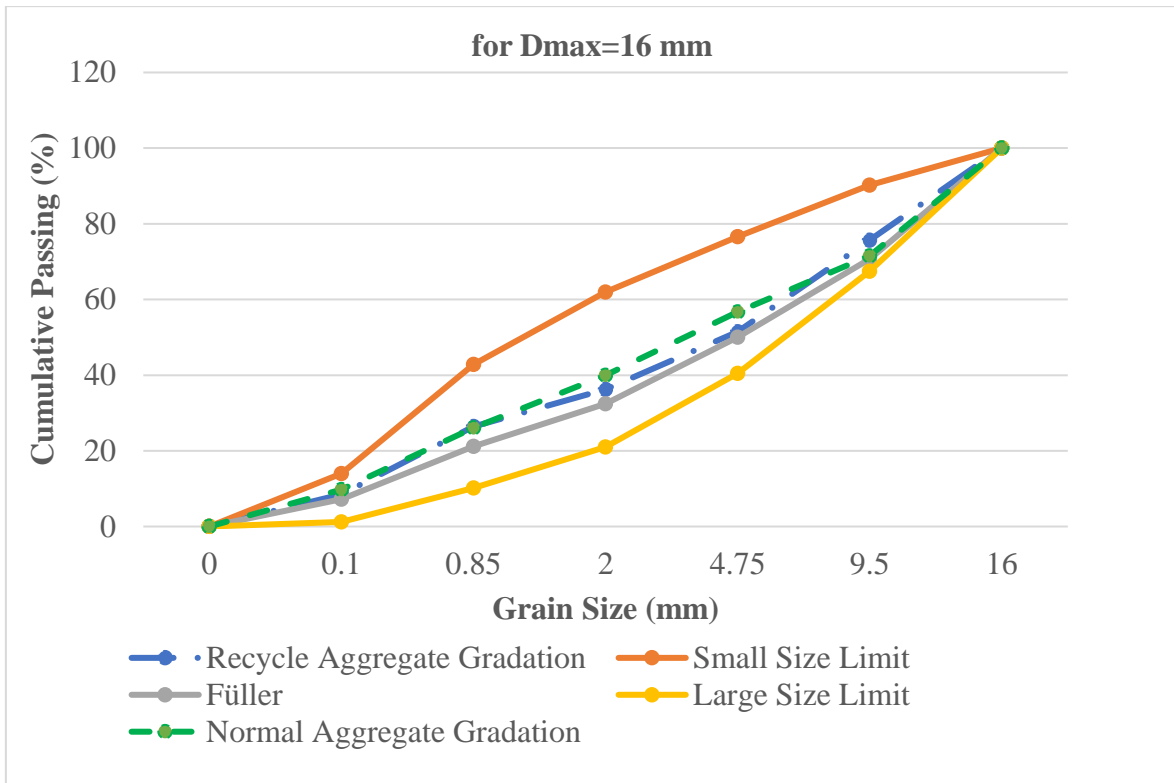


Figure 3.5. The gradation curve of the normal and recycle aggregate

### 3.5. Reinforcing Bars Detail

Each test beam was chosen to have a cross-section of 150x250mm and a length of 1100mm. The bottom longitudinal reinforcing steel was standard 10mm diameter deformed bars, while the top longitudinal reinforcing steel was 6mm diameter round bars. Round bars with a diameter of 6,5 mm were utilized for the stirrups. Three samples taken from different bar were tested in the laboratory to find the real yield strength and ultimate strength, as illustrated in Figure 3.6. Details of the rebar properties are listed in Table 3.7.

Table 3.7. Properties of reinforcing bar

Specimen numbers	Diameter (mm)	Nominal area (mm <sup>2</sup> )	Yield strength (MPa)	Ultimate strength (MPa)
1	6.42	32.37	327.4	451.0
2	6.52	33.39	329.4	449.3
3	6.48	32.98	333.5	448.8
Avarage	6.47	32.9	330.2	449.7
1	10.40	84.95	459.1	724.0
2	10.10	84.12	449.3	699.0
3	10.38	83.62	460.8	726.8
Avarage	10.29	83.2	456.4	716.6



Figure 3.6. Rebar test machine



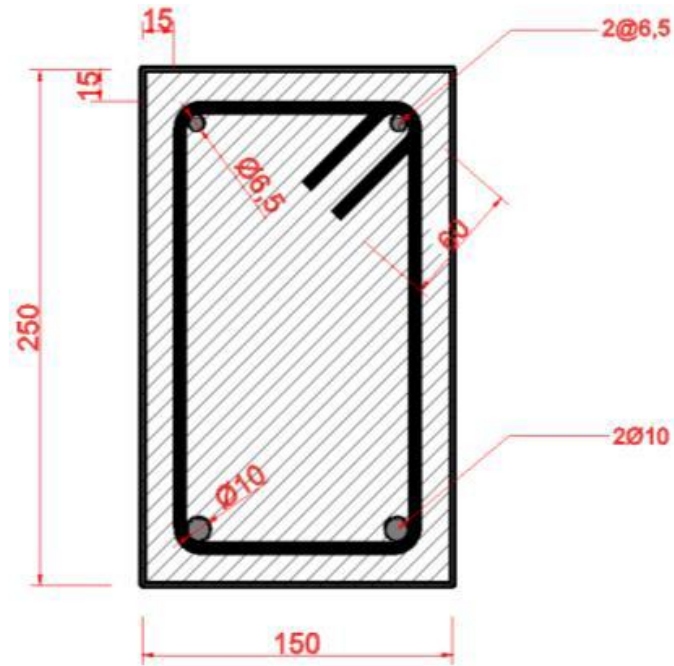


Figure 3.7. Beam cross-section

(All dimensions are given in mm)

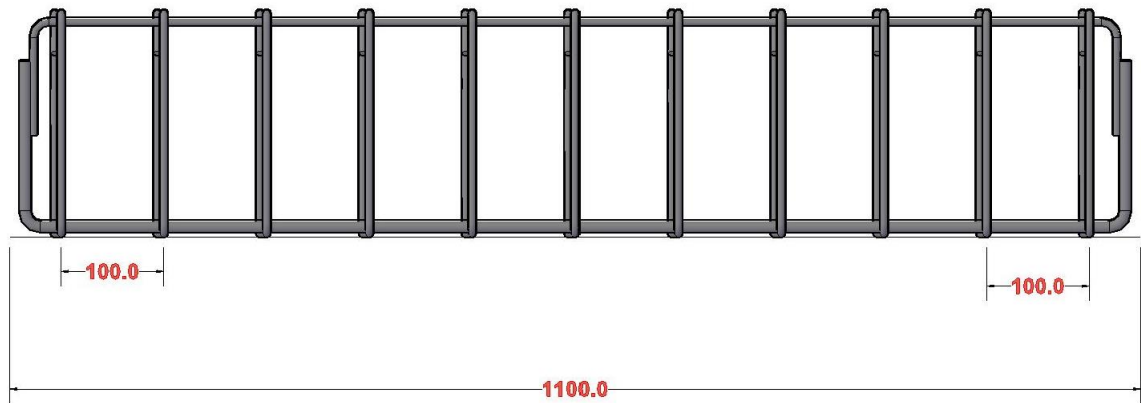


Figure 3.8. Beam reinforcing details

(All dimensions are given in mm)

In summary, the yield and maximum strength of the 10 mm (6.5 mm) steel bars were 456 MPa (330 MPa) and 716 MPa (449 MPa), respectively. Tie spacing was 100 mm over the beam length. All the ties were hooked to the core using 135° hooks to obey code-compliant detailing.



Figure 3.9. Stirrup dimensions

Concrete covers are used in the beam of 15 mm. In addition, the covers are not used in the plasticization zone of the beams so that they do not adversely affect their strength of it.

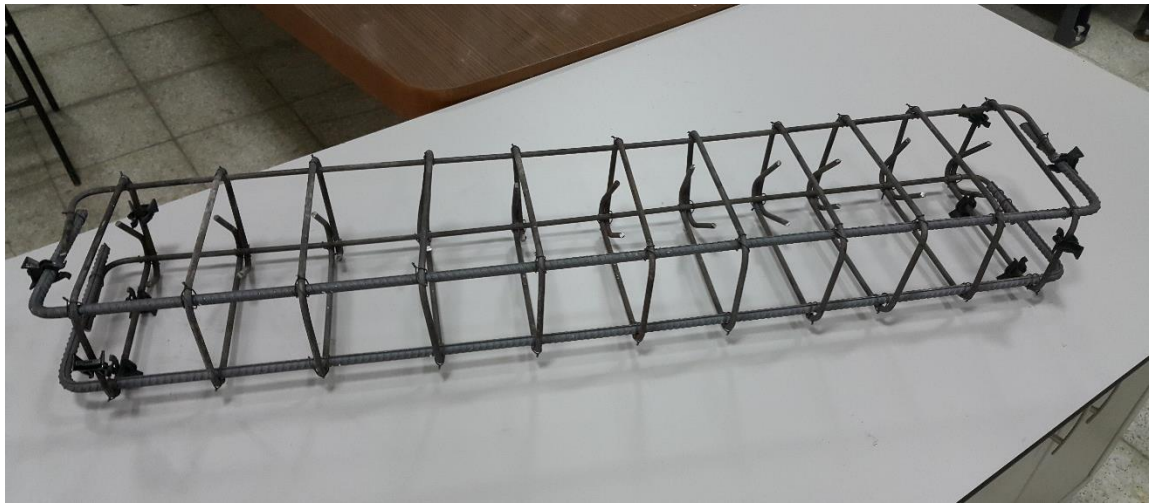


Figure 3.10. Cover and stirrup detail

### 3.6. Methodology

#### 3.6.1. Preparation of Mixtures

The production of geopolymer concrete samples was carried out by a simple mixing operation. Firstly, the powder components were weighed separately with a 0.1 g sensitivity and poured into a 50-liter Hobart mixer. The powders were then mixed for around 5 minutes to ensure homogeneous mixes, calcium hydroxide, and aggregate phase.

Sodium hydroxide in the liquid phase was combined with water and leaved to cool for one day at laboratory. Then, the sodium hydroxide mixture or solution, which was prepared, was added to the mixture of binder powder, afterward, sodium silicate in liquid form was added to the mixing, due to the rapid freezing of the sodium silicate used, it is added to the homogeneous mixture and mixing time is saved. Then, after the addition of sodium silicate, it is mixed for about 3 minutes and poured into molds immediately.



Figure 3.11. Preparation of NaOH Solution



Figure 3.12. Preparation of GPC mixture



Figure 3.13. Preparation of CVC mixture

### 3.6.2. Casting and Placing

After the preparation of the mixture, they were poured into the prepared molds. Then, molds were compacted by a vibrator appropriately.



Figure 3.14. Casting and placing procedure of CVC

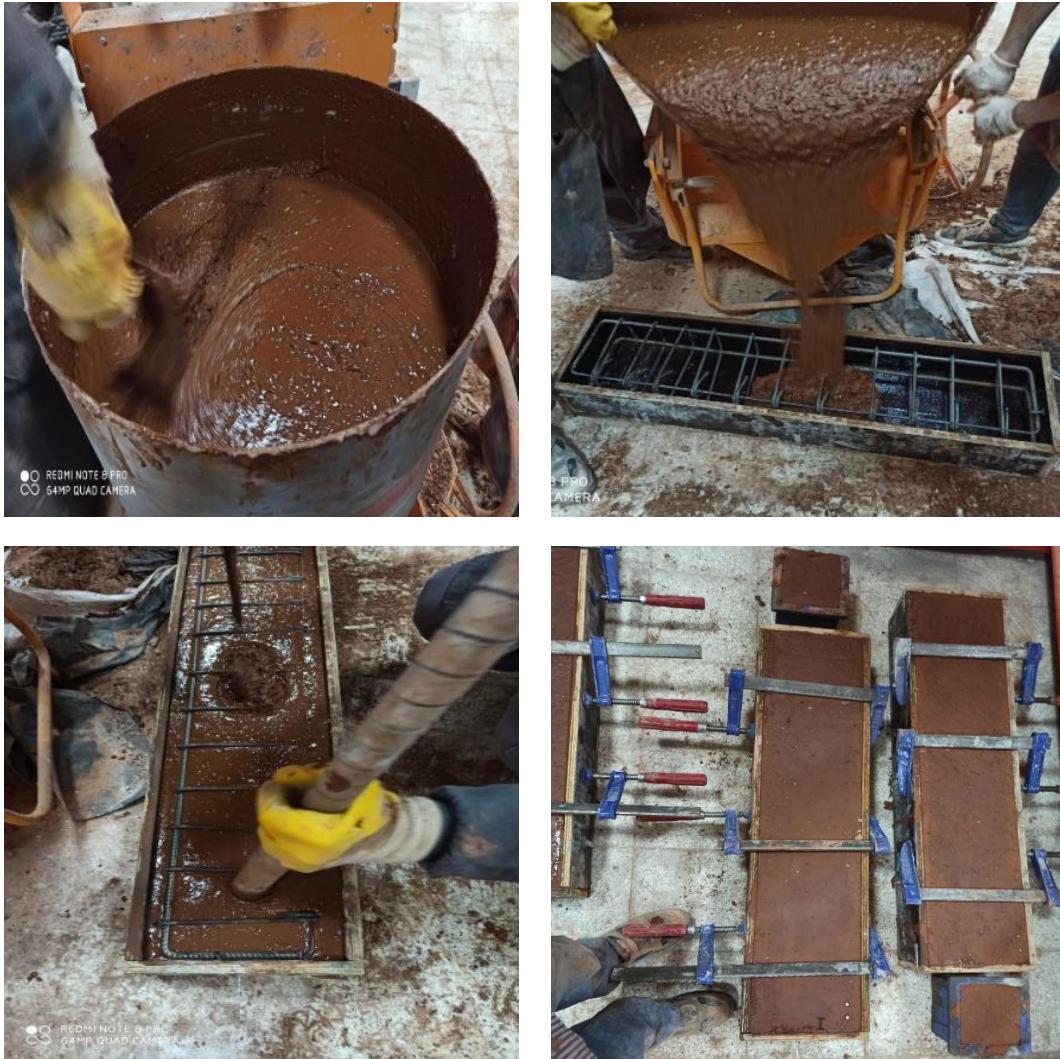


Figure 3.15. Casting and placing procedure of GPC

### 3.6.3. Curing Conditions

Beam samples, cubes, and cylinders were taken from the mold after one day of casting and cured in the water pool to eliminate water loss and to prevent drying shrinkage, as well as to ensure that the geopolymerization reactions continued. Furthermore, concrete samples were covered and applied moisture-curing until the test day, save from geopolymers.



Figure 3.16. Curing of the specimens, (a) geopolymer samples, (b) concrete samples

#### 3.6.4. Testing of Beams

The geometrical and reinforcement details of the tested specimen were selected from the first-story of a RC building designed according to TEC2018 [81]. The cross-section of the test beam was  $150 \times 250$ mm. A similar procedure to determine the inelastic performance of RC structural members in the literature was followed in this study [82-86]. Fine and coarse aggregates have been utilized in the production of geopolymer concrete. The target compressive strength was selected as 35 MPa. The average uniaxial cylinder compressive strength and the average splitting tensile strength of the test specimens are given in Table 4.1-Table 4.4 (i.e.,  $150 \times 300$ mm cylinders).

Three different concrete shear-span-to-depth ( $a/d$ ) ratios (i.e., 0.50, 1.00, and 1.65) were used in the testing program in order to observe the change in the failure pattern depending on the critical loading effects (i.e., shear-dominant behavior and flexure-dominant behavior). The beam specimens have the same reinforcement arrangements to examine the impact of the application of the geopolymer concrete and the recycled aggregate on the performance. All the reinforcement details are in compliance with the current seismic code in Turkey (i.e., TEC2018 [81]). The details of reinforcements used for all specimens are given in Figure 3.7-3.8. In addition, a schematic of all variables and all methods considered in the scope of this study was prepared for clarity (Figure 3.17).

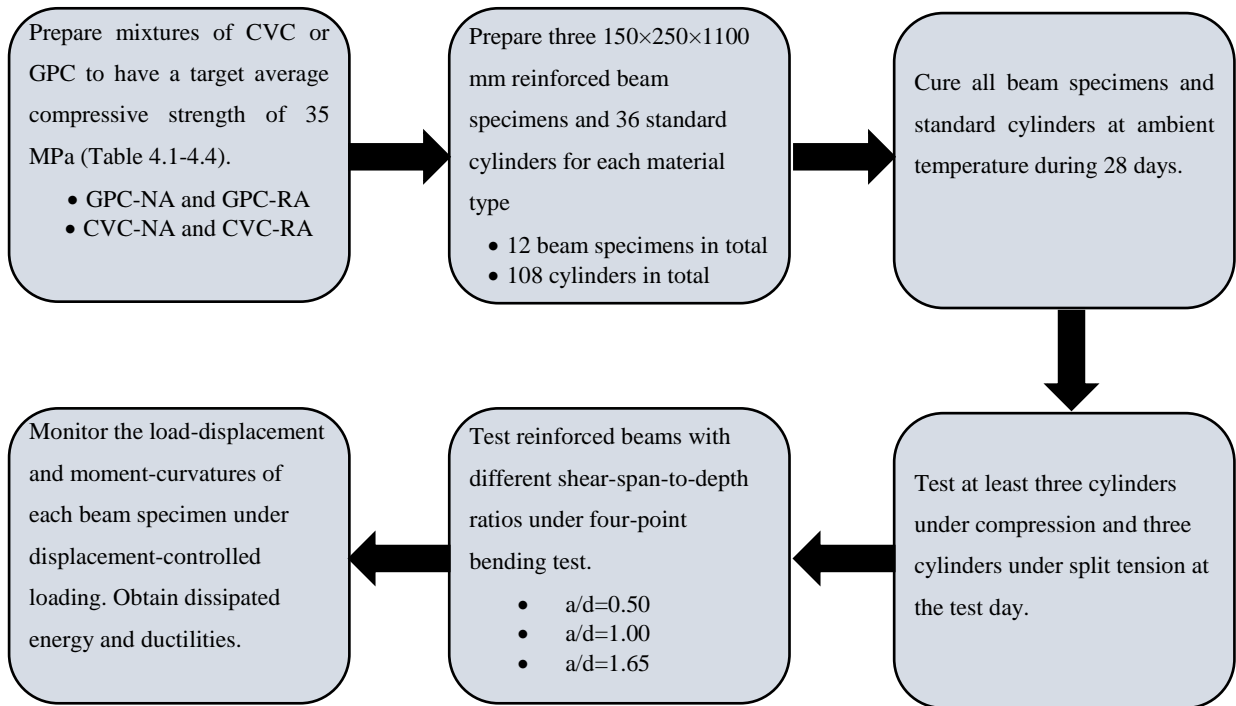


Figure 3.17. Schematic of Variables, Curing Procedures, and Mechanical Tests

In Tables 4.1- 4.4, the standard deviations of each test were also presented. It is apparent that the GPC mixtures had larger standard deviations compared to CVC mixtures.

### 3.6.5. Test setup and procedure

The test setup is shown in Figure 3.18. Vertical loads were utilized by a displacement-controlled hydraulic machine. The testing equipment was a product manufactured by BESMAK company. The system had a loading capacity of 40 tons. The testing equipment was designed to represent a closed system, eliminating the strong base anchorages of the system to the RC slab. It was equipped with an electrohydraulic servo valve with a displacement application rate range of 0.10 – 1 mm/min. The accuracy of the test was  $\pm 0.5\%$ . The tests in this study were performed with a constant loading rate of 0.30 mm/min. All samples were tested under a four-point loading system, i.e., subjected to two-point loads and supported on pin supports at both ends. The clear span of each specimen was 900 mm. For all specimens, applied vertical forces were applied with a load cell. The midspan vertical displacement was measured using Linear Variable Differential Transformers (LVDTs) placed at the center of the beam. The average curvature response of all specimens was also determined by placing lateral LVDTs (Figure 3.18). Lateral LVDTs were placed in beam specimens at 100-mm, 50-mm, and 100-mm intervals for left span, midspan, and right span,



respectively (Figure 3.18). The accuracy of each LVDT was  $\pm 0.1\%$ . All beam samples were tested under a four-point bending test demonstrated in Figure 3.18. Load deflection curves, moment-curve curves, and crack patterns were determined in order to compare the behavior of geopolymer concrete beams.

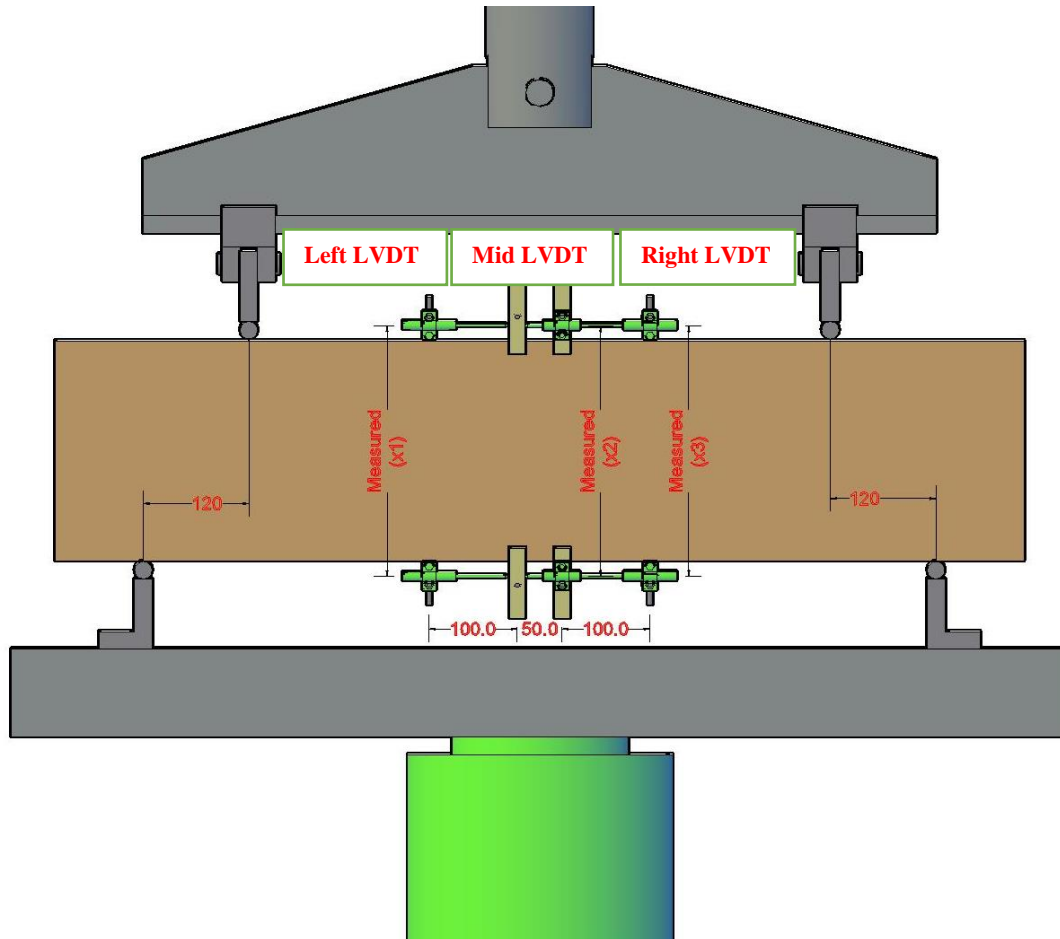


Figure 3.18. Test setup example

(All dimensions are given in mm.)

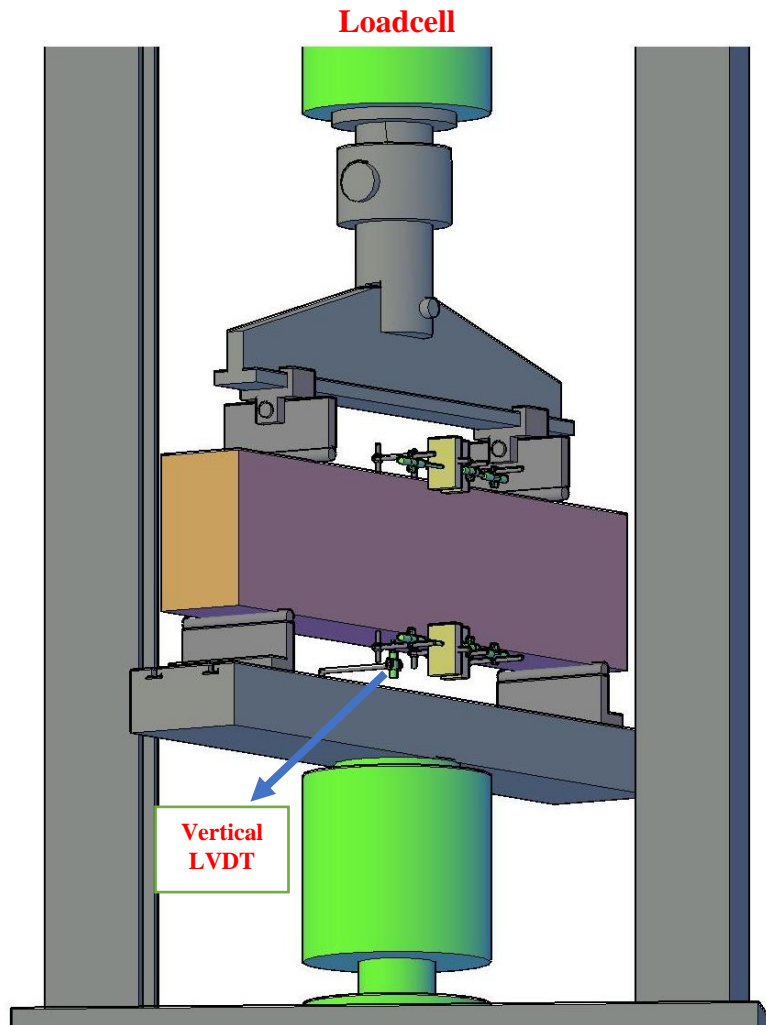


Figure 3.19. Details on Instrumentation

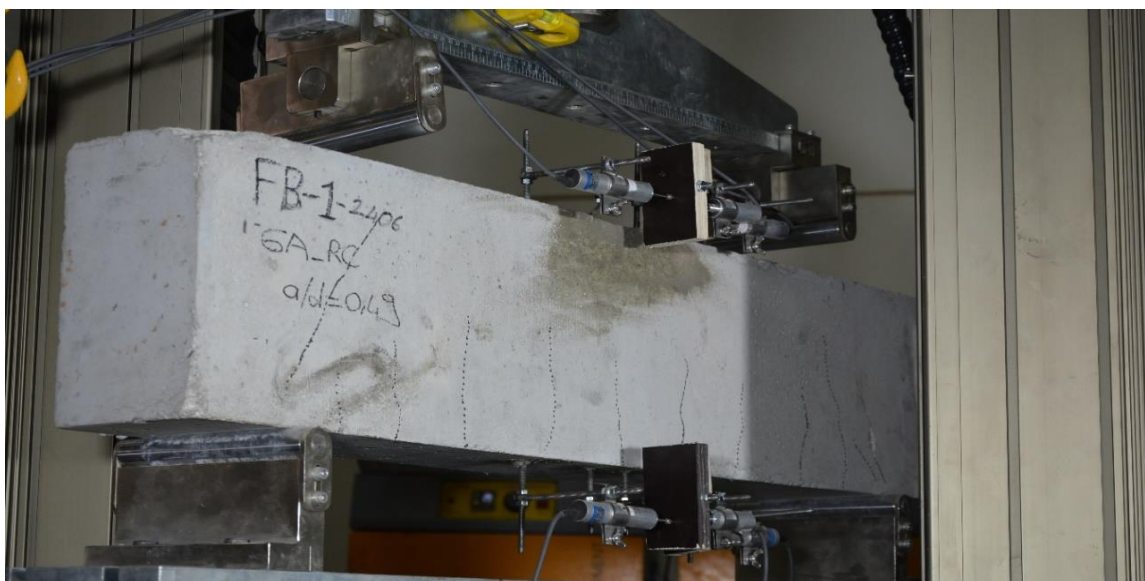


Figure 3.20. Details on Instrumentation

## EXPERIMENTAL RESULTS AND DISCUSSION

### 4.1. Introduction

In this section, the test results and the observed crack patterns during each experiment were documented. To this end, the vertical load-midspan displacement and the moment-curvature responses of all specimens are drawn and compared with different materials for a constant a/d ratio. For the sake of clarity, the ultimate force ( $F_u$ ), ultimate displacement ( $u_u$ : displacement corresponding to the end of the test or the 20% capacity drop), the yield force, and displacement ( $F_y$  and  $u_y$  were obtained by using the bilinearization procedure in FEMA356 [87]), the ductility of displacement ( $\mu_u$ :  $u_u / u_y$ ), the ultimate curvature ( $\phi_u$ : curvature corresponding to the end of the test or the 20% capacity drop), the yield curvature ( $\phi_y$ : yield curvature obtained from FEMA356 [87]), the curvature ductility ( $\mu_\phi$ :  $\phi_u / \phi_y$ ), the energy absorption capacity ( $E_t$ ) and the normalized energy capacity ( $E_n$ :  $E_t / (F_y \times u_y / 2)$ ) measured during the tests are tabulated. The damage photographs at different displacement levels are also presented. It should be noted that only one test was performed for each selected a/d ratio for all mixtures. The compressive strength and splitting tensile strength of each specimen were determined on the test day. Average strengths and their standard deviations are presented in Table 4.1-Table 4.4.

### 4.2. Compressive and Splitting-Tensile Strength of Geopolymer

At least nine cubic samples of 150 mm dimension were manufactured as part of the fabrication of geopolymer beam samples to test the compressive strength. The compressive strength of the manufactured samples was measured on 7, 28, and testing days. The loading rate is taken 0.30 mPA/s according to ASTM C39 [88].



Figure 4.1. Compressive Strength Test Setup and Experiment

Moreover, cylinder specimens poured from the same batch of beam specimens were tested at the testing days of the beams. The standard dimensions of the cylinder are 150\*300 mm. The splitting test is vital since the tensile strength of the specimens could be known by converting compression load to tensile strength with the help of this test. The formula of the splitting test is below. Similar to the compression test, the loading rate is taken 0.30 mPA/s according to ASTM C496 [89].

$$\sigma = \frac{2P}{\pi \times L \times D}$$

where,

$\sigma$ : Splitting-Tensile Strength (MPa)

P: Failure load of the cylinder specimen (N),

L: Length of the cylinder specimen (mm),

D: Diameter of the cylinder sample (mm).



Figure 4.2. Splitting-Tensile Strength Test Setup and Experiment

Table 4.1. Test Specimens of GPC\_NA

Specimens	Concrete Compressive Strength (MPa)*			Concrete Splitting Tensile Strength (MPa)*
	7 days	28 days	Testing date	Testing date
1	21.70	28.90	35.60	2.61
2	21.90	30.80	37.60	2.06
3	23.40	31.10	41.90	2.50
4	-	-	33.70	-
5	-	-	37.20	-
6	-	-	39.10	-
Average	22.33	30.27	37.50	2.39
Standard Deviation	0.93	1.19	2.83	0.29

Table 4.2. Test Specimens of GPC\_RA

Specimens	Concrete Compressive Strength (MPa)*			Concrete Splitting Tensile Strength (MPa)*
	7 days	28 days	Testing date	Testing date
1	24.00	29.30	33.30	2.02
2	25.30	31.20	36.90	2.61
3	23.38	-	38.90	2.69
4	-	-	37.40	2.16
5	-	-	-	2.12
Average	24.23	30.25	36.60	2.32
Standard Deviation	0.97	1.34	2.06	0.31

Table 4.3. Test Specimens of CVC\_NA

Specimens	Concrete Compressive Strength (MPa)*			Concrete Splitting Tensile Strength (MPa)*
	7 days	28 days	Testing date	Testing date
1	18.20	27.20	34.20	2.30
2	19.40	29.50	34.10	2.44
3	19.70	29.50	31.90	2.60
4	20.20	-	35.40	-
5	-	-	34.75	-
Average	19.37	28.73	34.10	2.45
Standard Deviation	0.85	1.33	1.32	0.15

Table 4.4. Test Specimens of CVC\_RA

Specimens	Concrete Compressive Strength (MPa)*			Concrete Splitting Tensile Strength (MPa)*
	7 days	28 days	Testing date	Testing date
1	24.30	28.70	35.40	2.43
2	23.30	31.00	35.40	2.19
3	-	31.00	34.10	-
4	-	-	35.80	-
5	-	-	36.90	-
6	-	-	36.30	-
7	-	-	32.10	-
8	-	-	33.90	-
9	-	-	37.00	-
Average	24.80	30.20	35.20	2.31
Standard Deviation	0.70	1.30	1.60	0.17

### 4.3. Geopolymer Concrete Beams

#### Normal Aggregate Flexural-Critical Geopolymer Beam 1 (GPC – NA – 0.50)

During the experiment, firstly, shear cracks were performed, then bending cracks were observed. Then, shear cracks of the beam were propagated until failure.

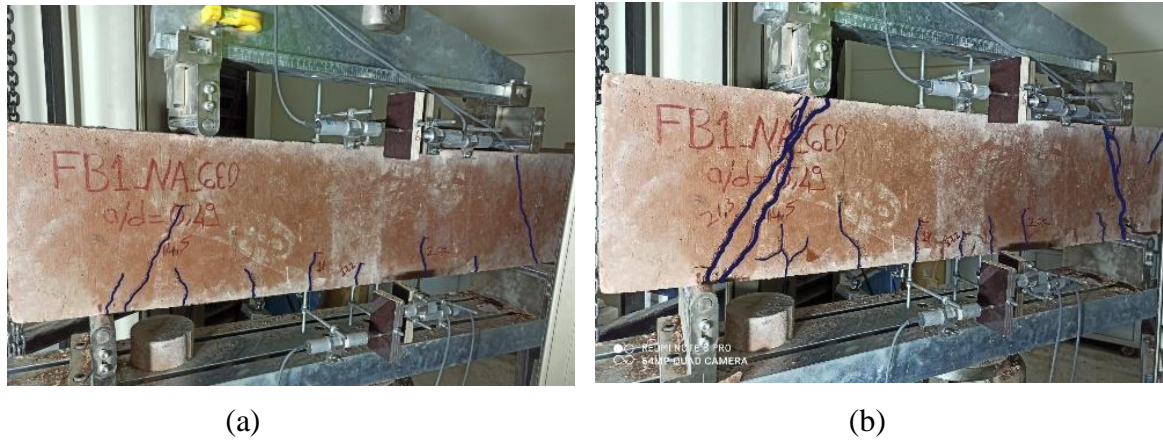


Figure 4.3. GPC – NA – 0.50 beam, (a) first cracks, (b) failure



Figure 4.4. GPC – NA – 0.50 shear crack detail



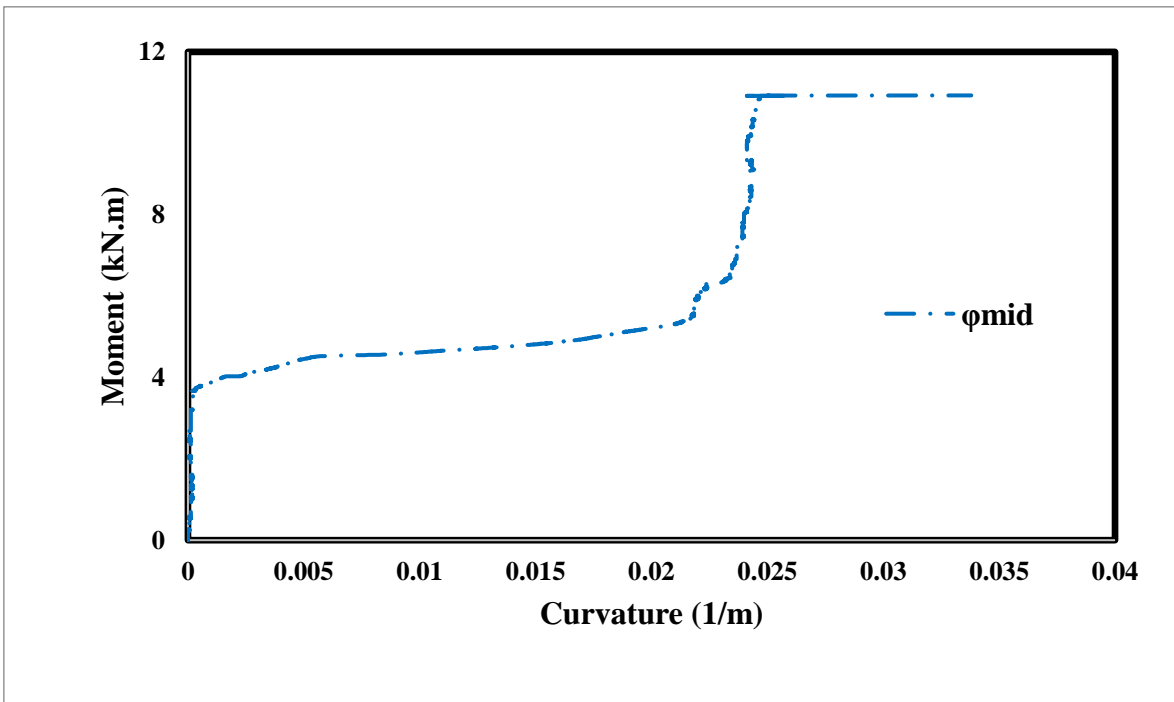
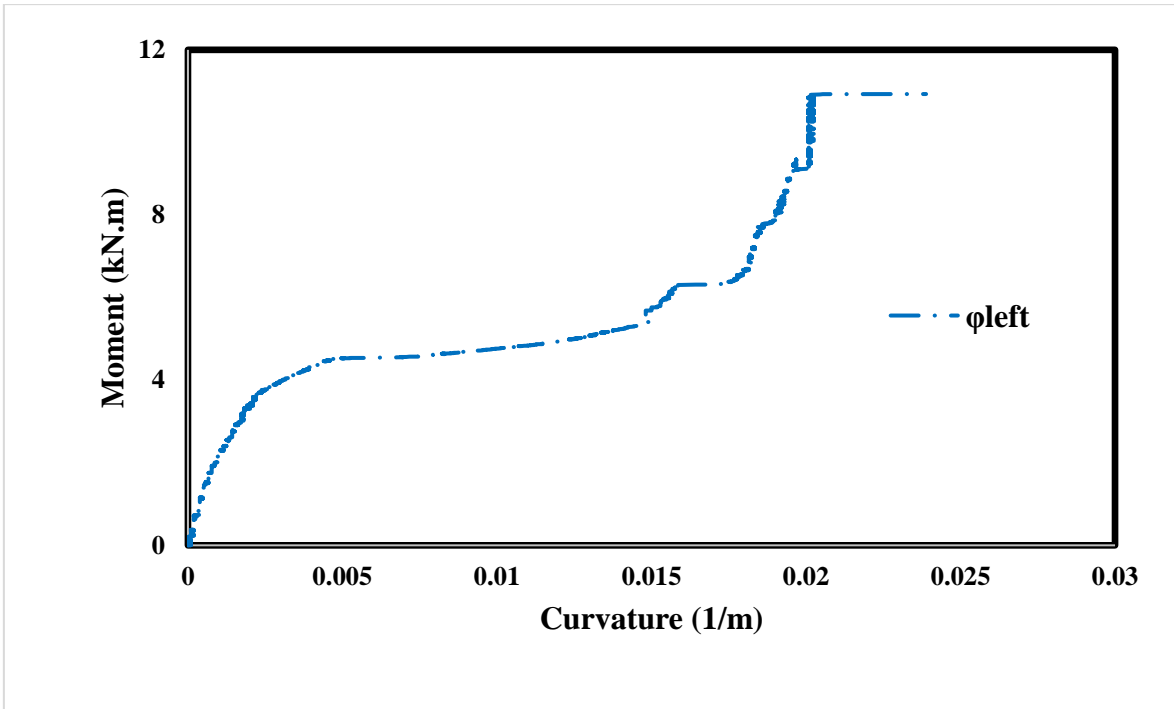


Figure 4.5. GPC – NA – 0.50 moment-curvature graph(continued)

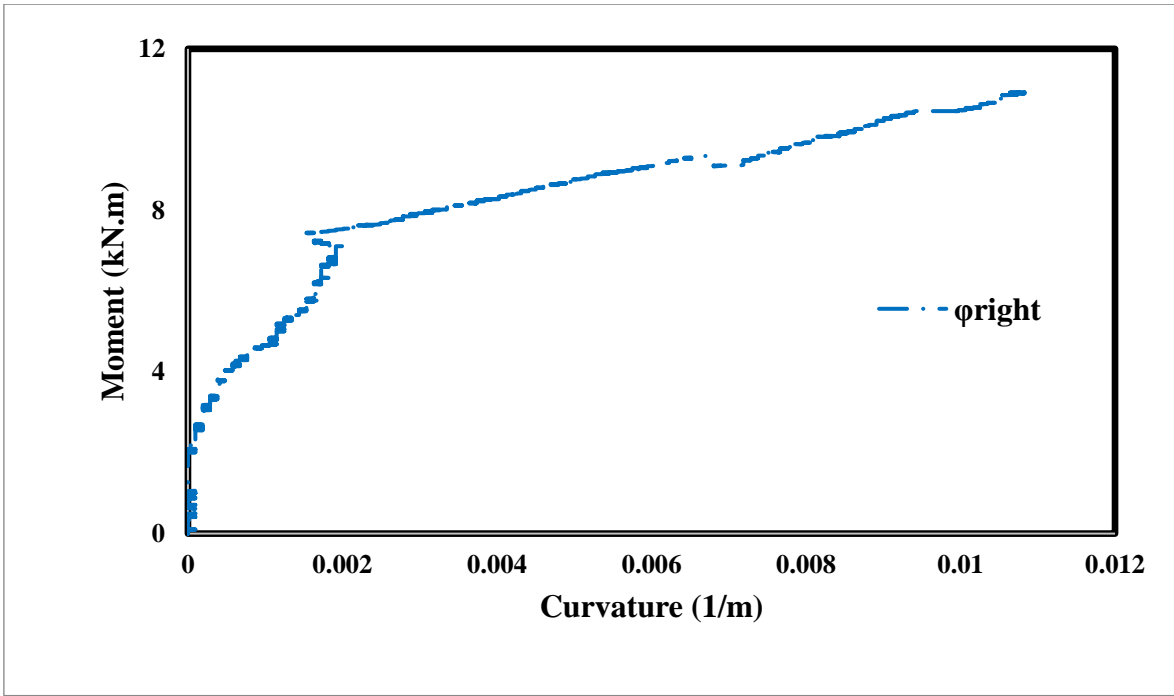


Figure 4.5. GPC – NA – 0.50 moment-curvature graph

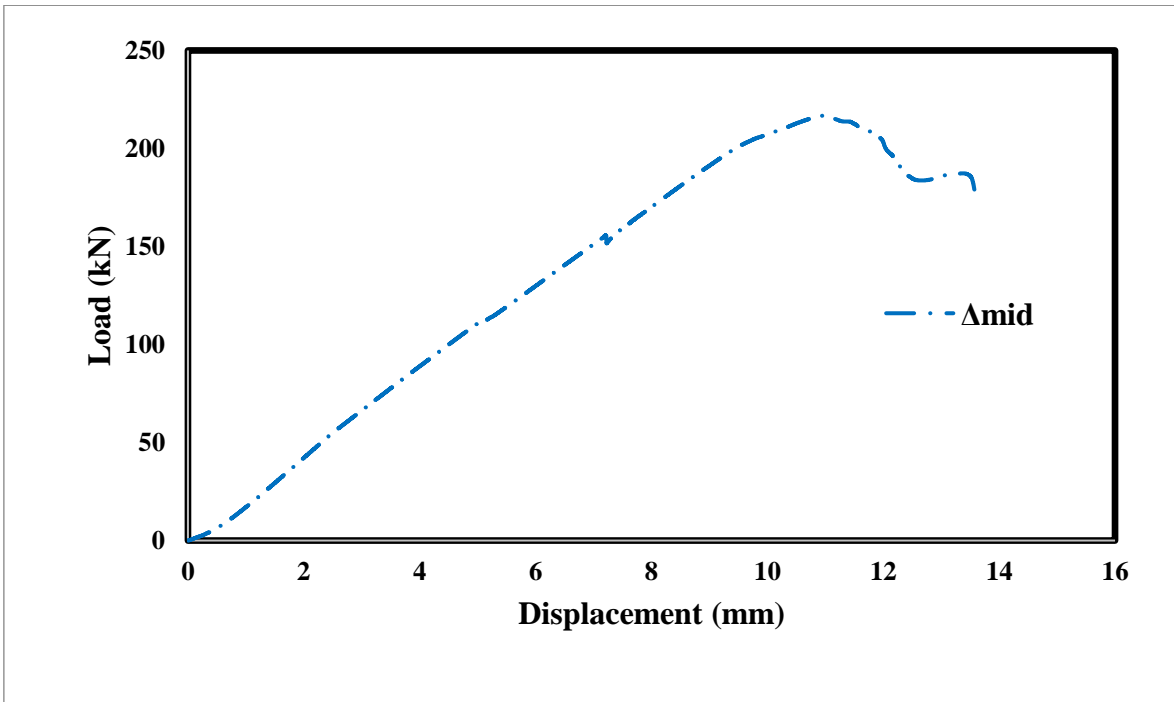


Figure 4.6. GPC – NA – 0.50 load-displacement graph

GPC – NA – 0.50 showed a brittle behavior, and in addition, it showed a limited or no post-yield response behavior. Shear cracks were observed in the geopolymer beam as expected during the experiment. Flexure cracks were also observed, but they were not propagated.

The moment-curvature curves were not ideal for examining the behavior of the specimen because inclined cracks formed between the load application point and the support, but the change in the curvature response over the beam was also provided for the sake of completeness.

### **Recycle Aggregate Flexural-Critical Geopolymer Beam 2 (GPC – NA – 1.00)**

During the experiment, firstly, shear cracks were performed, then bending cracks were observed. After that, shear cracks and flexure cracks were propagated until the final stage. Finally, shear cracks dominated, and the beam failed suddenly.

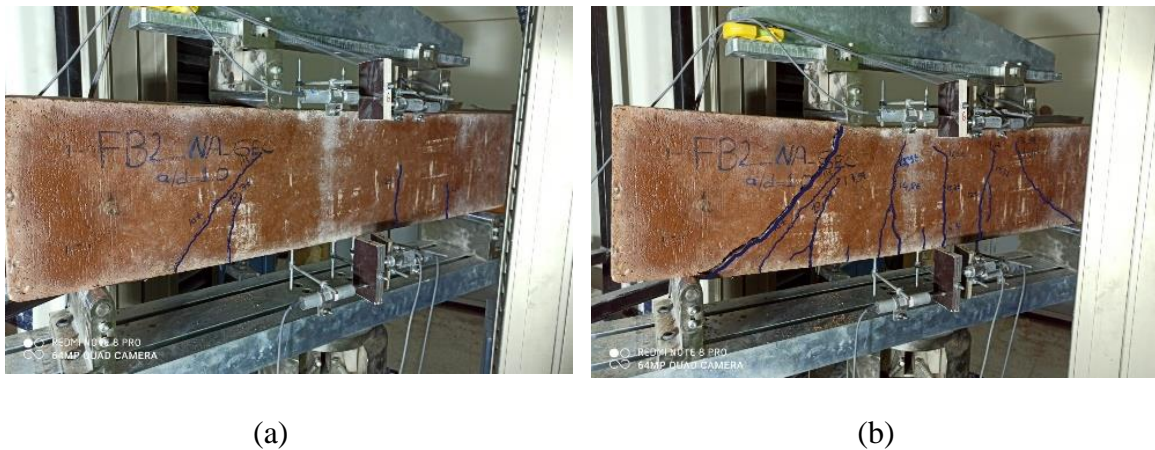


Figure 4.7. GPC – NA – 1.00 beam, (a) first cracks, (b) failure



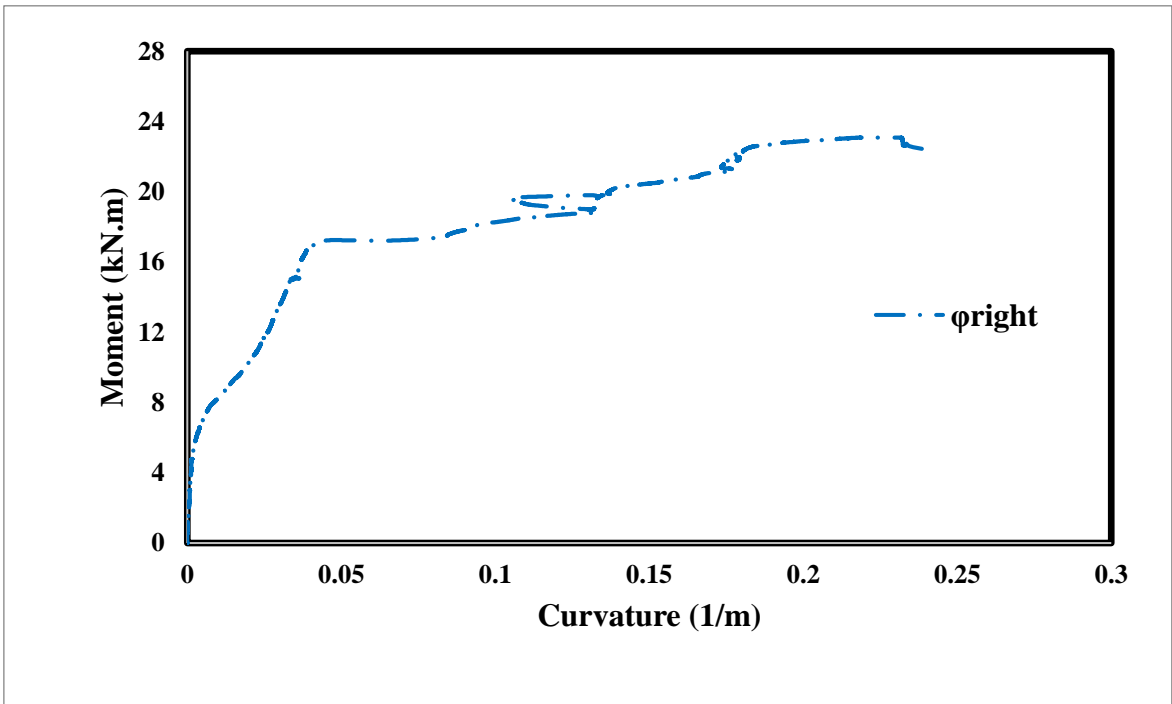
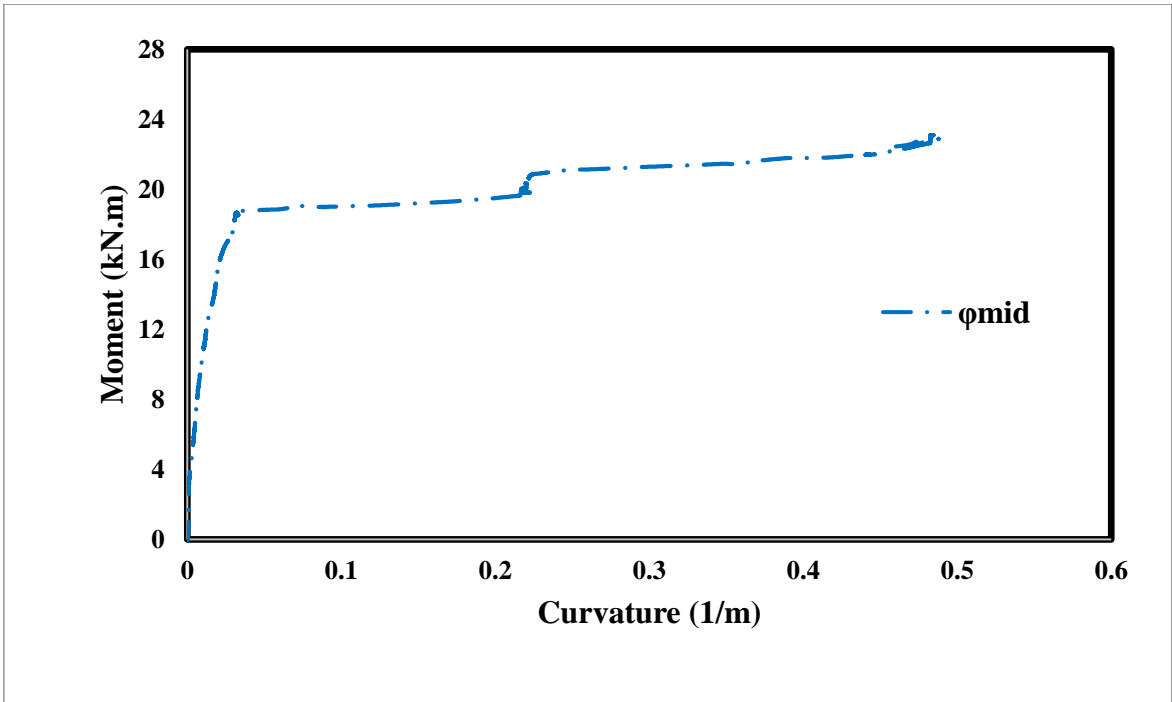


Figure 4.9. GPC – NA – 1.00 moment-curvature graphs

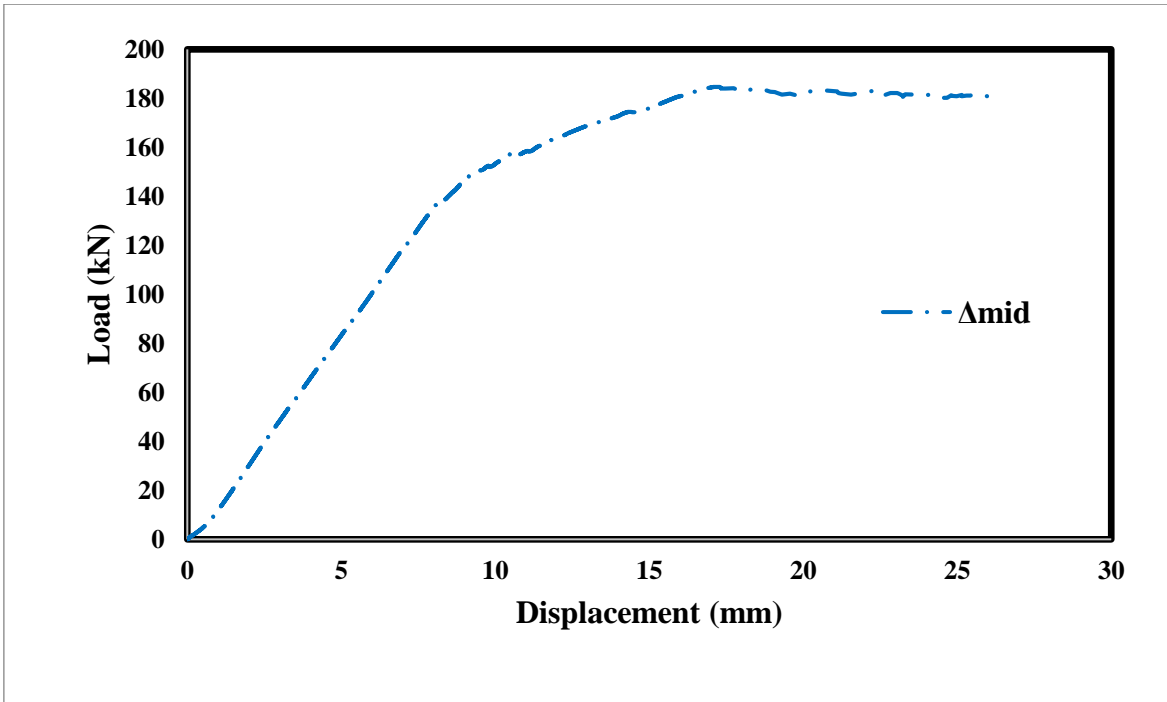


Figure 4.10. GPC – NA – 1.00 load-displacement graph

GPC – NA – 1.00 showed a flexure dominant behavior, namely, moment-curvature graphs showed post-yield response behavior. Shear cracks were observed in the geopolymer beam as expected during the experiment. Also, the full height of flexure cracks was observed as expected. Due to flexure dominant behavior of the specimen, the moment-curvature curves examined the behavior of reinforced concrete specimens in this case.

### Recycle Aggregate Flexural-Critical Geopolymer Beam 3 (GPC – NA – 1.65)

During the experiment, flexure dominant behavior was observed. Although some shear cracks were also observed, these micro-cracks not propagated fully.



(a)

(b)

Figure 4.11. GPC – NA – 1.65 beam, (a) first cracks, (b) failure



Figure 4.12. GPC – NA – 1.65 beam crushing

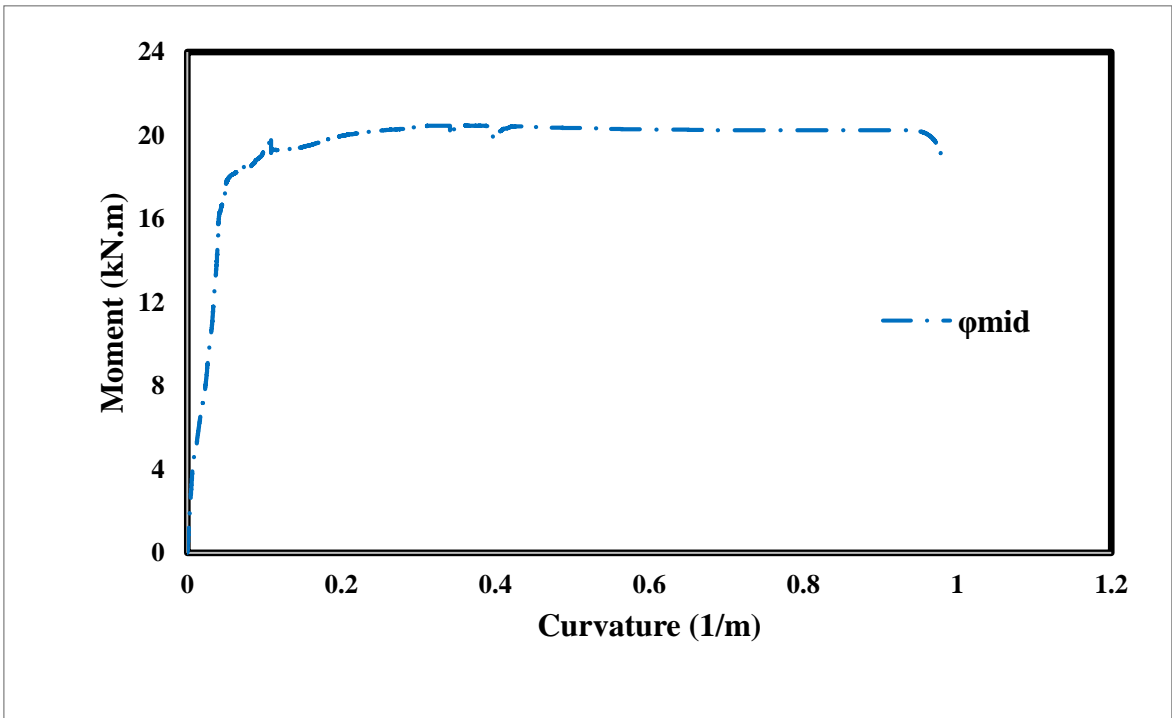
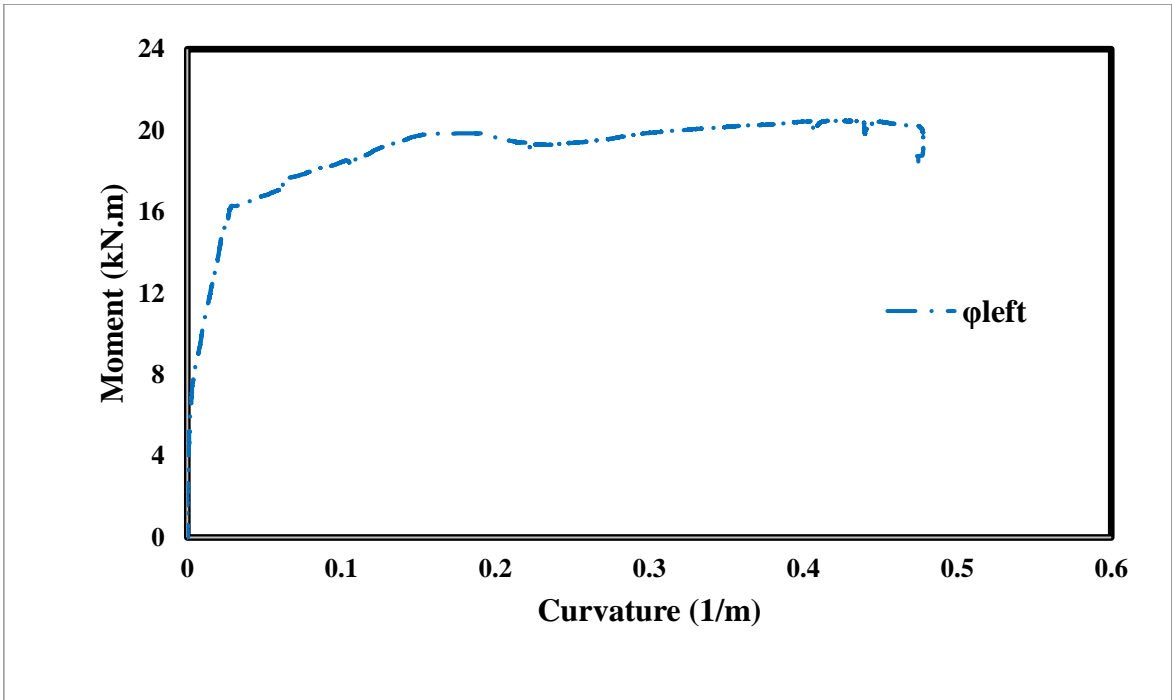


Figure 4.13. GPC – NA – 1.65 moment-curvature graphs(continued)



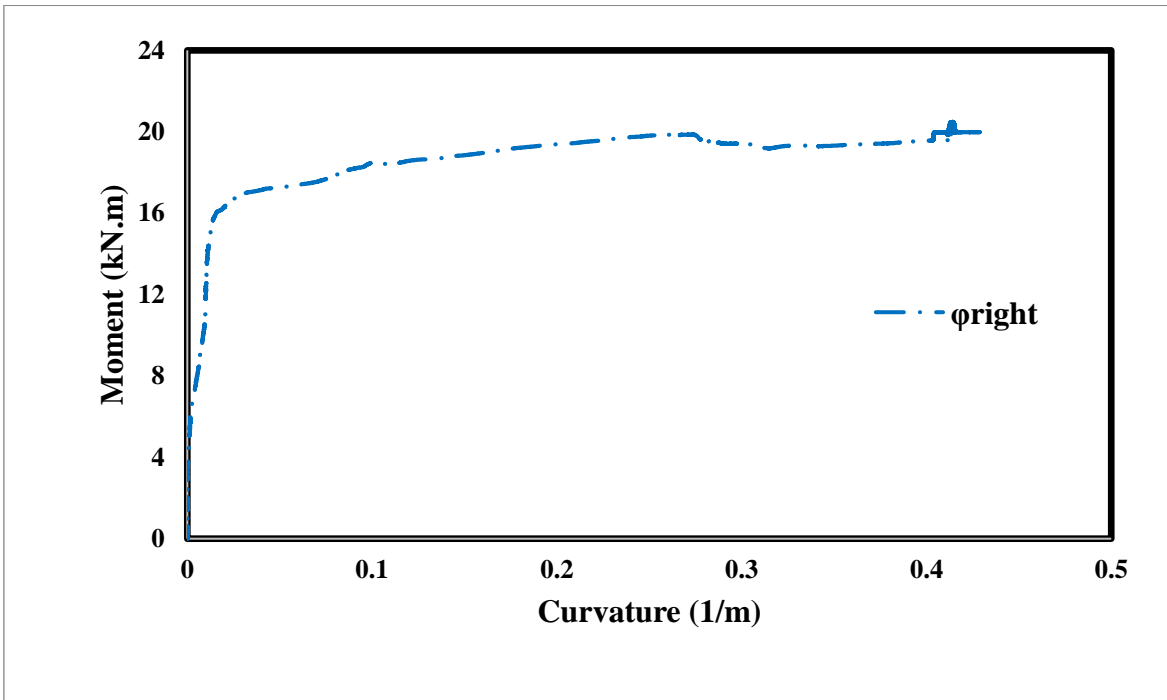


Figure 4.13. GPC – NA – 1.65 moment-curvature graphs

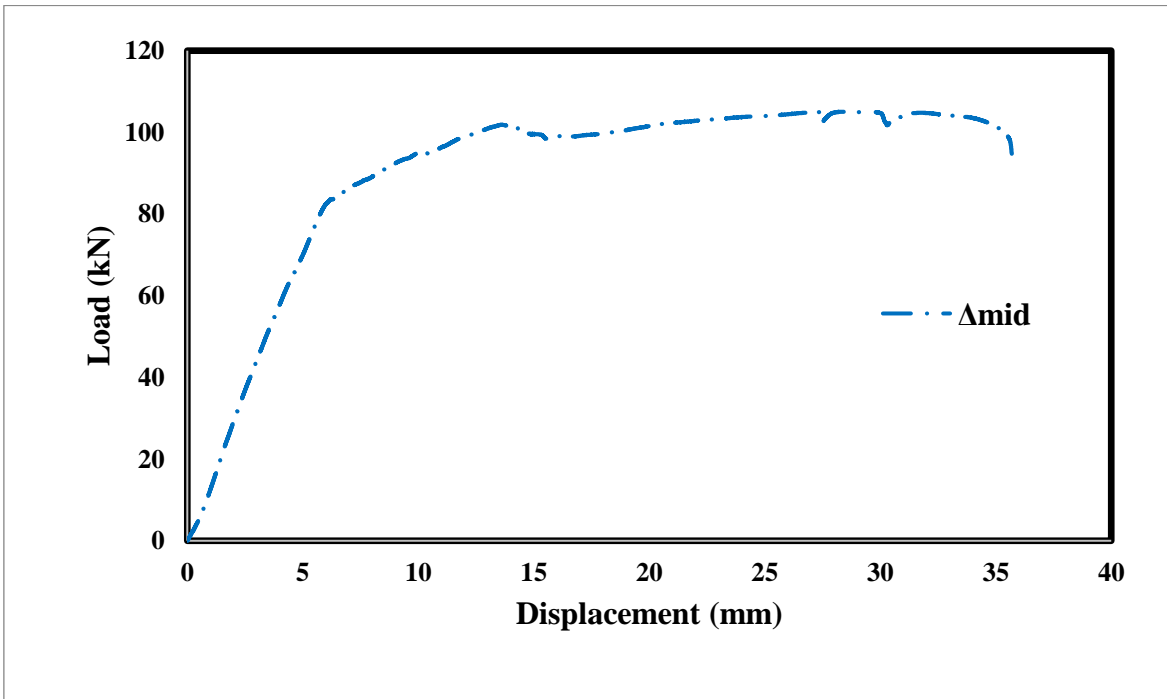


Figure 4.14. GPC – NA – 1.65 load-displacement graph

GPC – NA – 1.65 also showed a flexure dominant behavior; namely, moment-curvature graphs showed post-yield response behavior. Some micro shear cracks were observed in the

geopolymer beam as expected during the experiment. Also, the full height of flexure cracks was observed as expected. Due to flexure dominant behavior of the specimen, the moment-curvature curves examined the behavior of reinforced concrete specimens in this case.

### Recycle Aggregate Flexural-Critical Geopolymer Beam 1 (GPC – RA – 0.50)

In this test, crack propagation was similar to GPC – NA – 0.50.



Figure 4.15. GPC – RA – 0.50 beam, (a) first cracks, (b) failure

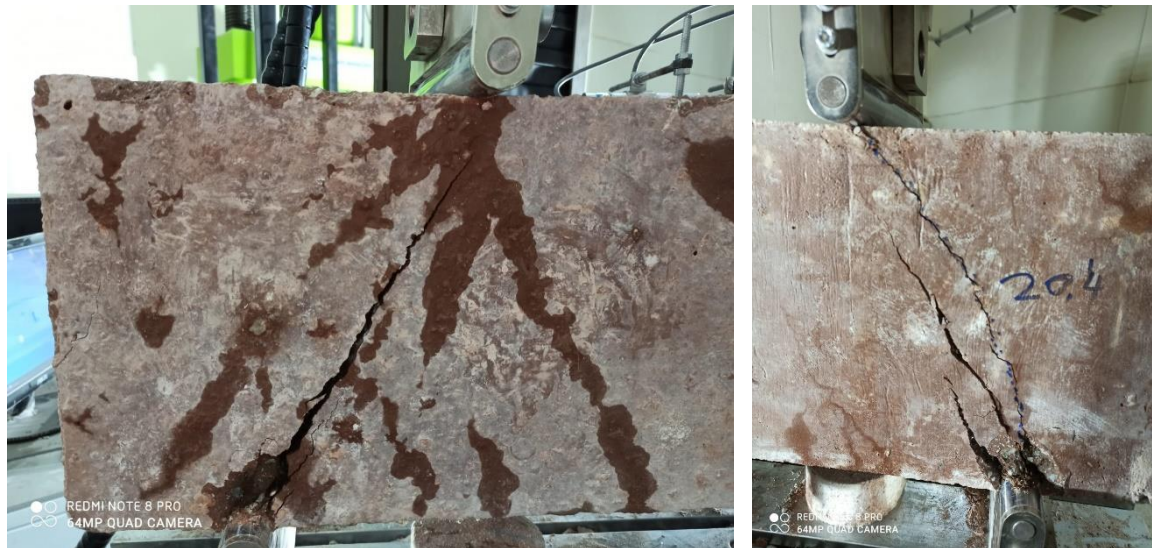


Figure 4.16. GPC – RA – 0.50 shear crack

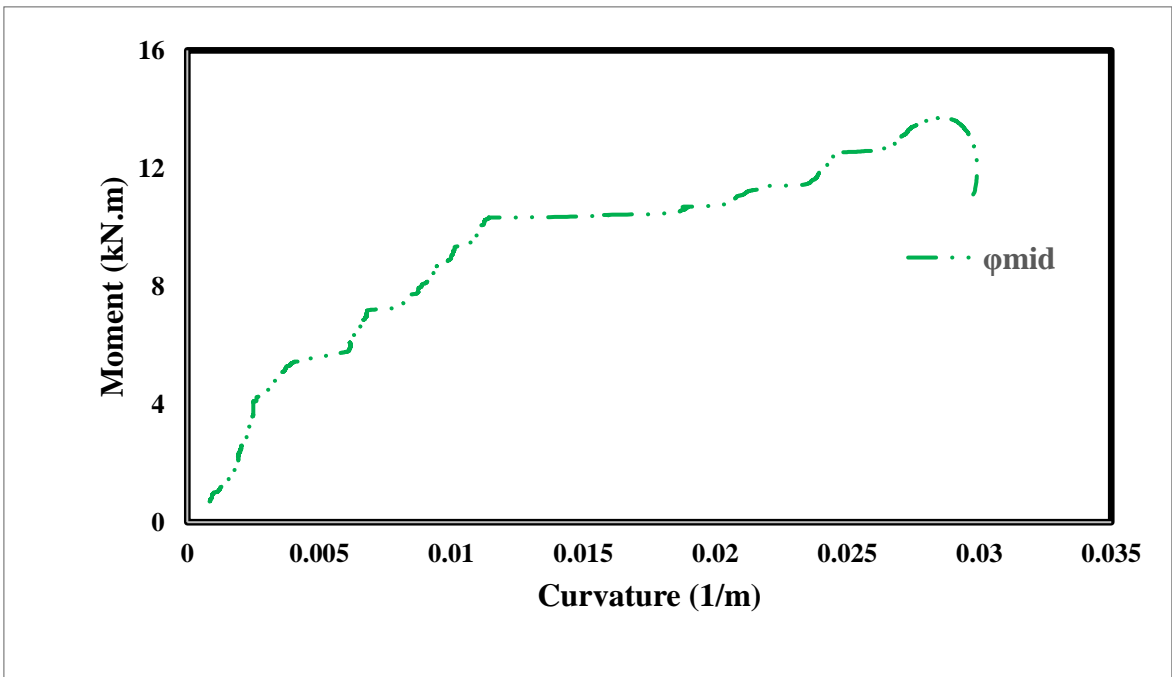
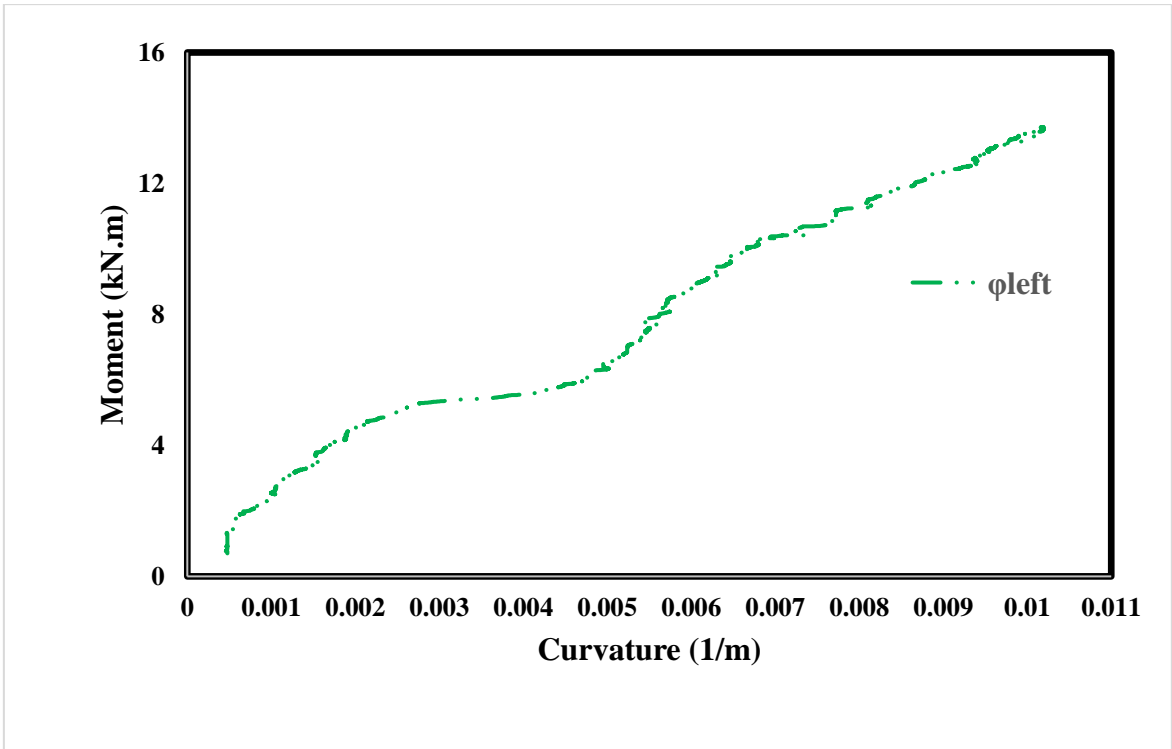


Figure 4.17. GPC – RA – 0.50 moment-curvature graphs(continued)

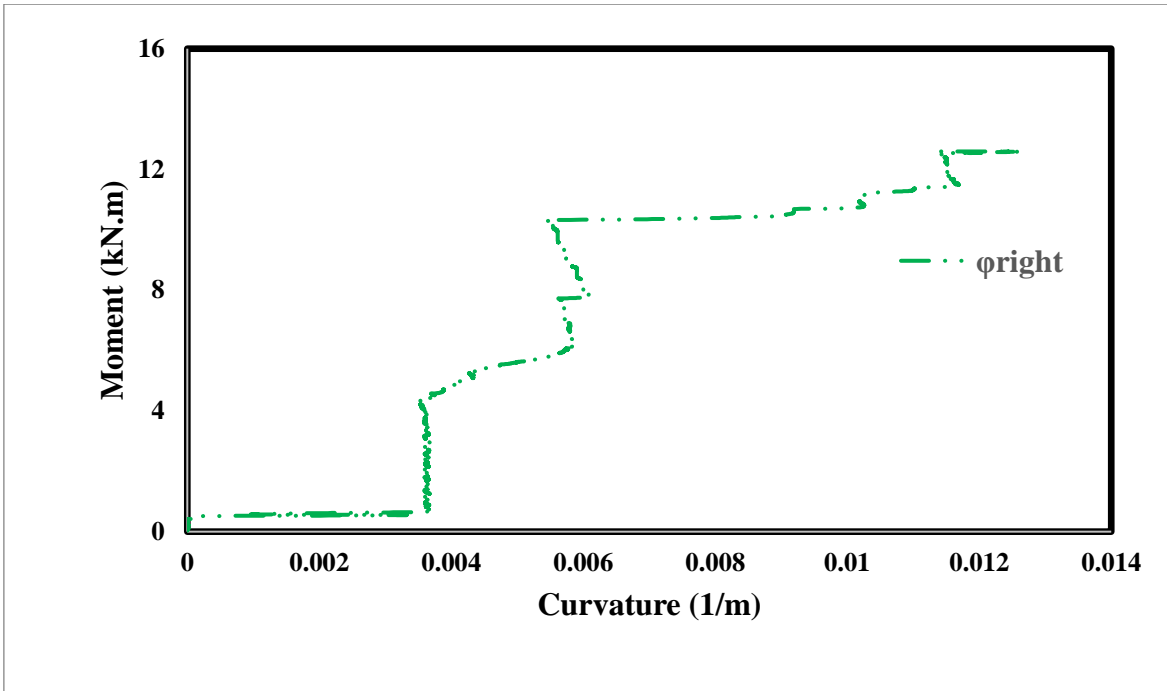


Figure 4.17. GPC – RA – 0.50 moment-curvature graphs

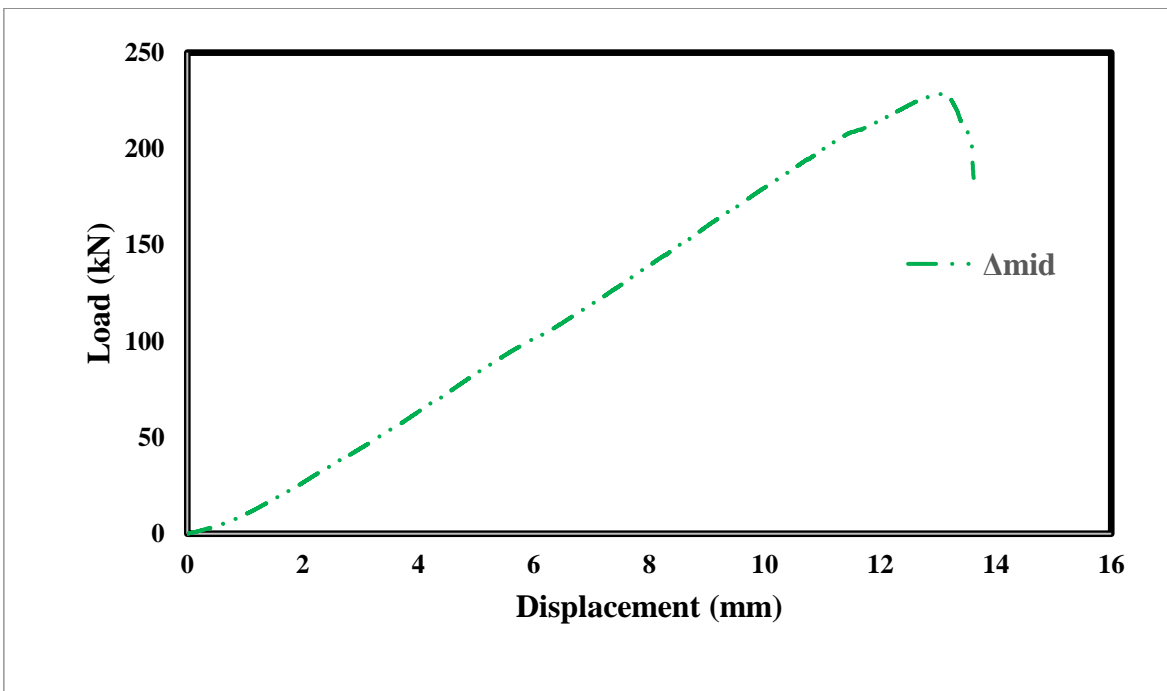


Figure 4.18. GPC – RA – 0.50 load-displacement graph

The moment-curvature curves were not ideal for examining the behavior of reinforced concrete specimens because inclined cracks formed between the load application point and

the support, but the change in the curvature response over the beam was also provided for the sake of completeness.

### Recycle Aggregate Flexural-Critical Geopolymer Beam 2 (GPC – RA – 1.00)

In this test, crack propagation was similar to GPC – NA – 1.00. In addition, except the right side of the beam was not deformed appropriately. Right support shear crack dissipated a large part of the energy.

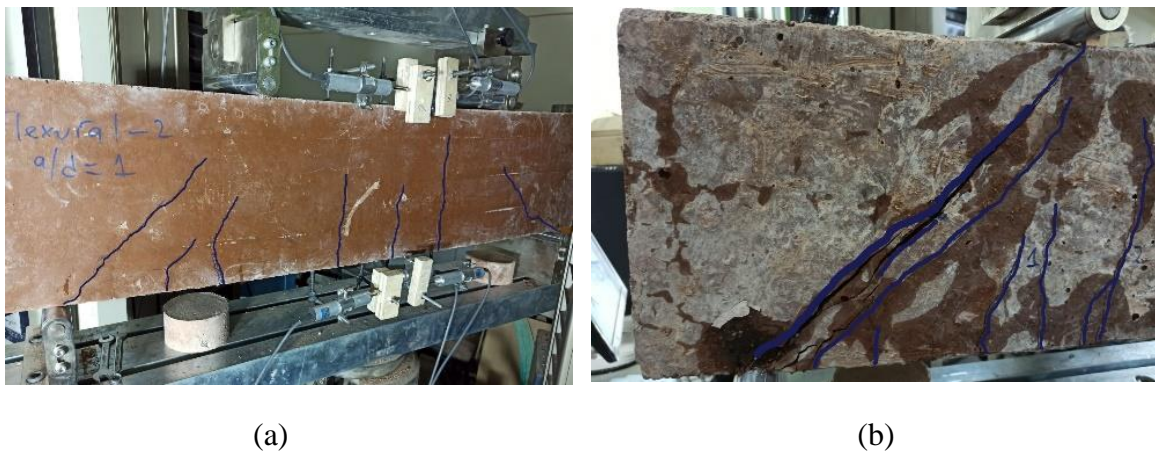


Figure 4.19. GPC – RA – 1.00 beam, (a) first cracks, (b) failure

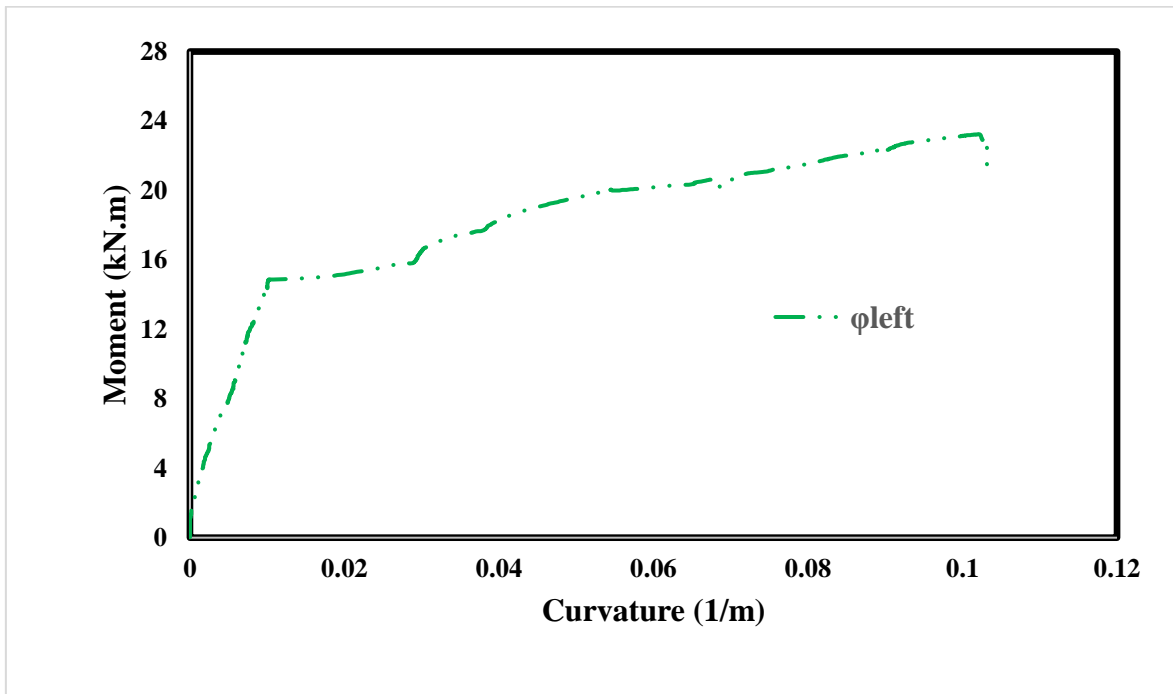


Figure 4.20. GPC – RA – 1.00 moment-curvature graphs(continued)

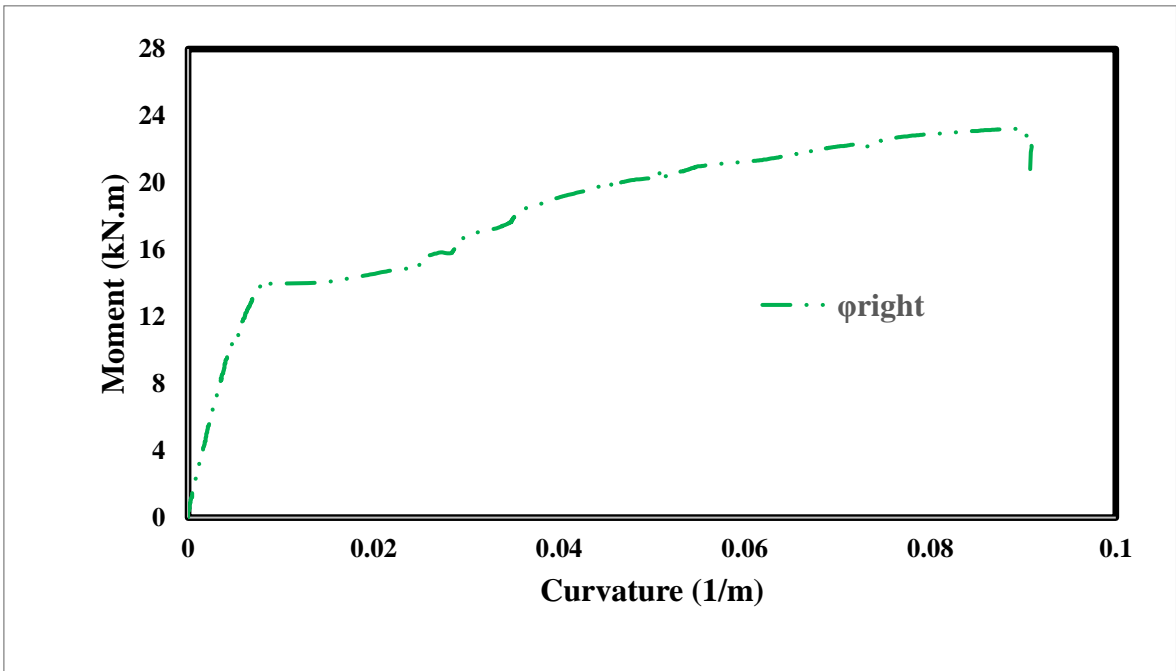
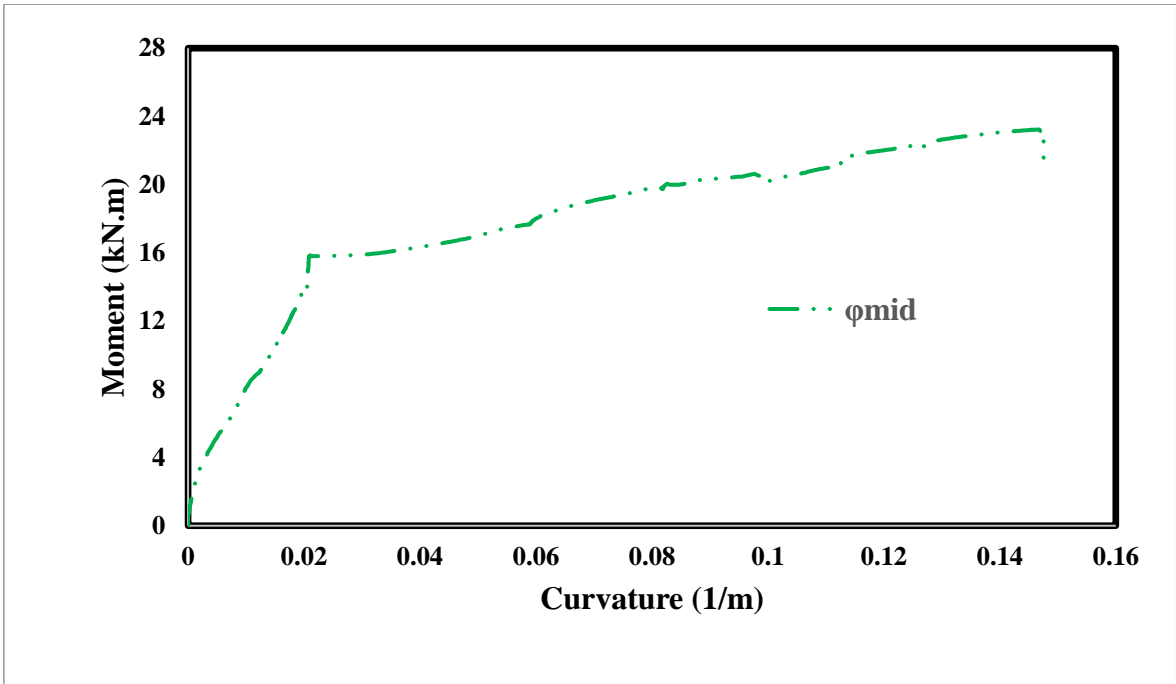


Figure 4.20. GPC – RA – 1.00 moment-curvature graphs

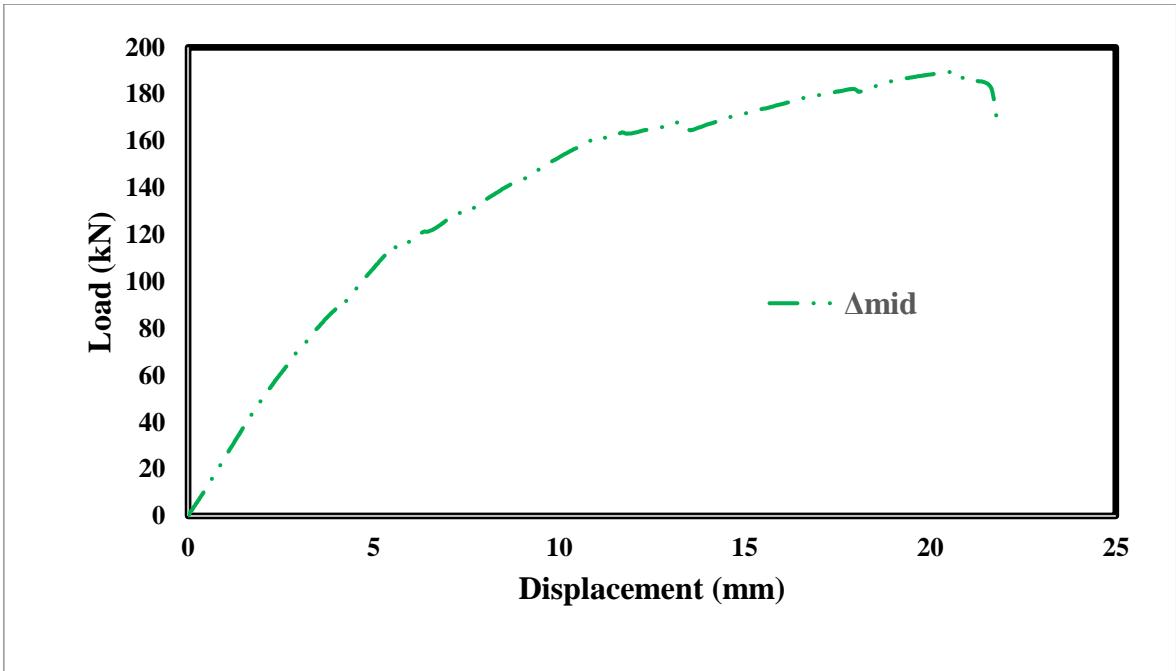


Figure 4.21. GPC – RA – 1.00 load-displacement graph

GPC – RA – 1.00 graphs also showed similar behavior to GPC – NA – 1.00.

**Recycle Aggregate Flexural-Critical Geopolymer Beam 3 (GPC – RA – 1.65)**

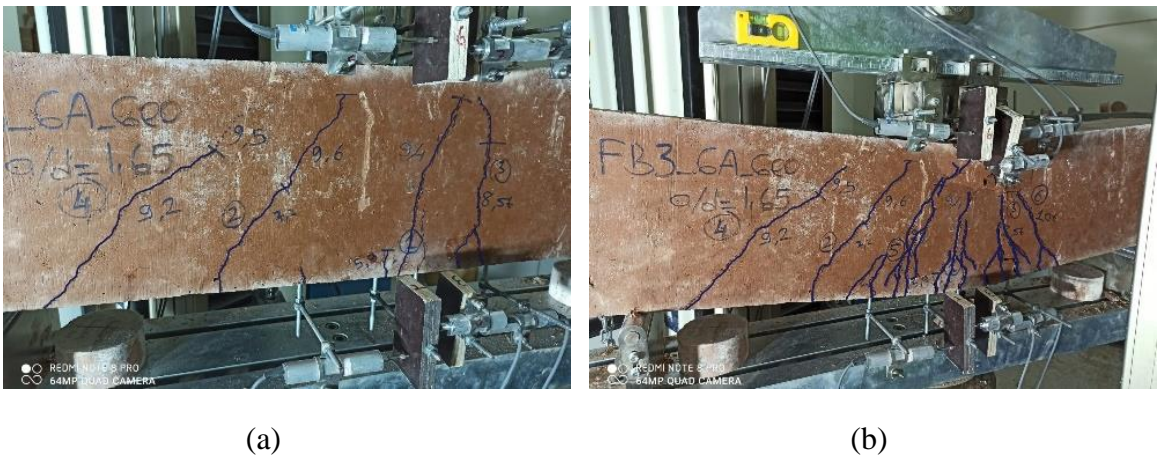


Figure 4.22. GPC – RA – 1.65 beam, (a) first cracks, (b) failure



Figure 4.23. GPC – RA – 1.65 buckling of reinforcement bar and crushing of geopolymer

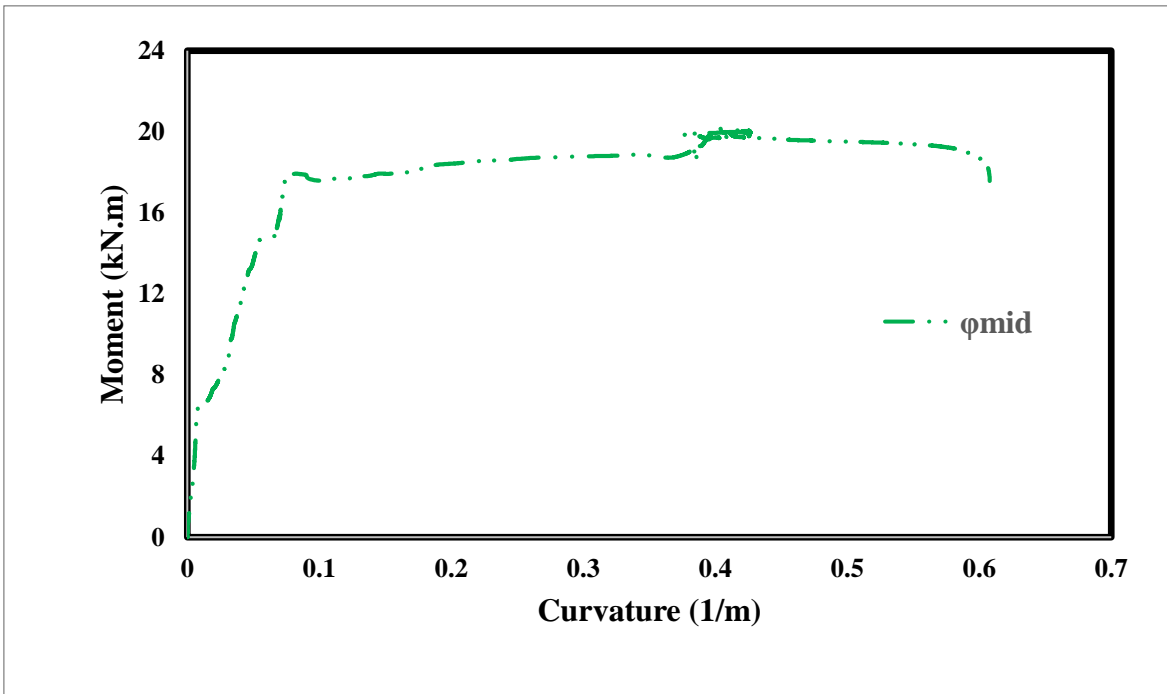


Figure 4.24. GPC – RA – 1.65 moment-curvature graphs(continued)



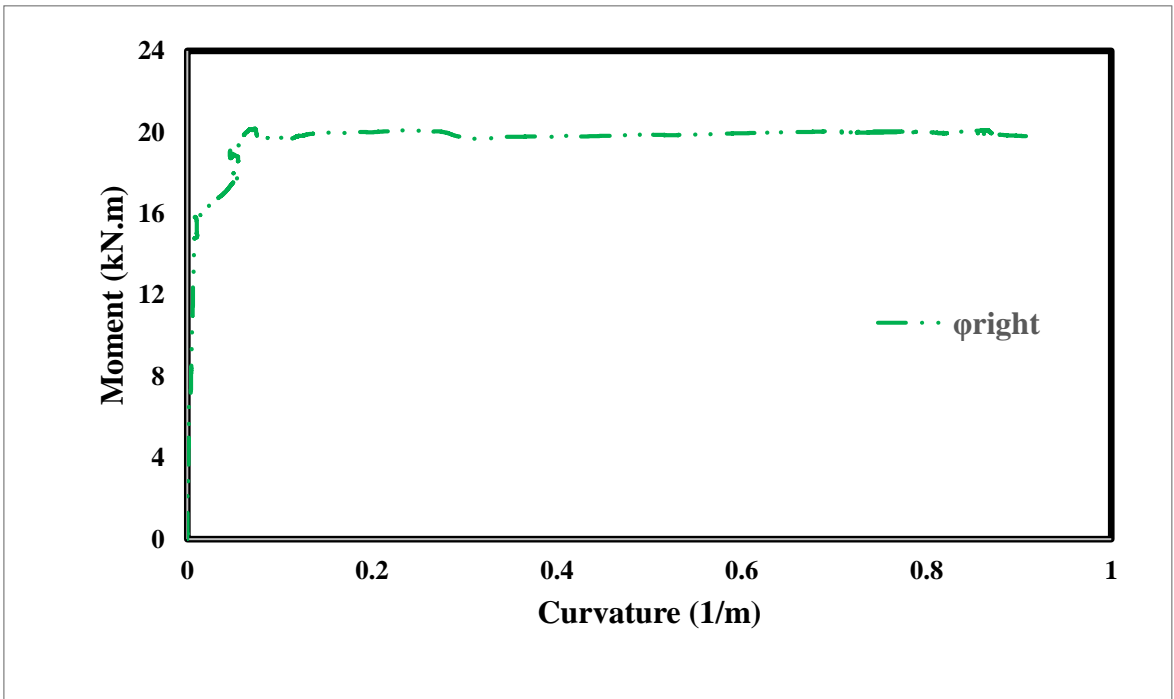
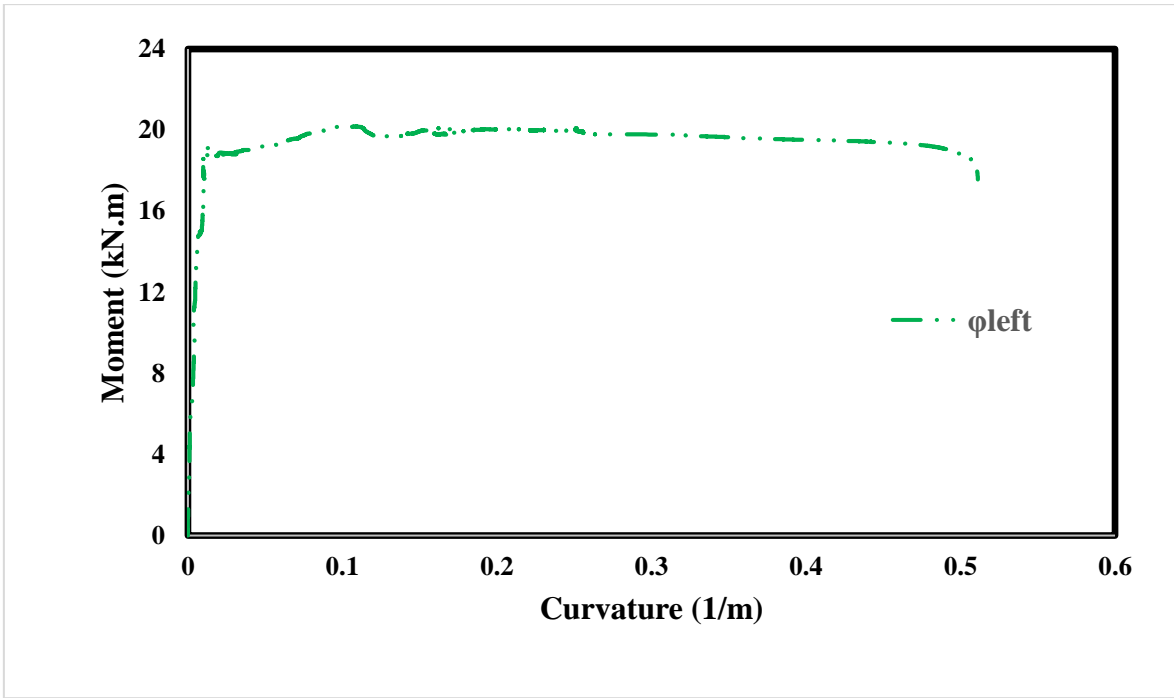


Figure 4.24. GPC – RA – 1.65 moment-curvature graphs

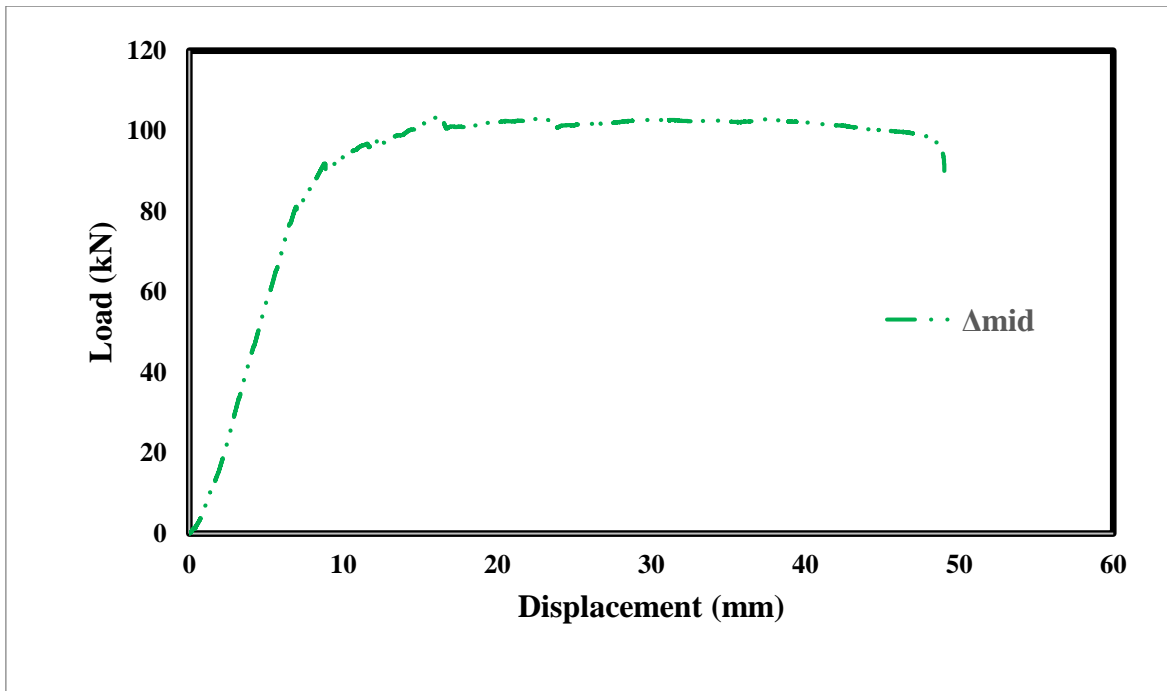


Figure 4.25. GPC – RA – 1.65 load-displacement graph

#### 4.4. Conventional Concrete Beams

In this part of the study, similar compressive strength conventional concrete beam samples were produced to compare mechanical properties of them under four points bending beam test. As a result of the test, moment-curvature and load-displacement graphs of the beams were obtained.

##### **Normal Aggregate Flexural-Critical Conventional Concrete Beam 1 (CVC – NA – 0.50)**

In this test, crack propagation and failure type were similar to geopolymer beam with the same  $a/d$  ratio. Contrary to the geopolymer beam, the left shear crack of the beam gave rise to failure.



Figure 4.26. CVC – NA – 0.50 beam, (a) first cracks, (b) failure



Figure 4.27. CVC – NA – 0.50 failure crack propagation

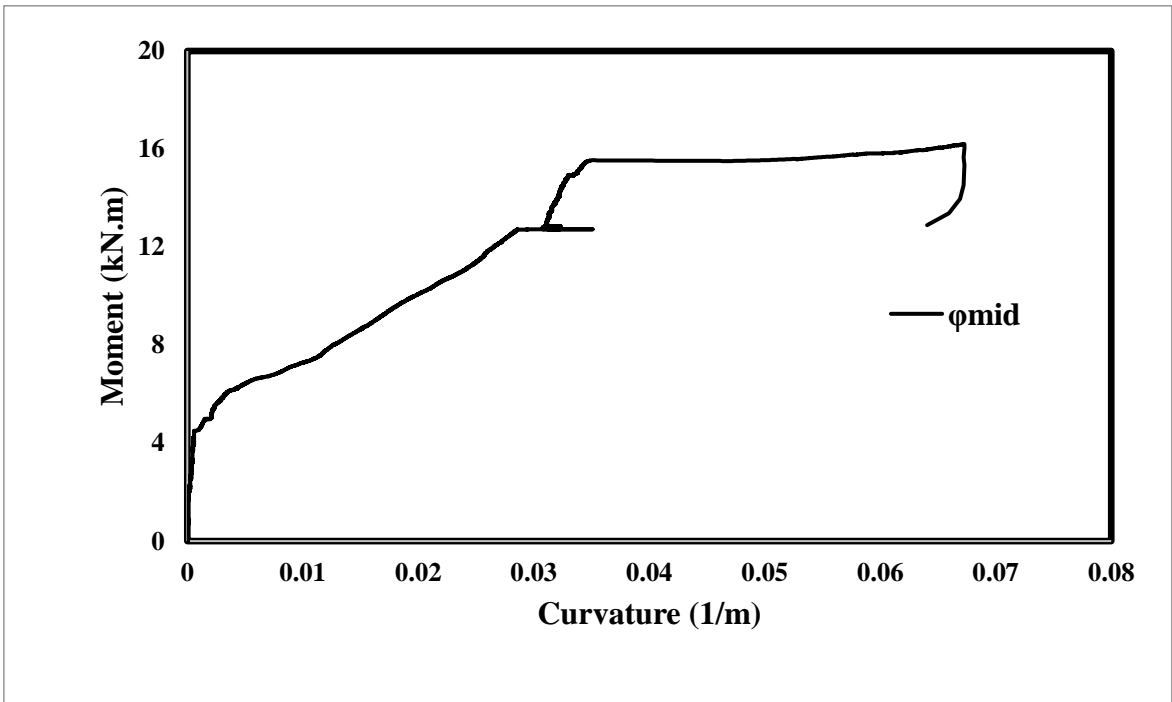
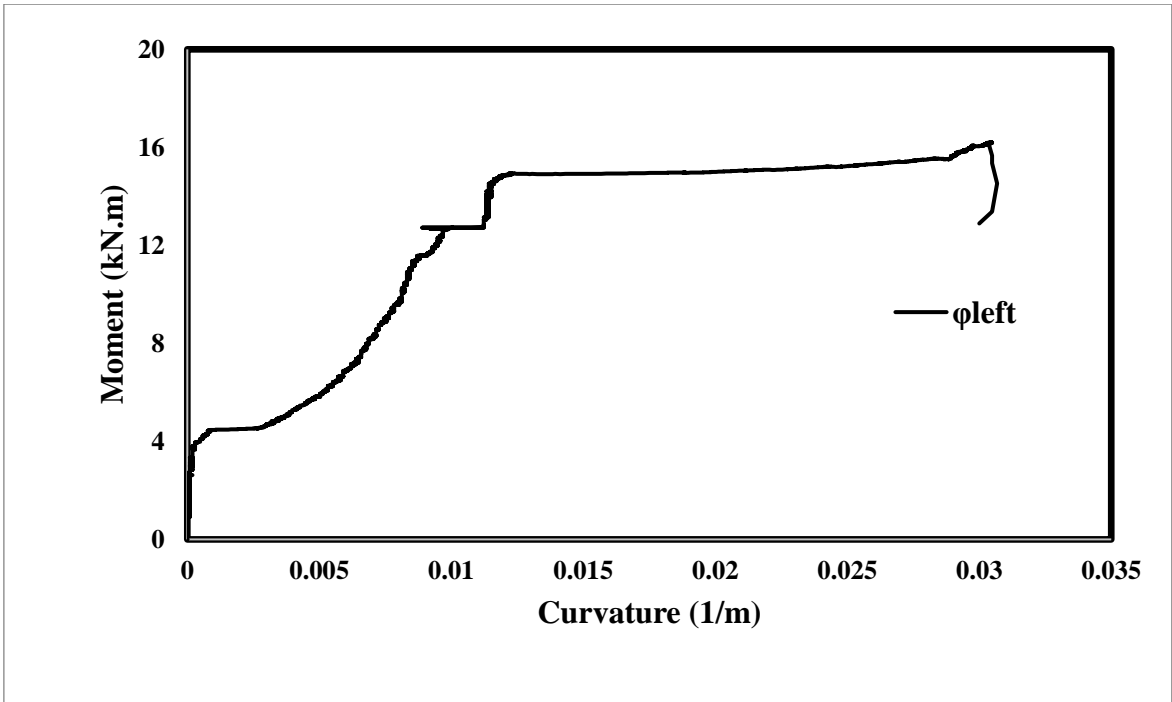


Figure 4.28. CVC – NA – 0.50 moment-curvature graphs(continued)

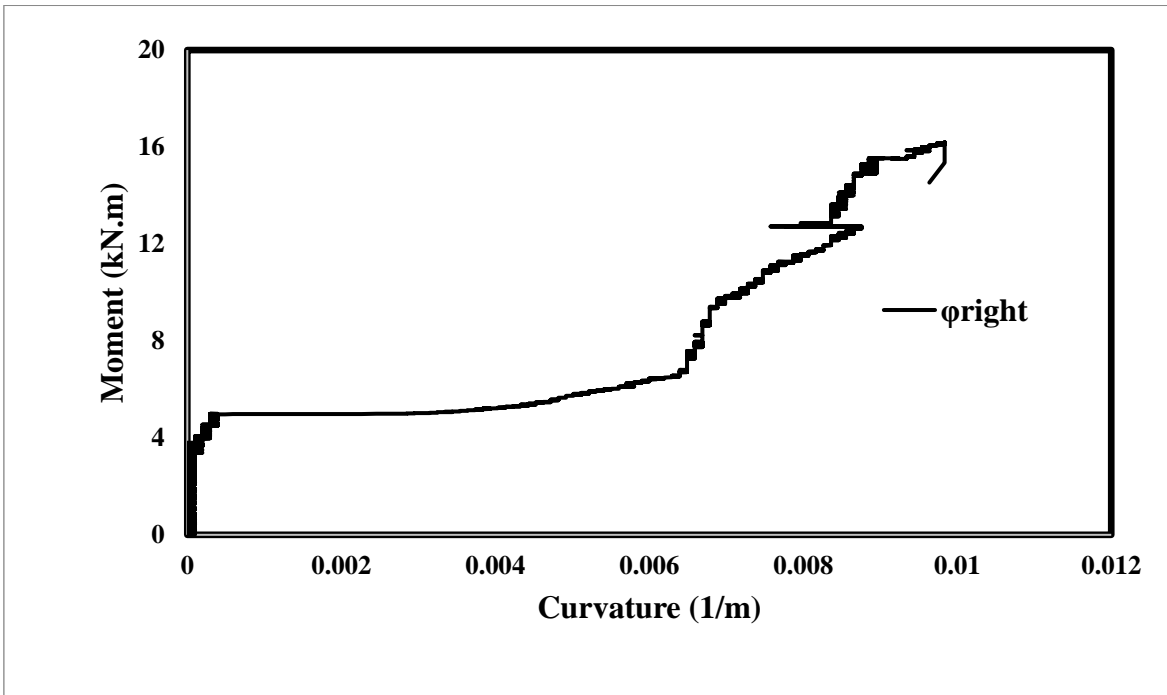


Figure 4.28. CVC – NA – 0.50 moment-curvature graphs

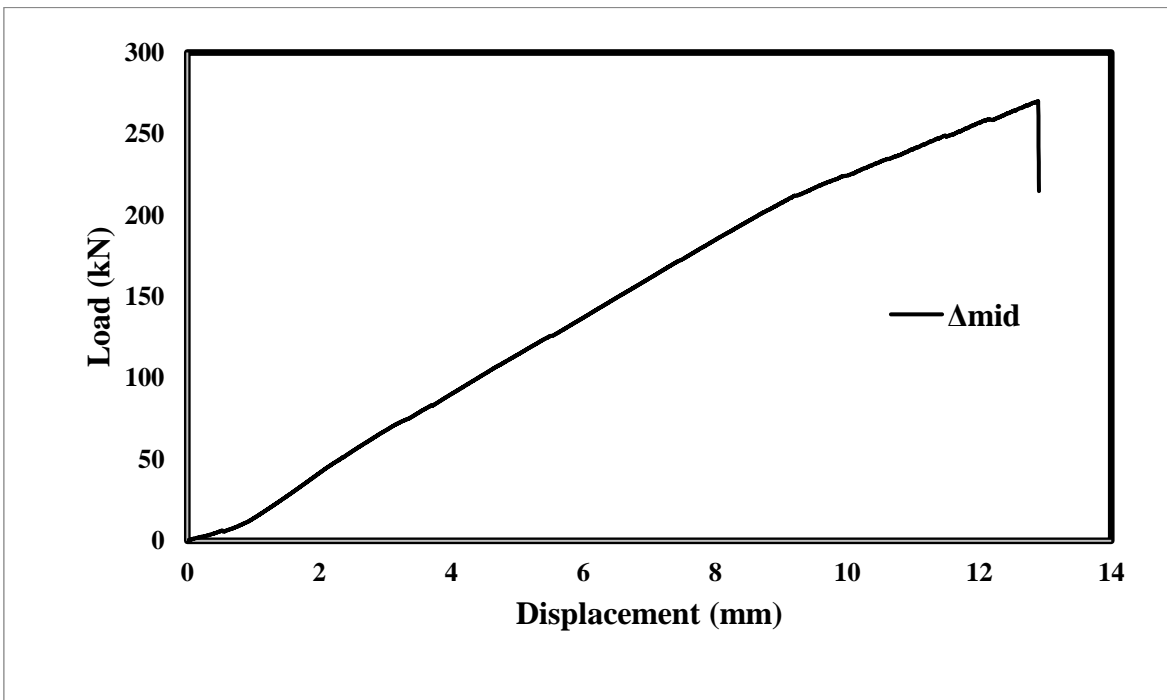


Figure 4.29. CVC – NA – 0.50 load-displacement graph

### Normal Aggregate Flexural-Critical Conventional Concrete Beam 2 (CVC – NA – 1.00)

In this test, crack propagation of the beam was similar to the geopolymer beams with same  $a/d$  ratio.



Figure 4.30. CVC – NA – 1.00 beam, (a) first cracks, (b) failure



Figure 4.31. CVC – NA – 1.00 shear dominant failure detailed picture

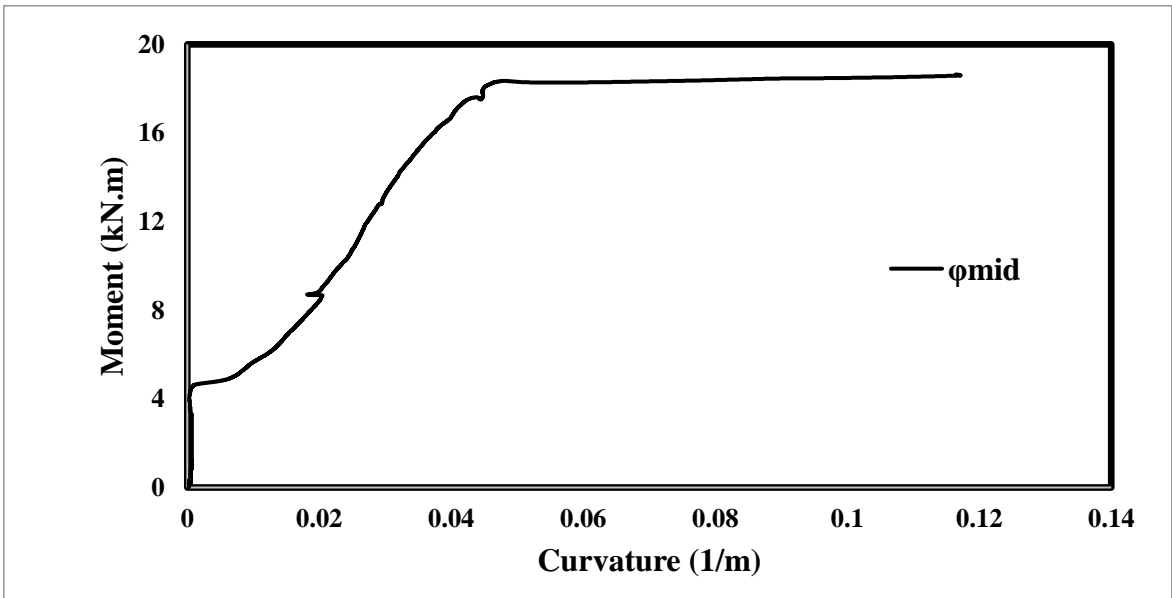
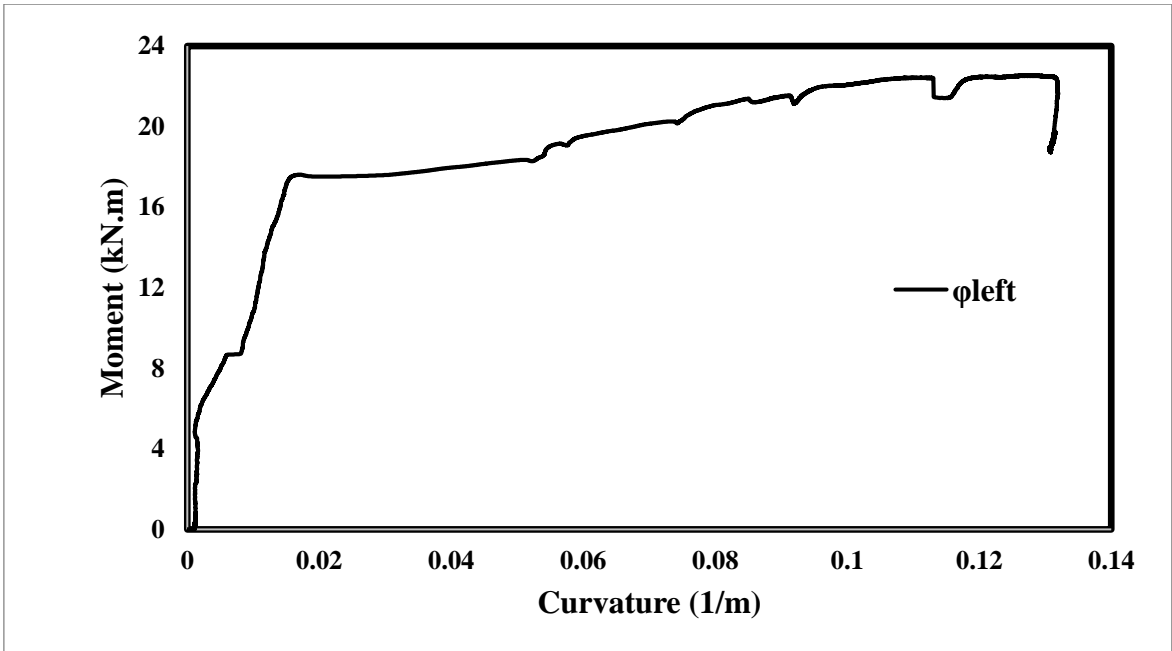


Figure 4.32. CVC – NA – 1.00 moment-curvature graphs(continued)

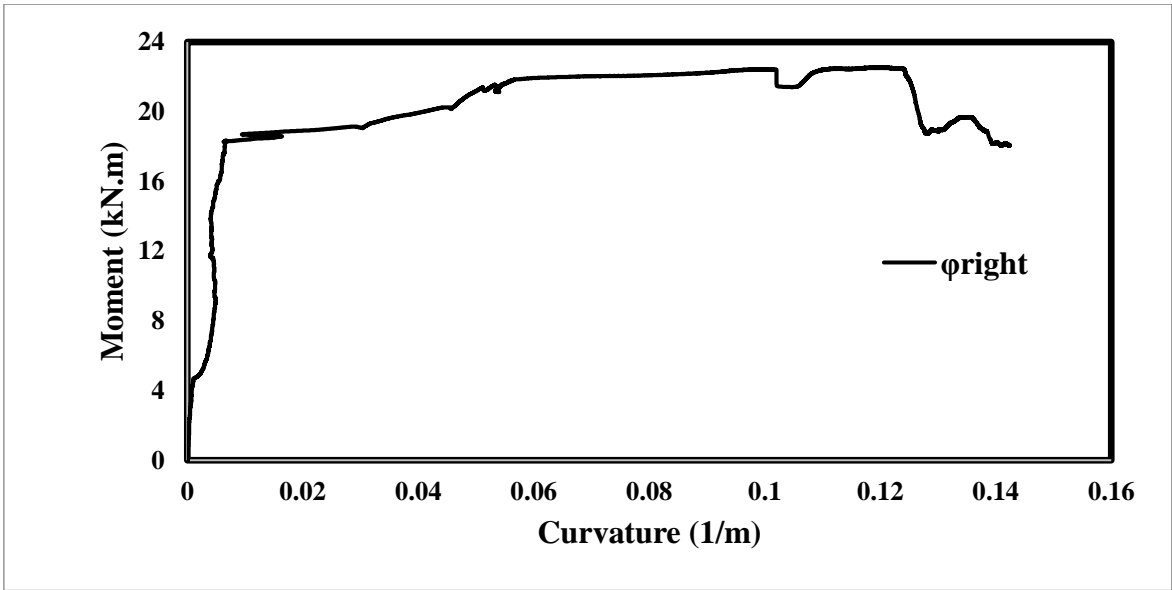


Figure 4.32. CVC – NA – 1.00 moment-curvature graphs

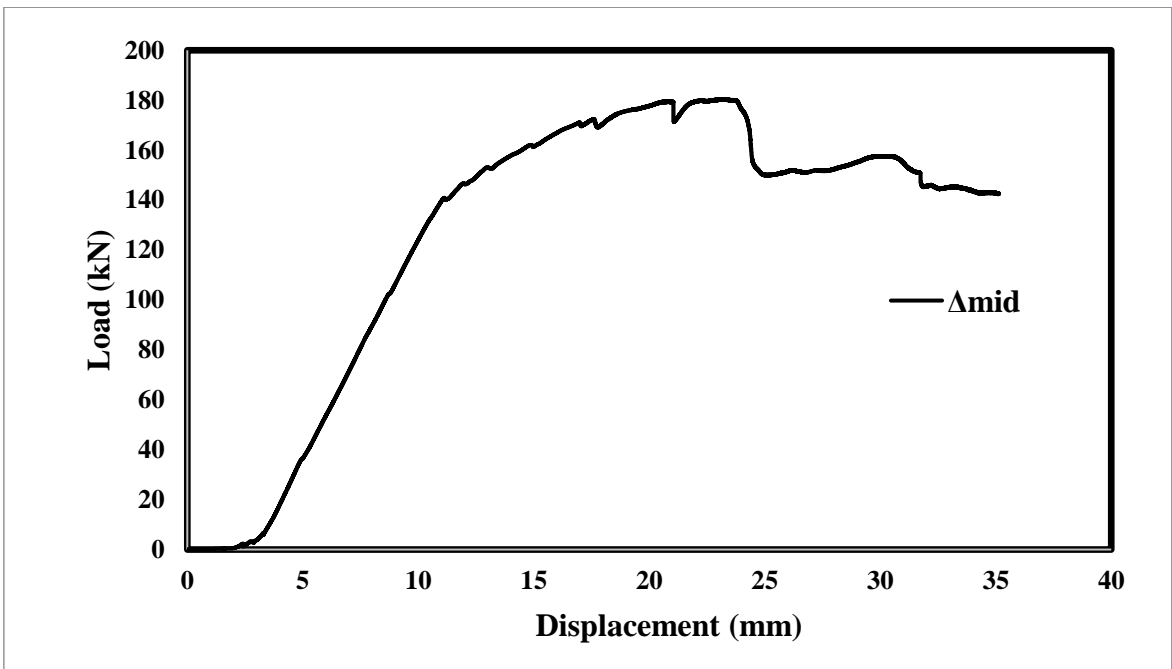


Figure 4.33. CVC – NA – 1.00 load-displacement graph



### Normal Aggregate Flexural-Critical Conventional Concrete Beam 3 (CVC – NA – 1.65)

In this test, crack propagation of the beam was similar to the geopolymer beams with the same  $a/d$  ratio.



Figure 4.34. CVC – NA – 1.65 beam, (a) first cracks, (b) failure



Figure 4.35. CVC – NA – 1.65 flexure dominant failure detailed picture

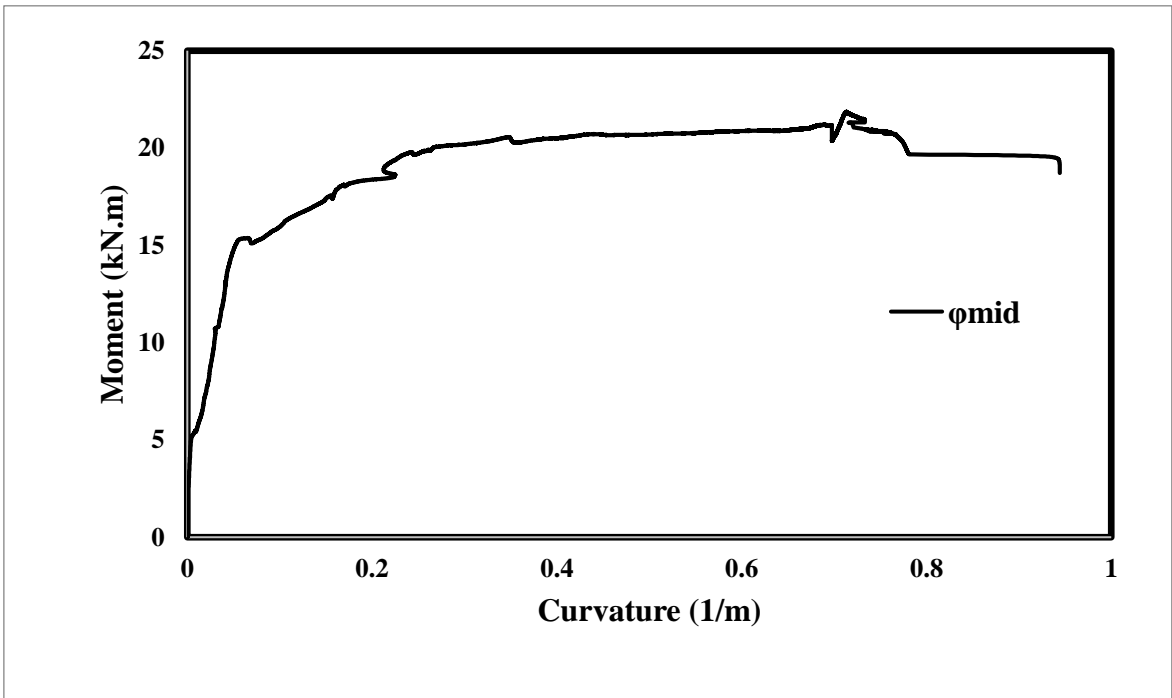
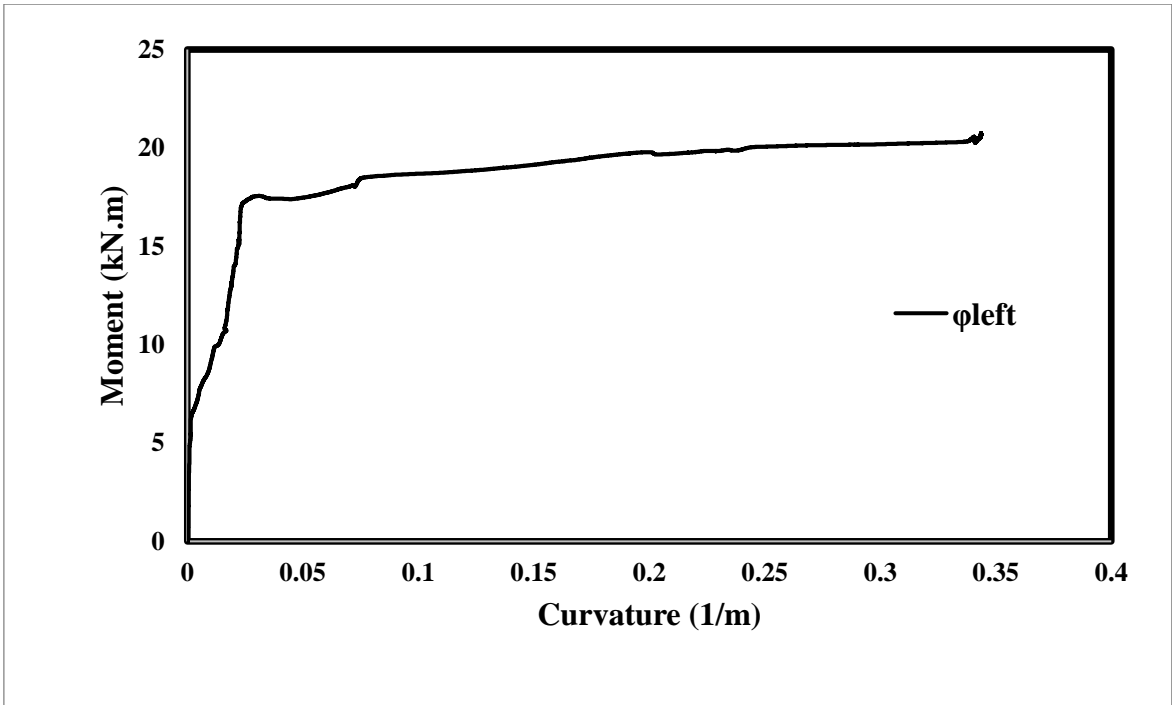


Figure 4.36. CVC – NA – 1.65 moment-curvature graphs(continued)

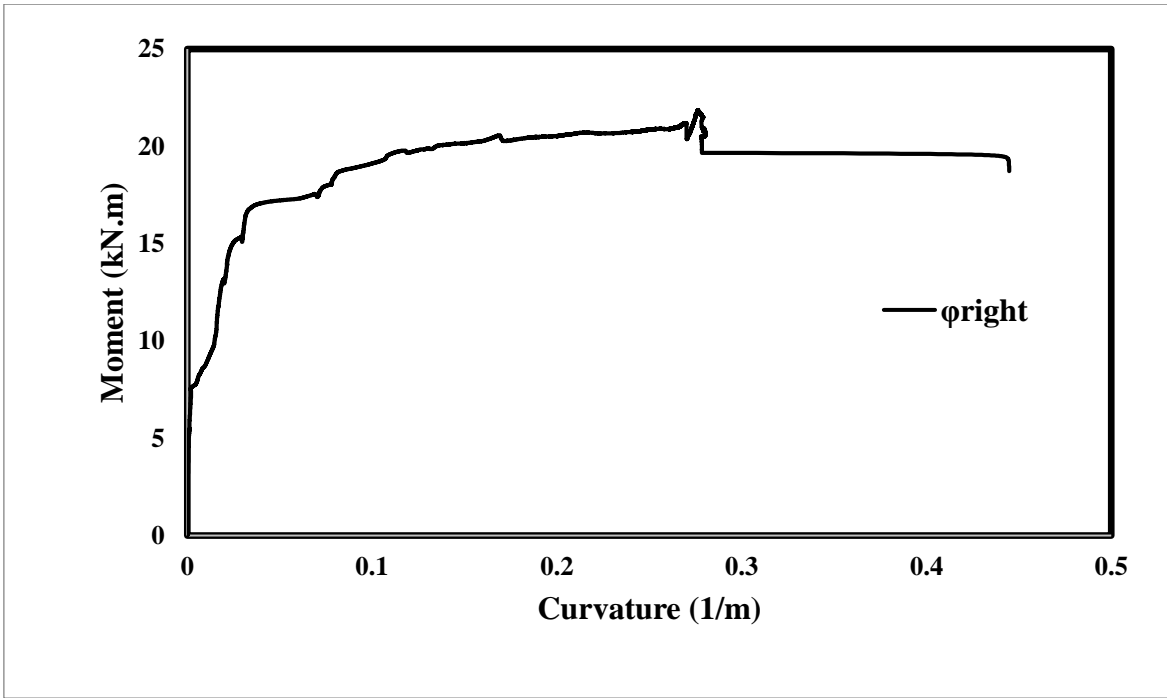


Figure 4.36. CVC – NA – 1.65 moment-curvature graphs

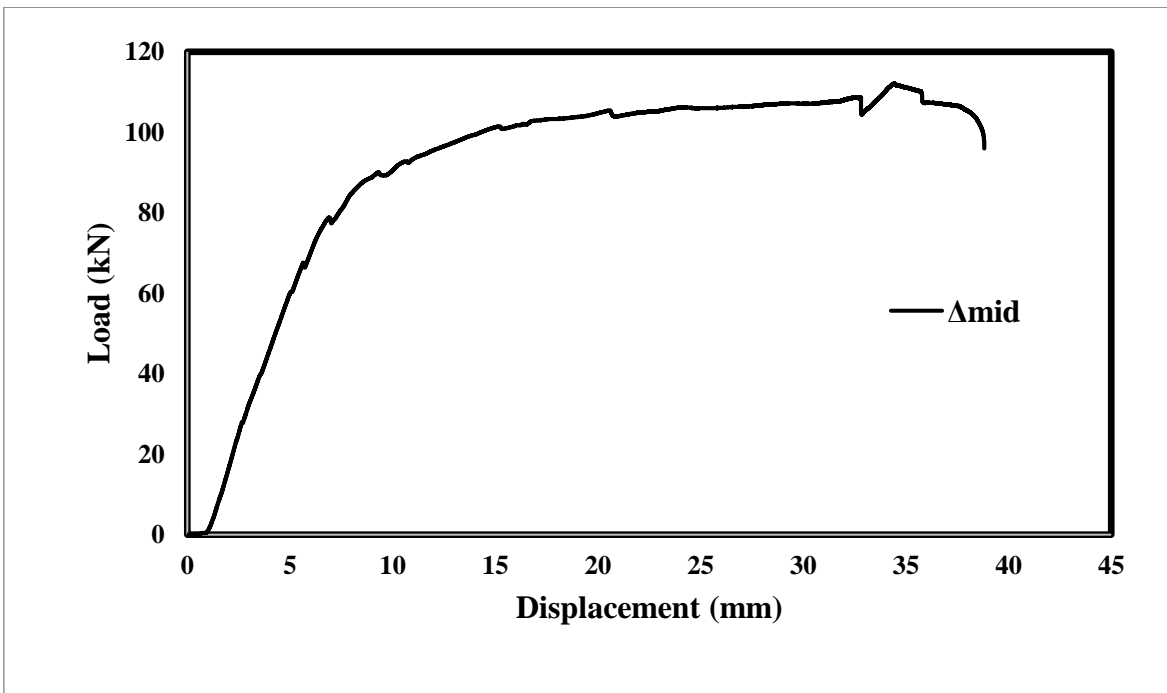


Figure 4.37. CVC – NA – 1.65 load-displacement graph

### Recycle Aggregate Flexural-Critical Conventional Concrete Beam 1 (CVC – RA – 0.50)

In this test, crack propagation of the beam was similar to the geopolymer beams with the same  $a/d$  ratio.



Figure 4.38. CVC – RA – 0.50 beam, (a) first cracks, (b) failure



Figure 4.39. CVC – RA – 0.50 shear dominant failure

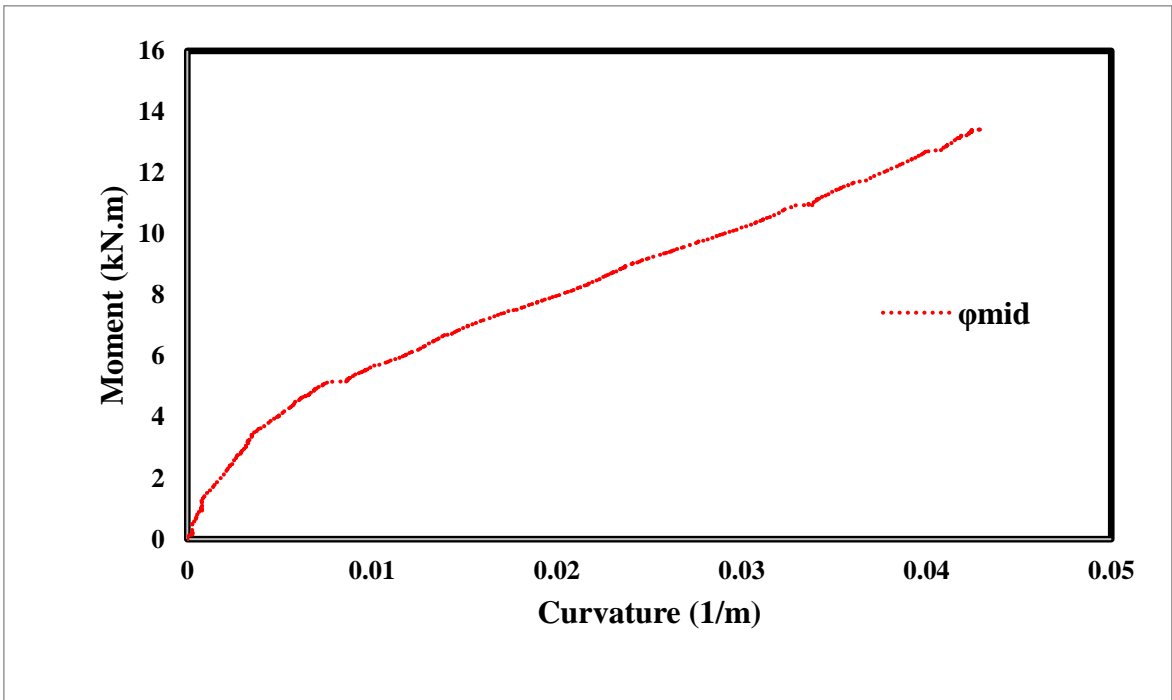
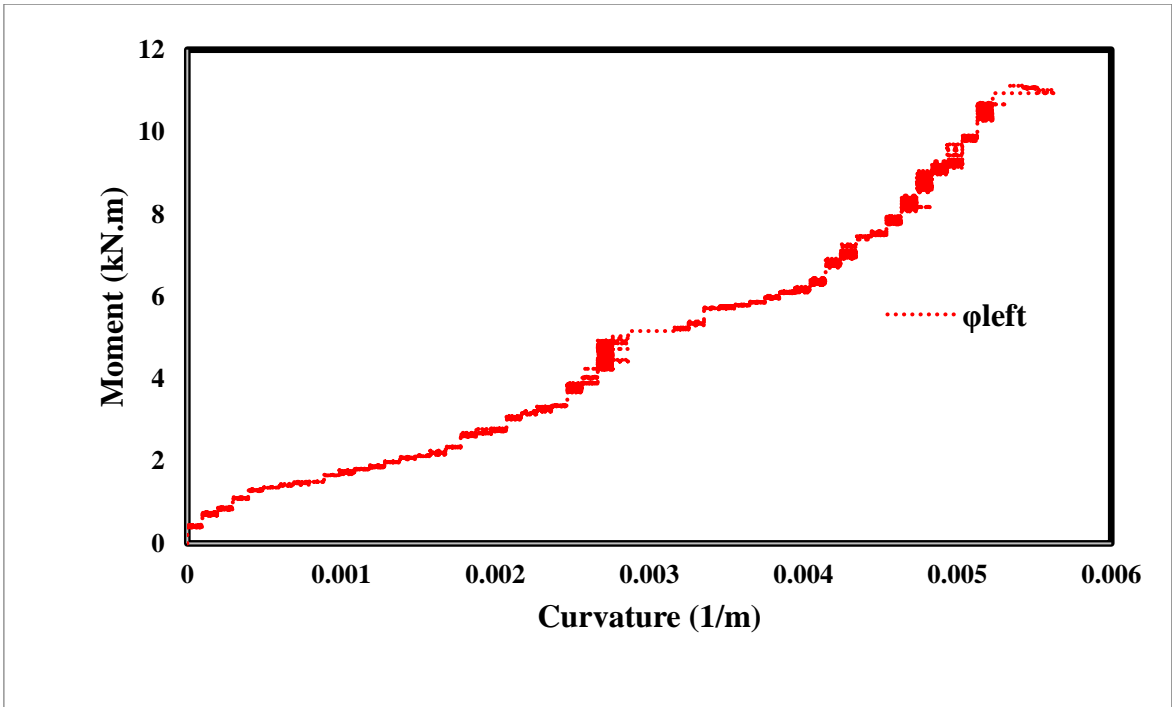


Figure 4.40. CVC – RA – 0.50 moment-curvature graphs(continued)

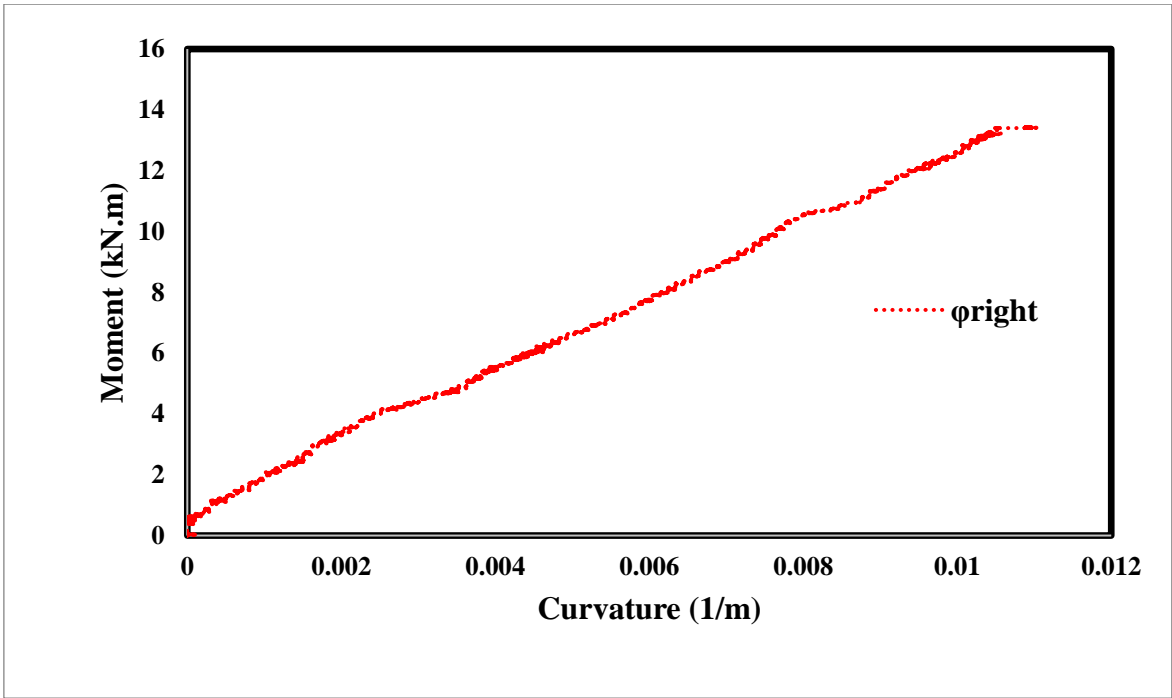


Figure 4.40. CVC – RA – 0.50 moment-curvature graphs

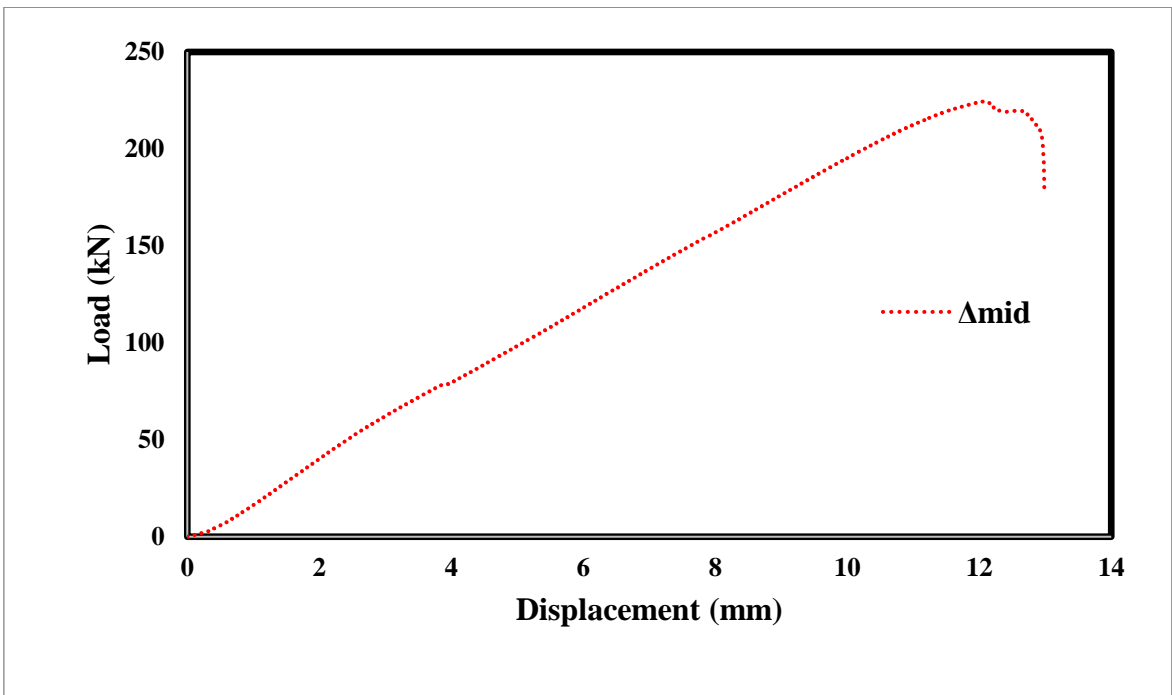


Figure 4.41. CVC – RA – 0.50 load-displacement graph

### Recycle Aggregate Flexural-Critical Conventional Concrete Beam 2 (CVC – RA – 1.00)

In this test, crack propagation of the beam was similar to the geopolymer beams with the same  $a/d$  ratio.



Figure 4.42. CVC – RA – 1.00 beam, (a) first cracks, (b) failure



Figure 4.43. CVC – RA – 1.00 shear dominant failure deatiled picture

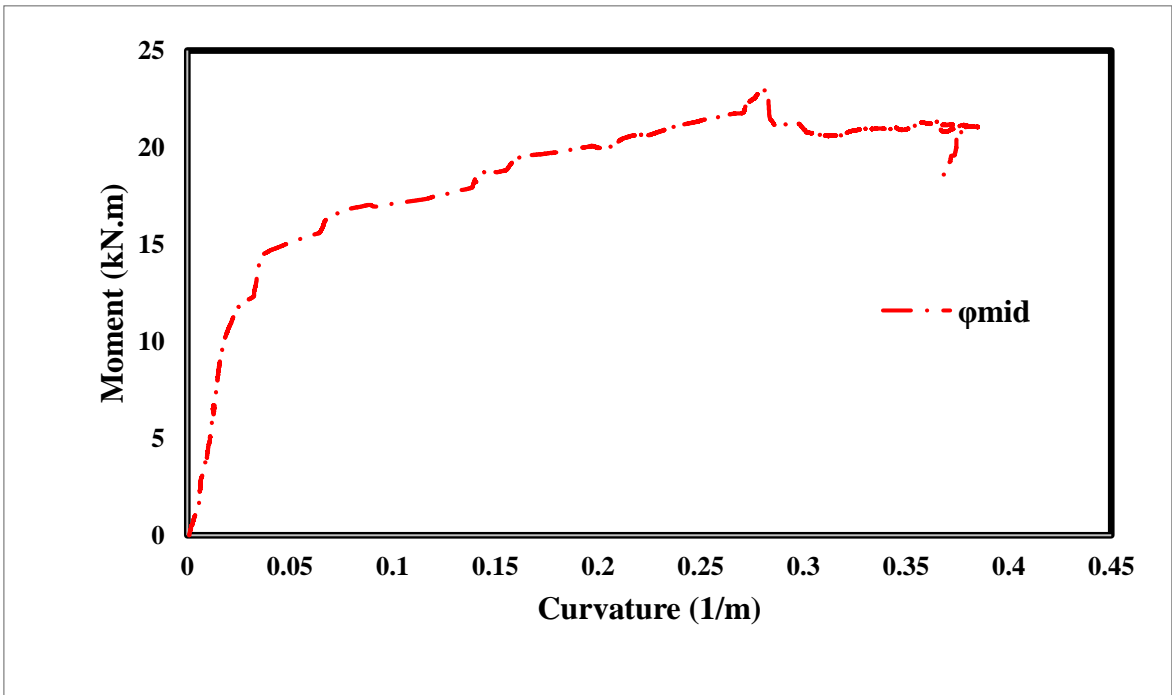
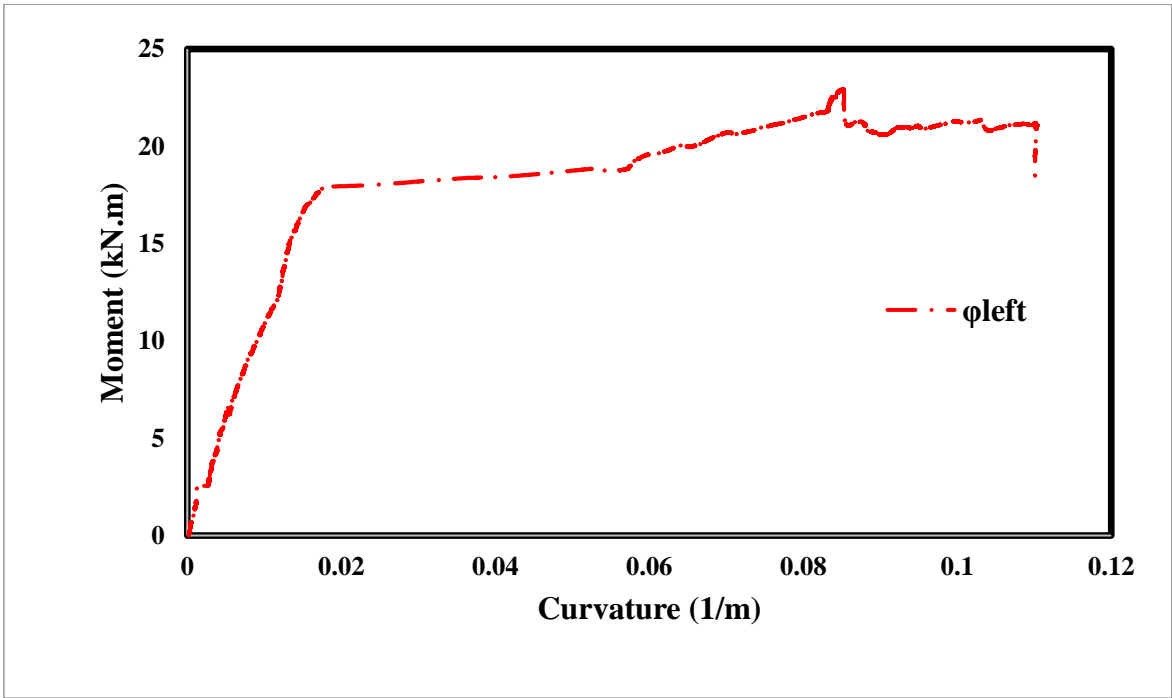


Figure 4.44. CVC – RA – 1.00 moment-curvature graphs(continued)



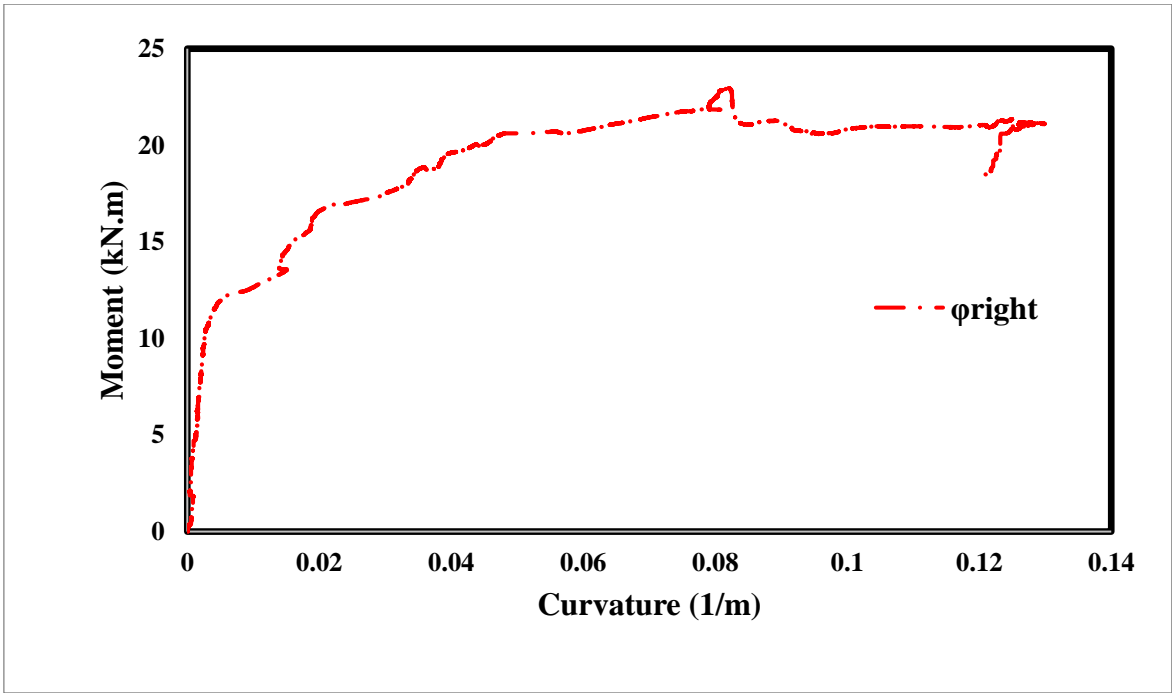


Figure 4.44. CVC – RA – 1.00 moment-curvature graphs

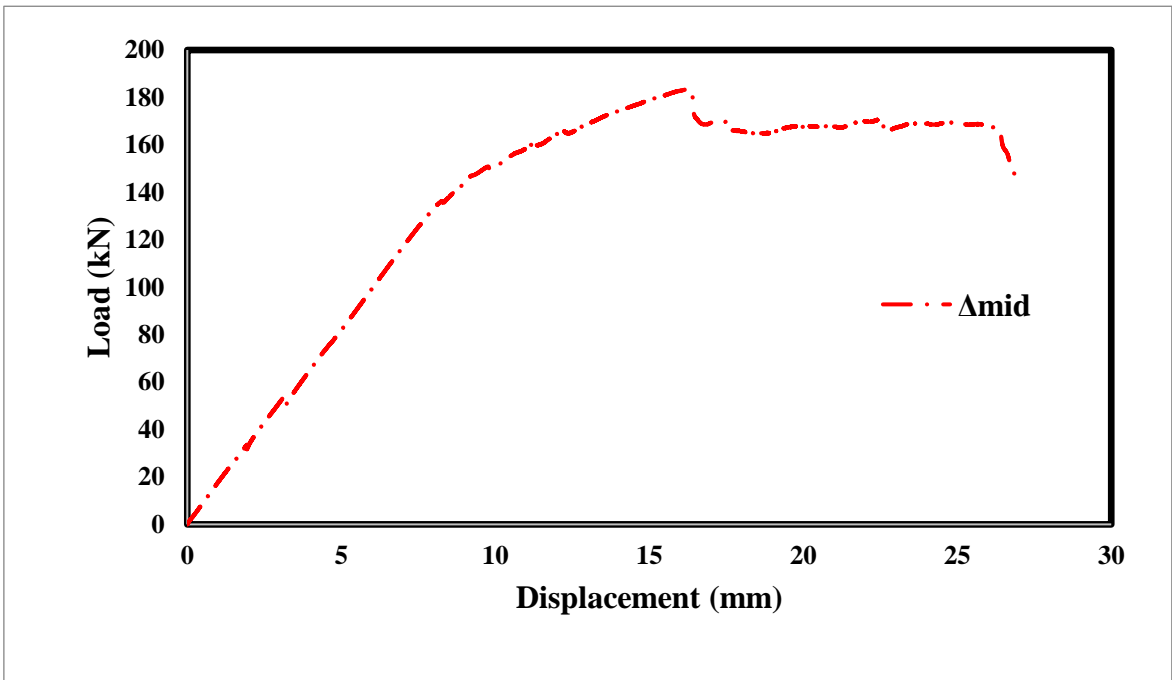


Figure 4.45. CVC – RA – 1.00 load-displacement graph

### Recycle Aggregate Flexural-Critical Conventional Concrete Beam 3 (CVC – RA – 1.65)

In this test, crack propagation of the beam was similar to the geopolymer beams with the same  $a/d$  ratio.

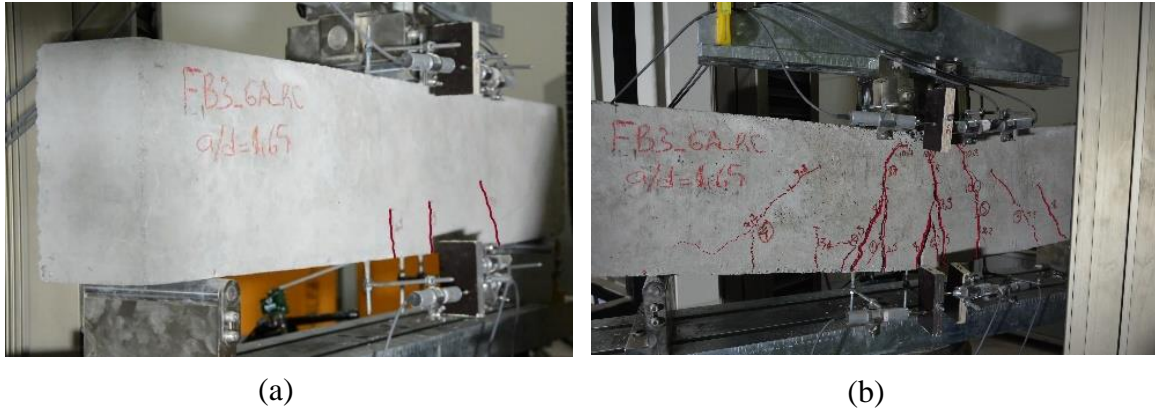


Figure 4.46. CVC – RA – 1.65 beam, (a) first cracks, (b) failure



Figure 4.47. CVC – RA – 1.65 flexure dominant failure picture

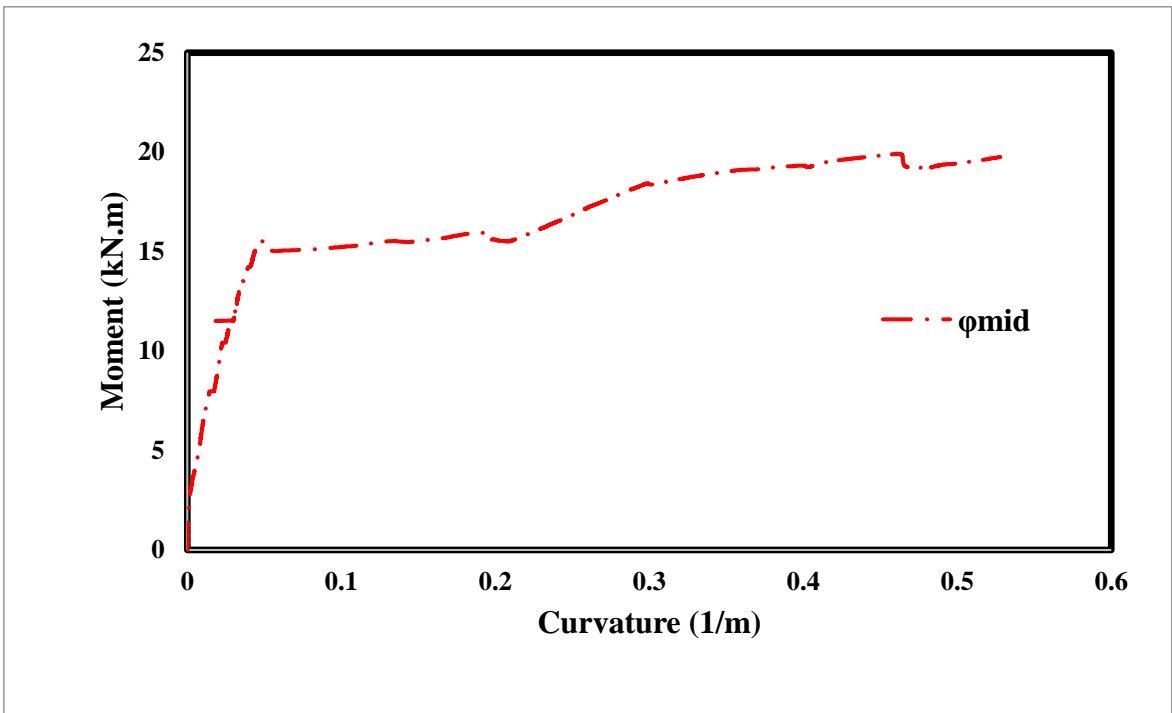
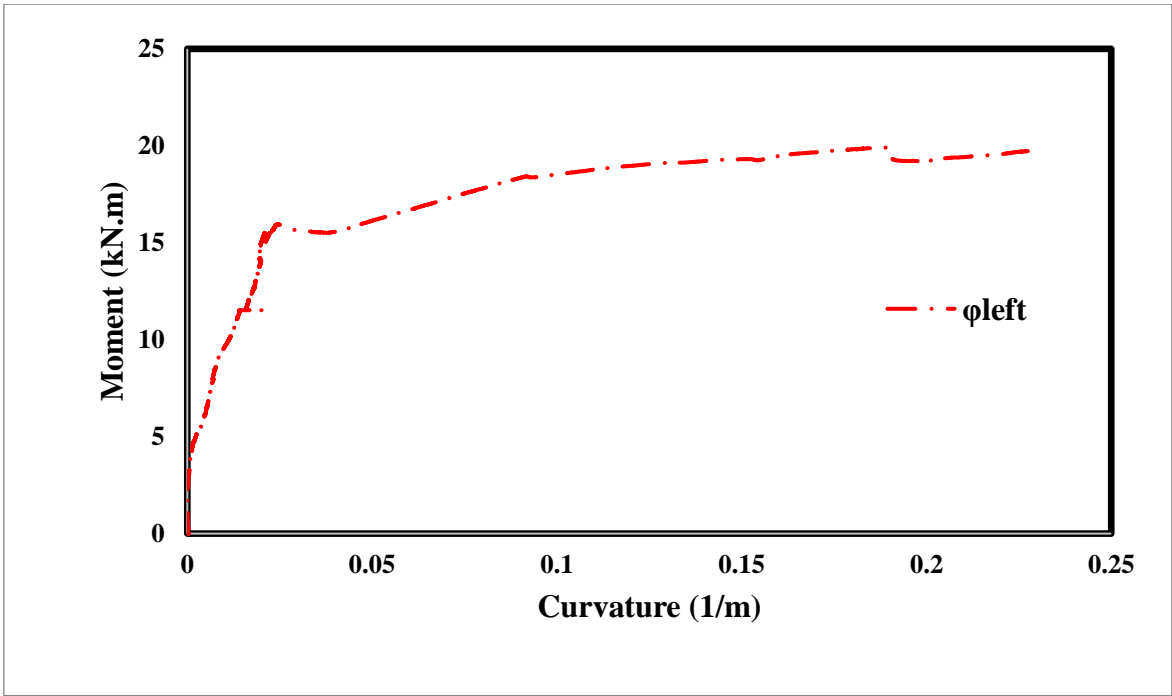


Figure 4.48. CVC – RA – 1.65 moment-curvature graphs(continued)

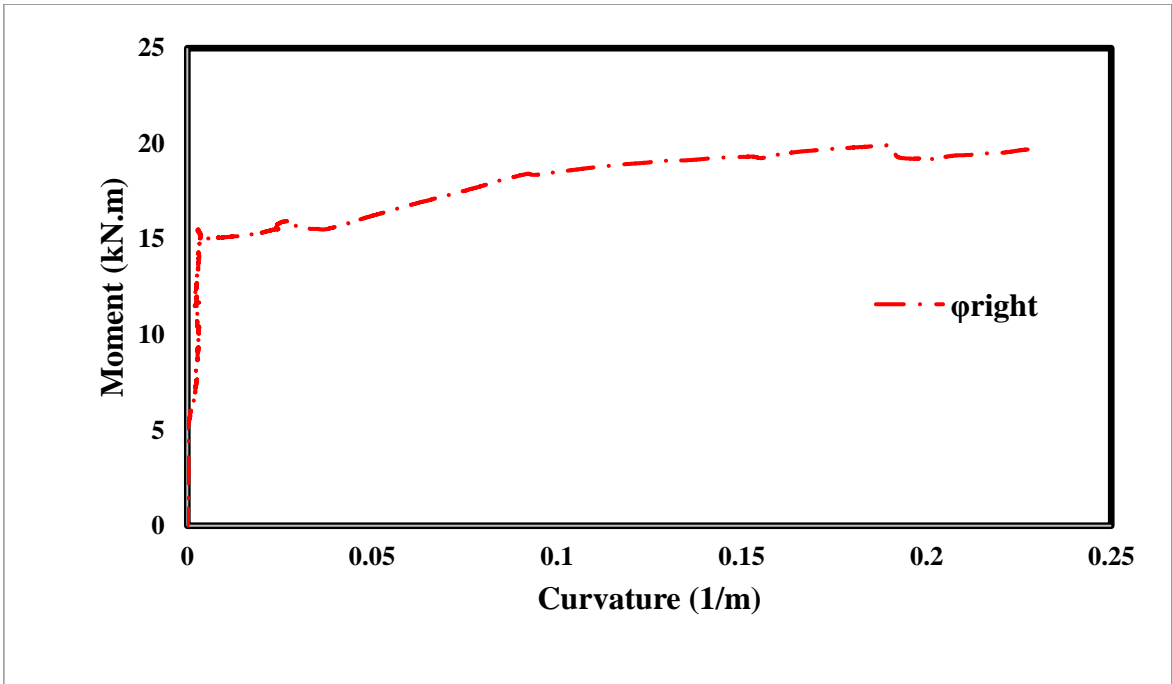


Figure 4.48. CVC – RA – 1.65 moment-curvature graphs

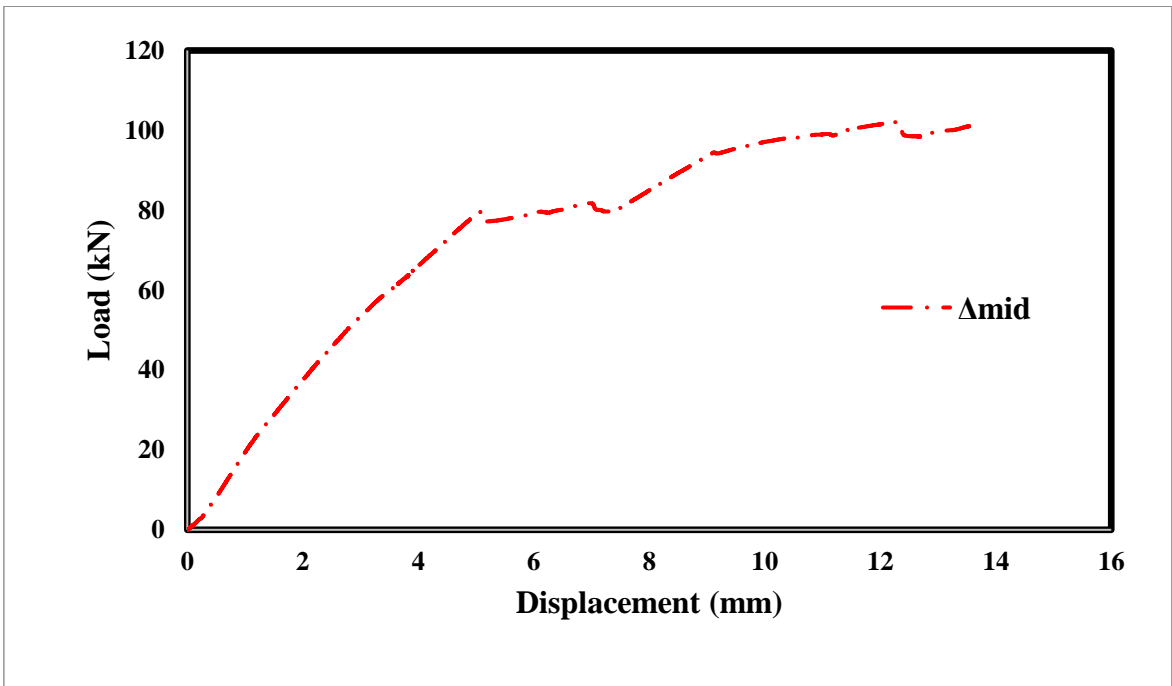


Figure 4.49. CVC – RA – 1.65 load-displacement graph

## 4.5. Summary of Beam Specimen Results

### 4.5.1. Test Results Summary of Beam Specimens with $a/d = 0.50$

The total vertical load-midspan displacement and the moment-curvature responses of CVC-NA-0.50, CVC-RA-0.50, GPC-NA-0.50, and GPC-RA-0.50 are given in Figure 4.50. It could easily be inferred from Figure 4.50 that the response of all specimens is brittle. Limited or no post-yield response was observed. This observation was also validated by the determined crack patterns (Figure 4.51). It is apparent from Figure 4.51 that all specimens failed by a shear – crack reaching the support. The yield and ultimate loads, yield and ultimate displacements, as well as the ductility indices, are presented in Table 4.5.

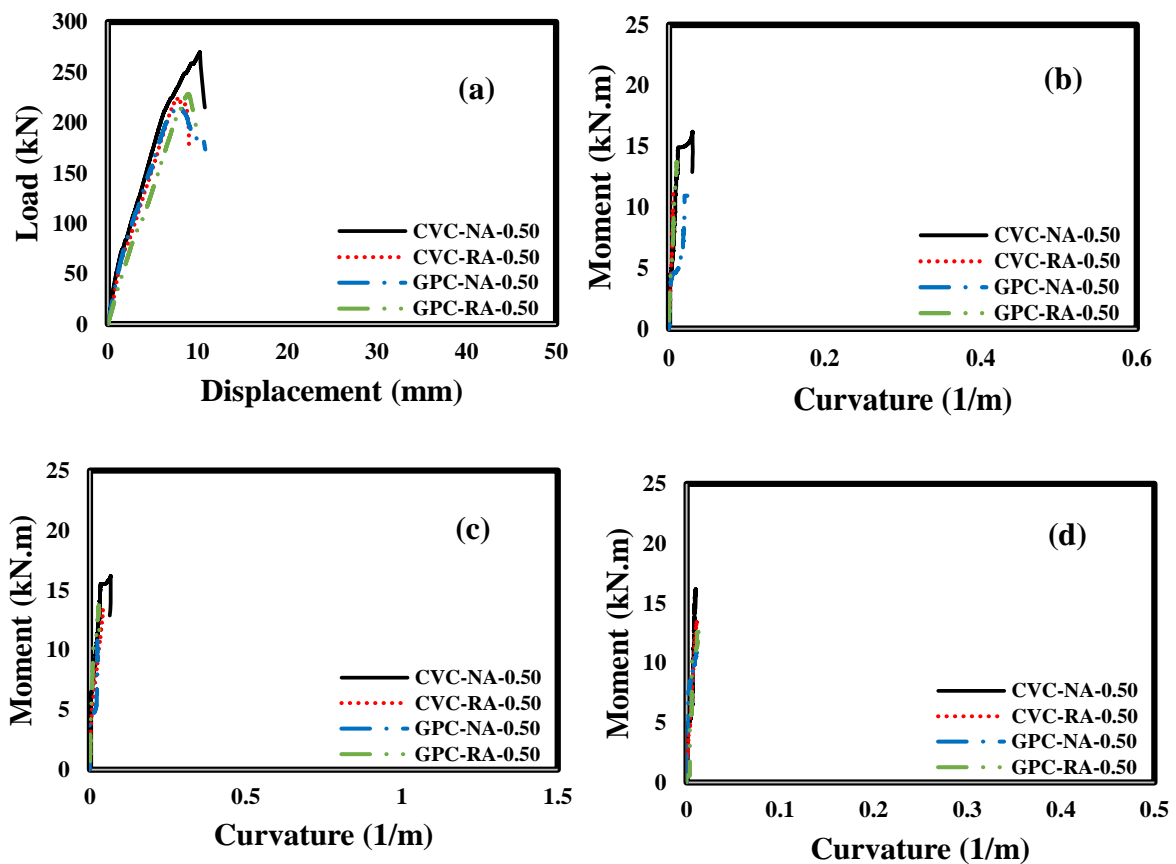


Figure 4.50. Test Results of Beam Specimens with  $a/d=0.50$ : (a) Total vertical load midspan displacement, (b) the moment-curvature curve from left LVDTs, (c) the moment-curvature curve from mid-LVDTs, and (d) the moment-curvature curve from right LVDTs









Specimen	Crack Initiation	Ultimate Stage
CVC - NA - 0.50	 <p>Handwritten text on specimen: FBI-NA-RC, a/d=0.43. A single vertical crack is visible on the left side.</p>	 <p>Handwritten text on specimen: FBI-NA-RC, a/d=0.43. Multiple vertical cracks are visible across the specimen.</p>
CVC - RA - 0.50	 <p>Handwritten text on specimen: FBI-GA-RC, a/d=0.43. A single vertical crack is visible on the left side.</p>	 <p>Handwritten text on specimen: FBI-GA-RC, a/d=0.43. Multiple vertical cracks are visible across the specimen.</p>
GPC - NA - 0.50	 <p>Handwritten text on specimen: FBI-NA-GED, a/d=0.43. A single vertical crack is visible on the left side.</p>	 <p>Handwritten text on specimen: FBI-NA-GED, a/d=0.43. Multiple vertical cracks are visible across the specimen.</p>
GPC - RA - 0.50	 <p>Handwritten text on specimen: FBI-GA-GED, a/d=0.43. A single vertical crack is visible on the left side.</p>	 <p>Handwritten text on specimen: FBI-GA-GED, a/d=0.43. Multiple vertical cracks are visible across the specimen.</p>

Figure 4.51. Observed Crack Patterns of Beam Specimens with  $a/d=0.50$

## FEMA 356 Bilinearization Method

In the FEMA method, to find the yield strength value of the curve, the iteration procedure is applied at the linear part of the curve. The stiffness line must be intersected at 60% of the estimated yield strength value. Moreover, Equal energy rule must also be applied.

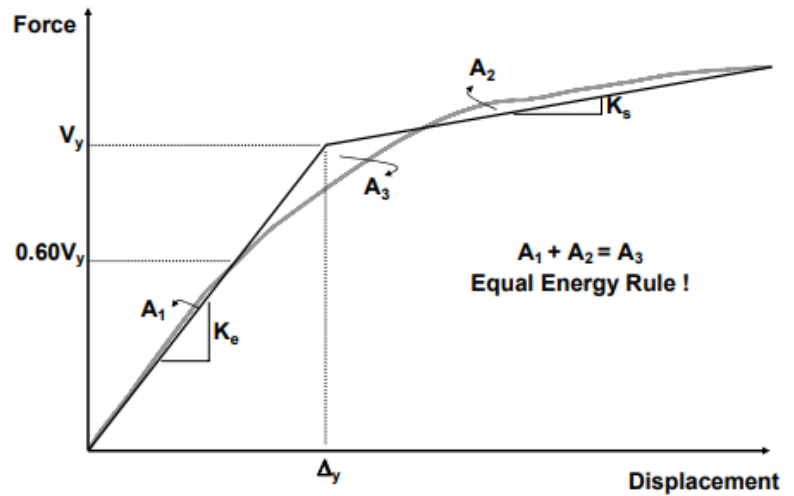


Figure 4.52. FEMA Idealization Method

Table 4.5. Summary of Test Results

Parameters	a/d = 0.50				a/d = 1.00				a/d = 1.65			
	CVC-NA	CVC-RA	GPC-NA	GPC-RA	CVC-NA	CVC-RA	GPC-NA	GPC-RA	CVC-NA	CVC-RA	GPC-NA	GPC-RA
<b>F<sub>y</sub> (kN)</b>	230.1	204.51	205.85	220.08	165.10	168.81	165.98	170.06	99.16	98.91	99.08	99.18
<b>F<sub>u</sub> (kN)</b>	270.05	224.46	216.82	228.58	180.40	183.63	184.68	189.66	112.08	102.11	105.04	103.5
<b>M<sub>y</sub> (kN.m)</b>	NA	NA	NA	NA	18.26	16.18	18.91	19.65	18.86	16.49	19.89	18.96
<b>M<sub>u</sub> (kN.m)</b>	16.20	13.46	13.00	13.71	22.10	22.49	23.23	21.85	19.91	20.48	20.18	20.18
<b>u<sub>y</sub> (mm)</b>	10.09	11.60	8.20	12.00	9.16	11.25	11.16	10.45	9.16	8.16	9.81	9.96
<b>u<sub>u</sub> (mm)</b>	13.18	13.63	14.11	15.5	20.89	27.91	26.18	21.78	39.81	26.63	37.68	26.02
<b>φ<sub>y</sub> (1/m)</b>	NA	NA	NA	NA	0.03	0.03	0.03	0.03	0.11	0.09	0.10	0.10
<b>φ<sub>u</sub> (1/m)</b>	NA	NA	NA	NA	0.13	0.11	0.12	0.10	0.96	0.65	0.98	0.72
<b>μ<sub>u</sub></b>	1.31	1.18	1.72	1.29	2.28	2.48	2.35	2.08	4.35	3.26	3.84	2.61
<b>μ<sub>φ</sub></b>	NA	NA	NA	NA	4.33	3.67	4.17	3.85	8.72	7.22	9.80	7.21
<b>E<sub>t</sub> (kN.m)</b>	1.90	1.69	1.87	1.88	4.23	3.67	4.43	3.00	3.53	2.31	3.23	2.27
<b>E<sub>n</sub></b>	1.64	1.42	2.22	1.43	5.60	3.87	4.78	3.37	7.77	5.72	6.65	4.60

### 4.5.2. Test Results of Beam Specimens with a/d = 1.00

The total vertical load-midspan displacement and the moment-curvature responses of CVC-NA-1.00, CVC-RA-1.00, GPC-NA-1.00, and GPC-RA-1.00 are given in Figure 4.53. It could easily be inferred from Figure 4.53 that the response of all specimens is less brittle than previous specimens. In these tests, it was observed that GPC specimens failed with a

limited or no post-yield response due to less amount of flexure cracks at the midspan. However, CVC specimens showed a mixed shear-flexure failure, resulting in more ductility. This observation was also validated by the determined crack patterns (Figure 4.54). The yield and ultimate loads, yield and maximum displacements, and the ductility indices, are presented in Table 4.5.

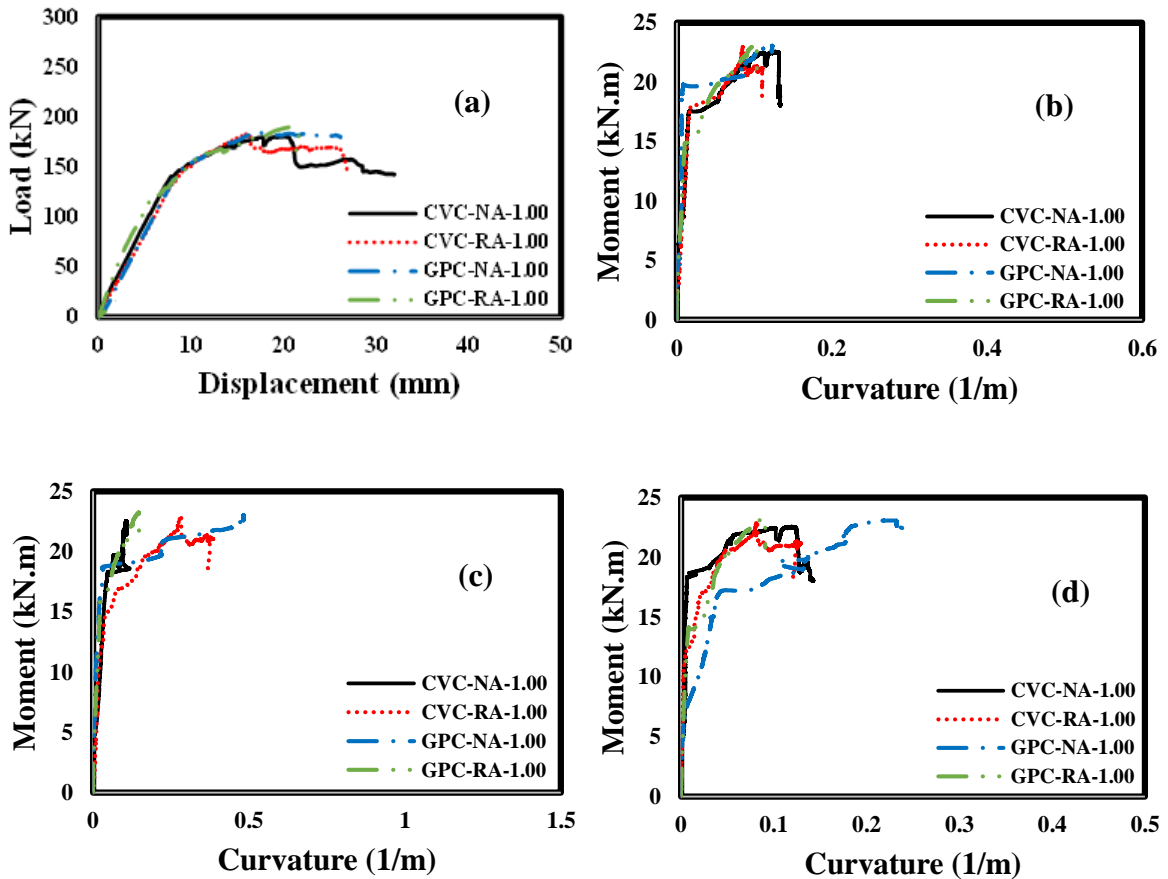


Figure 4.53. Test Results of Beam Specimens with  $a/d=1.00$ : (a) Total vertical load-midspan displacement, (b) the moment-curvature curve from left LVDTs, (c) the moment-curvature curve from mid LVDTs, and (d) the moment-curvature curve from right LVDTs



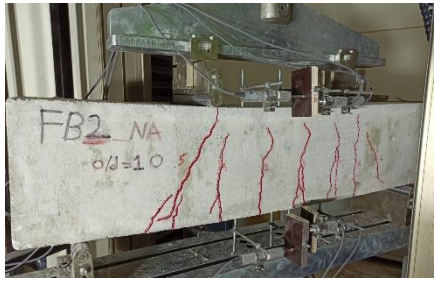
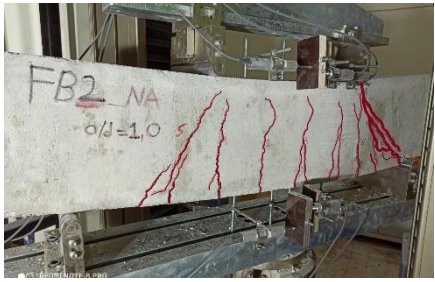
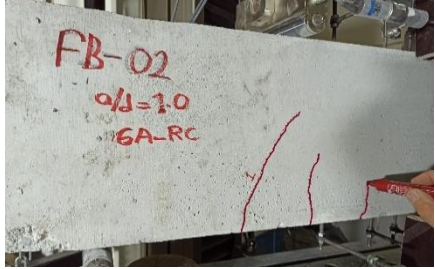



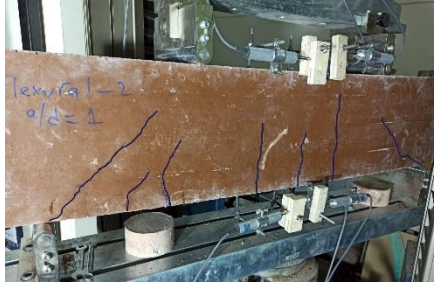
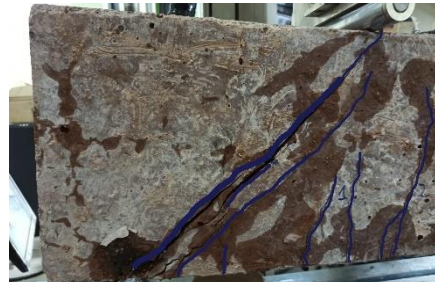
Specimen	Crack Initiation	Ultimate Stage
CVC - NA - 1.00	 <p>Handwritten text on specimen: FB2-NA, a/d=1.05. Red cracks are visible on the concrete surface.</p>	 <p>Handwritten text on specimen: FB2-NA, a/d=1.05. Multiple red cracks are visible, indicating failure.</p>
CVC - RA - 1.00	 <p>Handwritten text on specimen: FB-02, a/d=1.0, GA-RC. Red cracks are visible.</p>	 <p>Handwritten text on specimen: FB-02, a/d=1.0, GA-RC. Multiple red cracks are visible.</p>
GPC - NA - 1.00	 <p>Handwritten text on specimen: FB2-NA, a/d=1.0. Blue cracks are visible on the brown surface.</p>	 <p>Handwritten text on specimen: FB2-NA, a/d=1.0. Multiple blue cracks are visible.</p>
GPC - RA - 1.00	 <p>Handwritten text on specimen: lexura 1-2, a/d=1. Blue cracks are visible.</p>	 <p>Multiple blue cracks are visible on the brown surface.</p>

Figure 4.54. Observed Crack Patterns of Beam Specimens with  $a/d=1.00$

### 4.5.3. Test Results of Beam Specimens with $a/d = 1.65$

The total vertical load-midspan displacement and the moment-curvature responses of CVC-NA-1.65, CVC-RA-1.65, GPC-NA-1.65, and GPC-RA-1.65 are given in Figure 4.55. It could easily be inferred from Figure 4.55 that the response of all specimens is brittle. Limited or no post-yield response was observed. This observation was also validated by the determined crack patterns (Figure 4.56). It is apparent from Figure 4.56 that all specimens failed by a shear – crack reaching the support. The yield and maximum loads, yield and maximum displacements, and the ductility indices, are presented in Table 4.6.

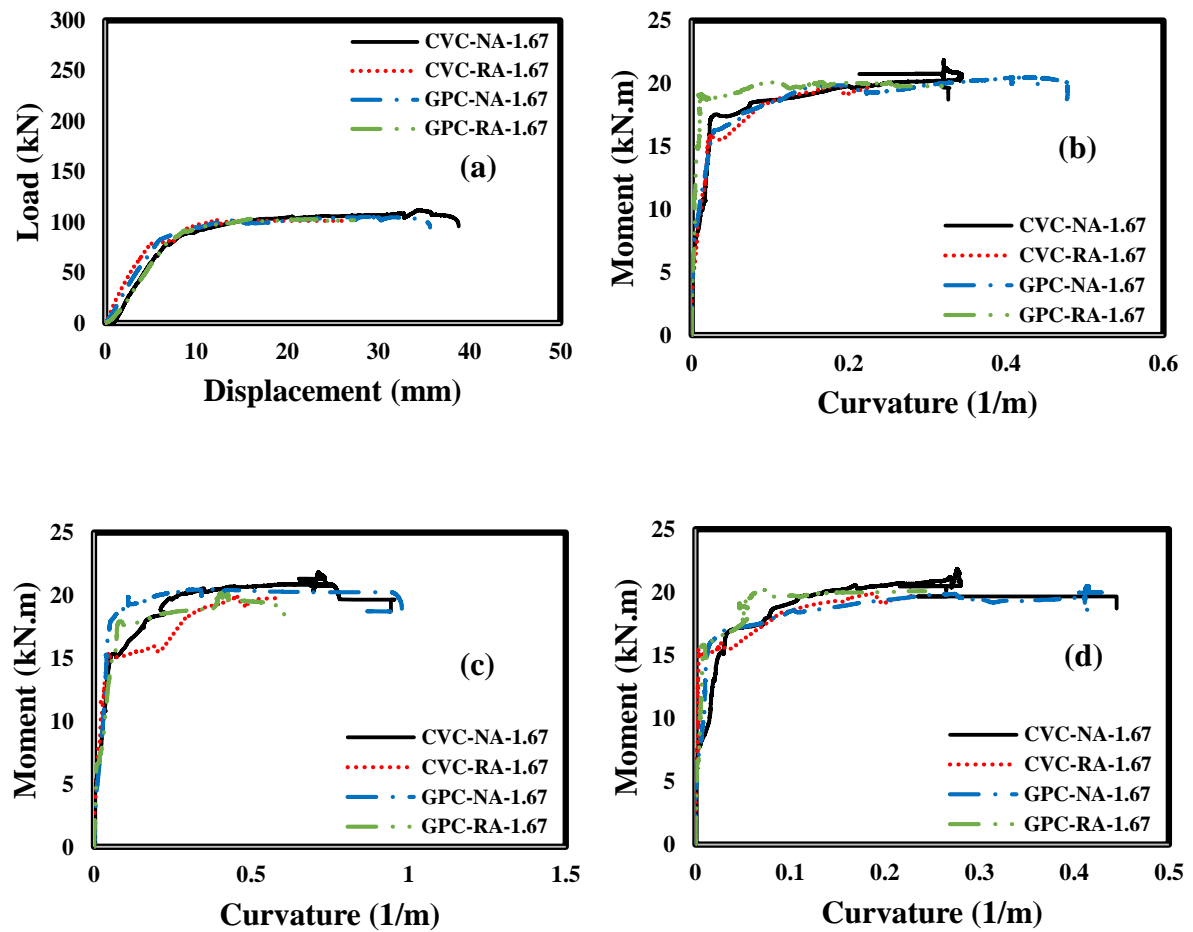


Figure 4.55. Test Results of Beam Specimens with  $a/d=1.65$ : (a) Total vertical load-midspan displacement, (b) the moment-curvature curve from left LVDTs, (c) the moment-curvature curve from mid LVDTs and (d) the moment-curvature curve from right LVDTs

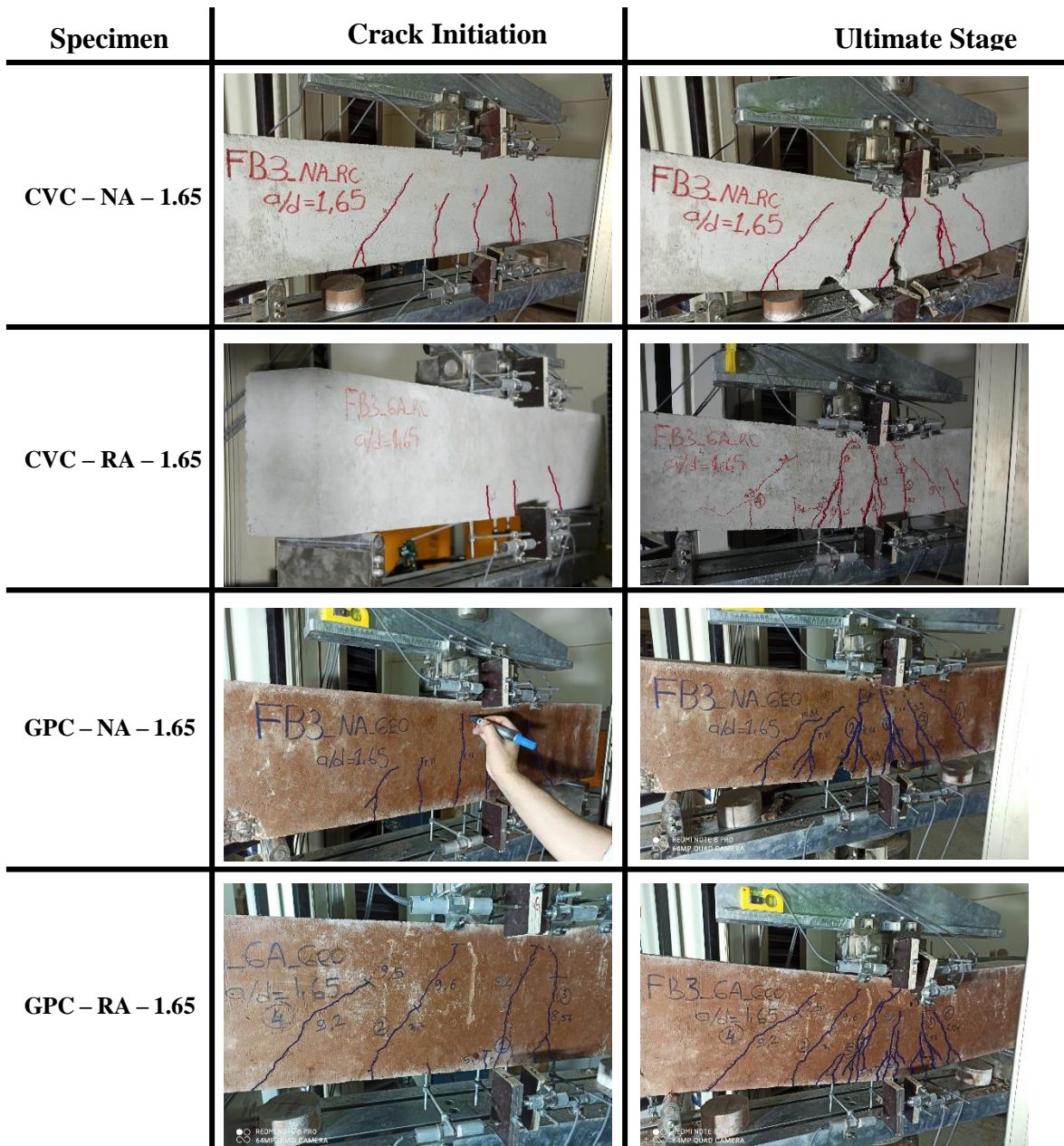


Figure 4.56. Observed Crack Patterns of Beam Specimens with  $a/d=1.65$

## 4.6. Analysis and Discussion

### 4.6.1. Effect of Material Type

The performances of beam specimens with different material properties are discussed in this part. Firstly, it should be noted that the GPC-NA specimens had similar behavior to CVC-NA specimens as far as the load and displacement capacities were considered. This observation was also verified with the curvature capacities. Also, the cracks in these specimens showed similar patterns. Therefore, it could easily be concluded that the proposed GPC mixture could perform as well as the CVC mixture.

However, the inclusion of recycled aggregates in the CVC and GPC mixtures gave rise to a critical change in the behavior. Although the effect of recycled aggregate on the load capacities was negligible, this effect on the displacement capacities was substantial. For instance, the reduction in the ultimate displacement capacities of CVC and GPC specimens were 35% and 30%, respectively. In addition, a second observation was that the effect of recycled aggregates was more pronounced for flexure-dominated specimens (i.e.,  $a/d=1.65$ ). This observation could be attributed to the secondary interfacial transition zone (ITZ) formation. Akbarnezhad et al. [90] claimed that the flexural ductility of beams depended on the adhesion of the aggregate and the paste. Since the most important factor affecting this bond strength is ITZ, a secondary ITZ formation was observed in mixtures with recycled aggregates due to formerly adhered mortar content surrounding the recycled aggregates. This secondary ITZ formation reduced the flexural capacity, postponing the shear cracks. This observation was also proved by comparing the flexural strengths of mixtures with and without recycled aggregates (Tables 4.1-4.4). It was apparent from Tables 4.1-4.4 that approximately a 10% reduction in the flexural strength of mixtures with recycled aggregates existed. It was, furthermore, known that the impact of ITZ depends significantly upon the water/binder ratio of mixtures using recycled aggregates [91], and the relatively high water/binder ratio in the Portland cement beams and free water in geopolymer beams were expected to produce a weaker ITZ formation.

The recycled aggregates caused a significant reduction in the normalized energy absorption capacities of CVC and GPC specimens. Independent from the different mixtures and different modes of failures, the reduction in the normalized energy absorption capacities reached nearly 30% in the usage of normal aggregates instead of recycled aggregates. This observation underlined the similarities of CVC and GPC specimens in terms of flexural behavior.

#### **4.6.2. Effect of Shear-span-to-depth Ratio**

The first shear-span-to-depth ratio was selected as 0.50 to investigate the possible shear failure for these code-conforming beam specimens. As expected, all specimens, independent from the construction material chosen, failed in shear and showed brittle load-deflection and moment-curvature responses. Although the moment-curvature curves were not suitable to analyze the behavior of reinforced concrete specimens due to the formation of inclined

cracks between the load application point and the support, the change in the curvature response over the beam was also provided for the sake of completeness. It could easily be inferred from Figure 4.50 that geopolymer concrete had very similar behavior compared to its conventional concrete counterparts in terms of load and deformation capacities. The failure patterns of all specimens were also detected to be similar (Figure 4.51). This observation proved that, for shear-dominant behavior, i) the recycled aggregate had a very limited impact on the performance of concrete, and ii) the reinforced geopolymer concrete could perform nearly the same as conventional reinforced concrete if the shear-dominant behavior was investigated. In addition, the displacement and curvature ductilities of all specimens (i.e., CVC-NA-0.50, CVC-RA-0.50, GPC-NA-0.50, and GPC-RA-0.50) were determined to be very low (Table 4.5). The other observation was that the normalized energy absorption capacities of all specimens with recycled aggregates were also less than other specimens without recycled aggregates (Table 4.5).

The second shear-span-to-depth ratio (i.e.,  $a/d=1.00$ ) was used to determine the mixed shear-flexure failure for code-conforming reinforced beam specimens. All CVC specimens failed in shear-flexure combined action, manifesting itself by inclined cracks between the support and load application point and vertical cracks at the midspan. However, GPC specimens failed with a limited or no post-yield response due to fewer flexure cracks at the midspan. Unlike the first  $a/d$  ratio (i.e., 0.50), there exists some ductility, implied by the yield plateau in load-displacement and moment-curvature curves in Figure 4.53. It should be stated that the mid LVDTs attached to specimens CVC-NA-1.00 and GPC-RA-1.00 stopped recording at a load value of 81kN and 96kN, respectively. Therefore, the curvature ductility comparisons of all specimens were made by using left LVDTs. The curvature ductility values of each specimen ranged between 3.67 and 4.33. It was clear from Table 4.5 that geopolymer concrete had a curvature ductility of close to 4. If the curvature values determined from the mid LVDTs and left LVDTs were compared, the maximum curvature demand (i.e., mid LVDTs) at the midspan resulted in nearly three times the curvature demand at the left span (i.e., mid LVDTs). The reinforced geopolymer concrete could perform almost the same as the conventional reinforced concrete if the shear-flexure-dominant behavior was investigated. The other observation was that the normalized energy absorption capacities of all specimens with recycled aggregates were also less than other specimens without recycled aggregates (Table 4.5). The decrease in normalized energy absorption capacity for CVC and GPC specimens was 30.89% and 29.50%, respectively.

The last shear-span-to-depth ratio (i.e.,  $a/d=1.65$ ) was utilized to study the flexure-dominant failure for code-conforming reinforced beam specimens with different materials. All specimens failed in flexure-dominant action, manifesting themselves by nearly vertical cracks concentrated at the midspan. In all of these tests, there exists a significant amount of ductility, implied by the large yield plateau in load-displacement and moment-curvature curves in Figure 4.55. The curvature ductility comparisons of all specimens were made by using midspan LVDTs. The curvature ductility values of each specimen ranged between 7.21 and 9.80. It was clear from Table 4.5 that geopolymer concrete had a curvature ductility of close to 10, which is near twice the curvature ductility of specimens with an  $a/d$  ratio of 1.00. The failure patterns of all specimens were also detected to be similar (Figure 4.56). This observation proved that the reinforced geopolymer concrete could perform nearly the same as the conventional reinforced concrete if the flexure-dominant behavior was investigated. However, the recycled aggregate had a negative effect on the performance of concrete, i.e., some reduction in ductility and hence energy absorption capacity was observed (Table 4.5).

The capacity estimation performances of two current codes: ACI318-19 [92] and TS500 [93], were also investigated in the scope of this study. The nominal shear capacity and the nominal moment capacities of each specimen were calculated by using proposed equations in ACI318-19 [92] and TS500 [93] and are presented in Table 4.6. In Table 4.6, the estimated capacity ( $V_{cap}$ ) was obtained from the minimum of the nominal shear strength ( $V_n$ ) and the ratio of nominal moment capacity ( $M_n$ ) to the moment arm. It could easily be inferred that the estimation performance of TS500 [93] is slightly better than the estimation performance of ACI318-19 [92]. It should also be noted that the estimation performance of codes is independent of the material type and the use of recycled aggregates. Besides, the estimation performance is slightly better for shear-dominant failures.

## TS500 and ACI318-19 Formulation Procedure

### TS500

$$V_r = V_c + V_s$$

$$V_s = \frac{A_{sw}}{s} \cdot f_{yw} \cdot d$$

$$V_c = 0,8 \cdot V_{cr}$$

$$V_{cr} = 0,65 \cdot f_{ct} \cdot b_w \cdot d$$

$$M_r = A_s \cdot f_{yk} \cdot j \cdot d$$

### ACI318-19

$$V_r = V_c + V_s$$

$$V_c = 0,75 \cdot (0,17 \cdot \sqrt{f_{ck}} \cdot b_w \cdot d)$$

$$V_s = 0,75 \cdot (A_v \cdot f_{yk} \cdot \frac{d}{s})$$

$$M_r = A_s \cdot f_{yk} \cdot \phi \cdot (d - a/2)$$

\*These formulas obtained from the defined code standards.

Table 4.6. Estimation Performance of Code Proposed Equations

Specimens	Experiment			TS500 Estimations				ACI318-19 Estimations			
	$M_{max}$ (kN.m)	$F_{max}$ (kN)	$V_{max}$ (kN)	$M_n$ (kN.m)	$V_n$ (kN)	$V_{cap}$ (kN)	Error (%)	$M_n$ (kN.m)	$V_n$ (kN)	$V_{cap}$ (kN)	Error (%)
<b>CVC-NA-0.50</b>	16.2	270.1	135.0	15	91.6	91.60	-32.1	12.7	89.2	89.2	-33.9
<b>CVC-RA-0.50</b>	13.5	224.5	112.2	15.1	96.5	96.50	-14.0	12.8	93.8	93.8	-16.4
<b>GPC-NA-0.50</b>	13.0	216.8	108.4	15	95.1	95.10	-12.3	12.8	92.5	92.5	-14.7
<b>GPC-RA-0.50</b>	13.7	228.6	114.3	15	94.6	94.60	-17.2	12.8	92.1	92.1	-19.4
<b>CVC-NA-1.00</b>	22.1	180.4	90.2	15	91.6	61.22	-32.1	12.7	89.2	51.84	-42.5
<b>CVC-RA-1.00</b>	22.5	183.6	91.8	15.1	96.5	61.63	-32.9	12.8	93.8	52.24	-43.1
<b>GPC-NA-1.00</b>	22.6	184.7	92.3	15	95.1	61.22	-33.7	12.8	92.5	52.24	-43.4
<b>GPC-RA-1.00</b>	23.2	189.7	94.8	15	94.6	61.22	-35.4	12.8	92.1	52.24	-44.9
<b>CVC-NA-1.67</b>	21.9	112.1	56.0	15	91.6	38.46	-31.3	12.7	89.2	32.56	-41.8
<b>CVC-RA-1.67</b>	19.9	102.1	51.1	15.1	96.5	38.72	-24.2	12.8	93.8	32.82	-35.8
<b>GPC-NA-1.67</b>	20.5	105.0	52.5	15	95.1	38.46	-26.7	12.8	92.5	32.82	-37.5
<b>GPC-RA-1.67</b>	20.2	103.5	51.8	15	94.6	38.46	-25.7	12.8	92.1	32.82	-36.6

## CONCLUSION

In this thesis, the structural properties of reinforced geopolymer concrete beams produced from 100% CDW-based materials were determined by performing laboratory experiments. In addition, the impact of the inclusion of recycled aggregate in the mixtures was investigated. To this end, bending tests were performed on reinforced conventional concrete beam specimens and reinforced geopolymer concrete beam specimens. Twelve specimens were tested to compare the structural behavior of geopolymer concrete beams with conventional concrete beams. The selected parameters in this study are three different shear span ratios and the inclusion of recycled aggregates in the concrete mixture. Therefore, the structural performance of beams was, firstly, compared for mixtures without recycled aggregates to control the possible side effects of 100% recycled concrete construction. Load-deflection curves, moment-curvature curves, and crack patterns were utilized to study the performance of geopolymer concrete. The following significant interpretations can be drawn based on the results of the conducted test in this study:

- 1- The GPC-NA specimens had similar behavior to CVC-NA specimens as far as the load and displacement capacities were considered. This observation was also verified with the curvature capacities. Also, the cracks in these specimens showed similar patterns.
- 2- The inclusion of recycled aggregates in the CVC and GPC mixtures gave rise to a critical change in the behavior. Although the effect of recycled aggregate on the load capacities was negligible, this effect on the displacement capacities was significant (up to 30% difference). In addition, the effect of recycled aggregates was more pronounced for flexure-dominated specimens (i.e.,  $a/d=1.65$ ). This observation could be attributed to the secondary interfacial transition zone (ITZ) formation.
- 3- The recycled aggregates resulted in a notable reduction in the normalized energy absorption capacities of CVC and GPC specimens. Independent from the different mixtures and different modes of failures, the reduction in the normalized energy absorption capacities reached nearly 30% in the case of the replacement of normal aggregates with recycled aggregates.
- 4- The geopolymer concrete had a significant amount of ductility if flexure-dominant behavior could be enforced on the designed structural element. The curvature ductility of geopolymer concrete was proven to be comparable to conventional concrete. Therefore, geopolymer concrete could be a possibly strong replacement candidate.



- 5- The failure patterns of all specimens were also detected to be similar except for shear-flexure dominant behavior. This implies that geopolymer concrete obeyed nearly the same failure surface.
- 6- The normalized energy absorption capacities of all specimens with recycled aggregates were also less than other specimens without recycled aggregates. The decrease in normalized energy absorption capacity for CVC and GPC specimens was approximately 30%. However, the recycled aggregate had a very limited impact on the load capacity.
- 7- The reinforced geopolymer concrete was similarly performed to the conventional reinforced concrete for especially flexure-dominated  $a/d$  ratios as far as the load capacity, displacement capacity, and energy absorption capacity were considered. The percentage deviations for the listed parameters were all less than 10%.
- 8- The test observations clearly showed that construction demolition waste could be recycled to produce new constructional components, considering its advantage of promoted sustainability.
- 9- Code estimations failed to have low deviations and insignificant percentage errors. The percentage of errors reached as large as 45%. Although the authors are aware of the fact that the code formulations should result in conservative estimations, it should be noted that the code calculations in this study did not include the material factors. Therefore, the estimates should be reconsidered when the material and load factors are applied to them. The material factor along with the load factors would result in a further reduction in the estimations in the order of approximately 2. Thus, the code estimations would give a factor of safety of around 4 for the tested specimens.

## REFERENCES

- [1]. Rashid K, Razzaq A, Ahmad M, Rashid T, Tariq S. Experimental and analytical selection of sustainable recycled concrete with ceramic waste aggregate. *Constr Build Mater* **2017**;154: 829–40.
- [2]. Louise K Turner, Frank G, Collins, **2013** "Carbon dioxide equivalent (CO<sub>2</sub>-e) emissions between Geopolymer and OPC cement concrete" *Construction and Building materials*, vol.43, pp.125-130.
- [3]. De Brito J, Saikia N. Recycled aggregate in concrete: use of industrial, construction and demolition waste. Springer Science & Business Media; **2012**.
- [4]. Rashid K, Yazdanbakhsh A, Ul Rehman M, Sustainable selection of the concrete incorporating recycled tire aggregate to be used as medium to low strength material. *Journal of Cleaner Production*. 0959-6526-**2019**.
- [5]. Yildirim, G., A Kul, A., Özçelikci, E., Sahmaran, M., Aldemir, A. 533 Figueira, D. and Ashour, A.F. (**2020**), "Development of Alkali-Activated Binders from Recycled Mixed Masonry-originated Waste", *Journal of Building Engineering*. 33: 101690
- [6]. Ulugöl, H., Kul, A., Yıldırım, G., Şahmaran, M., Aldemir, A., Figueira, D. and Ashour, A.F. (**2020**), "Mechanical and microstructural characterization of geopolymers from assorted construction and demolition waste-based masonry and glass", *Journal of Cleaner Production*.
- [7]. Davidovits J., **1991**. "Geopolymers: inorganic polymeric new materials", *Journal of Thermal Analysis*, 37, pp. 1633–1656.
- [8]. Pelisser F, Silva B. V, Menger M. H, Frasson B. J, Keller T. A, Torii A. J, Lopez R. H, Structural analysis of composite metakaolin-based geopolymer concrete. Volume 11, Number 3 (June **2018**) p. 535 – 543 • ISSN 1983-4195.
- [9]. K. H. Mo, U. J. Alengaram, and M. Z. Jumaat, "Structural performance of reinforced geopolymer concrete members: A review," *Construction and Building Materials*, vol. 120, pp. 251– 264, **2016**.
- [10]. P. Duxson, J. L. Provis, G. C. Lukey, and J. S. J. V. Deventer, "The role of inorganic polymer technology in the development of green concrete," *Cement & Concrete Research*, vol. 37, no. 12, pp. 1590–1597, **2007**.
- [11]. Kumar S, Pradeepa J, Ravindra P M and Rajendra S,"Flexural Behavior Of Fly Ash Based Reinforced Geopolymer Concrete Beams," *International Journal of Structural and Civil Engineering Research*, ISSN 2319 – 6009 www.ijscer.com Vol. 3, No. 3, August **2014**.
- [12]. Mehta, P. K. (**2001**). Reducing the environmental impact of concrete. *Concrete International*, 23(10), 61–66.

- [13]. Madhava, T. V., Manjunath, G., & Venugopal, K. (2013). Phenomenological Model to Re-proportion the Ambient Cured Geopolymer Compressed Blocks. *International Journal of Concrete Structures Materials*, 7(3), 193–202.
- [14]. Kar, A., Ray, I., Halabe, U. B., Unnikrishnan, A., & Dawson-Andoh, B. (2014). Characterizations and quantitative estimation of alkali-activated binder paste from microstructures. *International Journal of Concrete Structures Materials*, 8(3), 213–228.
- [15]. Nguyen K T, Le T A, Lee K, “Experimental Study on Flexural Strength of Reinforced Geopolymer Concrete Beams” *World Academy of Science, Engineering and Technology International Journal of Civil and Environmental Engineering Vol:10, No:4, 2016.*
- [16]. Luhar, S., Chaudhary, S., & Luhar, I. (2019). Development of rubberized geopolymer concrete: Strength and durability studies. *Construction and Building Materials*, 204, 740–753. <https://doi.org/10.1016/j.conbuildmat.2019.01.185>.
- [17]. Khale, D., & Chaudhary, R. (2007). Mechanism of geopolymerization and factors influencing its development: a review. *Journal of Materials Science*, 42(3), 729–746. <https://doi.org/10.1007/s10853-006-0401-4>.
- [18]. Duxson, P., Provis, J. L., Lukey, G. C., & Van Deventer, J. S. J. (2007). The role of inorganic polymer technology in the development of ‘green concrete’. *Cement and Concrete Research*, 37(12), 1590–1597. <https://doi.org/10.1016/j.cemconres.2007.08.018>.
- [19]. Ahmed H Q, Jaf D K and Yaseen S A, Flexural Capacity and Behaviour of Geopolymer Concrete Beams Reinforced with Glass Fibre-Reinforced Polymer Bars, *International Journal of Concrete Structures and Materials*, (2020) <https://doi.org/10.1186/s40069-019-0389-1>.
- [20]. Monteiro PJM, Miller SA, Horvath A. Towards sustainable concrete. *Nat Mater* 2017; 16:698–9.
- [21]. Flower, D. J., & Sanjayan, J. G. (2007). Green house gas emissions due to concrete manufacture. *The international Journal of life cycle assessment*, 12(5), 282-288.
- [22]. U.S. Environmental Protection Agency (EPA). Advancing sustainable materials management: 2017 fact sheet.
- [23]. AECOM Asia Company Limited. People’s Republic of China: Construction and Demolition Waste Management and Recycling. 2018.
- [24]. Davidovits, J. (2015). False values on CO2 emission for geopolymer cement/concrete published in scientific papers. Technical paper, 24, 1-9.[c] Błaszczyński, T., & Król, M. (2015). Usage of green concrete technology in civil engineering. *Procedia Engineering*, 122, 296-301.
- [25]. Liu, J., Huang, Z., & Wang, X. (2020). Economic and Environmental Assessment of Carbon Emissions from Demolition Waste Based on LCA and LCC. *Sustainability*, 12(16), 6683.

- [26]. Fořt, J., Vejmelková, E., Koňáková, D., Alblová, N., Čáchová, M., Keppert, M., ... & Černý, R. (2018). Application of waste brick powder in alkali activated aluminosilicates: functional and environmental aspects. *Journal of cleaner production*, 194, 714-725.
- [27]. Torres-Carrasco, M., & Puertas, F. (2015). Waste glass in the geopolymer preparation. Mechanical and microstructural characterisation. *Journal of cleaner production*, 90, 397-408.
- [28]. Youssef, N., Rabenantoandro, A. Z., Dakhli, Z., Chehade, F. H., & Lafhaj, Z. (2019). Environmental evaluation of geopolymer bricks. In *MATEC Web of Conferences* (Vol. 281, p. 03005). EDP Sciences.
- [29]. Roy, D. (1999). Sulfoaluminate-Belite Cement From Low-Calcium Fly Ash and Sulfur-Rich and Other Industrial by-Products”, *Cement and Concrete Research*, 29(8):1305-1311.
- [30]. Wongpa, J.; Kiattikomol, K.; Jaturapitakkul, C.; Chindaprasirt, P. Compressive strength, modulus of elasticity, and water permeability of inorganic polymer concrete. *Mater. Des.* 2010, 31, 4748–4754.
- [31]. Davidovits, J., *The need to create a new technical language for the transfer of basic scientific information. Transfer and Exploitation of Scientific and Technical Information*, EUR 7716. Luxembourg, Commission of the European Communities, 1982.
- [32]. Davidovits, J. (1991). Geopolymers: inorganic polymeric new materials. *Journal of Thermal Analysis and calorimetry*, 37(8), 1633-1656.
- [33]. Davidovits, J. High-alkali cements for 21st century concretes. *Spec. Publ.* 1994, 144, 383–398
- [34]. Wastiels, J., Wu, X., Faignet, S. and Patfoort, G. (1993) Mineral polymer based on fly ash. *Proceedings of the 9th International Conference on Solid Waste Management*, Philadelphia, PA, 8pp.
- [35]. Barrer, R. M. and Mainwaring, D. E. (1972) Chemistry of soil minerals. Part XI. Hydrothermal transformations of metakaolinite in potassium hydroxide. *Journal of the Chemical Society – Dalton Transactions*, 1254–1265. doi: 10.1039/DT9720001254.
- [36]. Wastiels, J., Wu, X., Faignet, S., & Patfoort, G. (1994). Mineral polymer based on fly ash. *Journal of Resource Management and Technology*, 22 (3), 135-141.
- [37]. Duxson, P., Fernández-Jiménez, A., Provis, J. L., Lukey, G. C., Palomo, A., & van Deventer, J. S. (2007). Geopolymer technology: the current state of the art. *Journal of materials science*, 42(9), 2917-2933
- [38]. Provis J. and van Deventer J.S.J. (eds) (2009), *Geopolymers: structure, processing, properties and industrial applications*, Woodhead Publishing Limited. Cambridge.
- [39]. Wang S.D., Pu X.C., Scrivener K.L. and Pratt P.L. (1995), ‘Alkali-activated slag: a review of properties and problems’, *Cem. Concr. Res.* 17(27), 93–102.

- [40]. Hong, S. Y., & Glasser, F. P. (1999). Alkali binding in cement pastes: Part I. The CSH phase. *Cement and Concrete Research*, 29(12), 1893-1903.
- [41]. Gruskovnjak, A., Lothenbach, B., Holzer, L., Figi, R., & Winnefeld, F. (2006). Hydration of alkali-activated slag: comparison with ordinary Portland cement. *Advances in cement research*, 18(3), 119-128.
- [42]. Li, Z., & Liu, S. (2007). Influence of slag as additive on compressive strength of fly ash-based geopolymer. *Journal of Materials in civil engineering*, 19(6), 470-474.
- [43]. Kurt, C. and Bittner, J.: Sodium hydroxide. In: Ullmann's Encyclopedia of Industrial Chemistry, Wiley-VCH Verlag (2006)
- [44]. Provis, J. L., & Van Deventer, J. S. (Eds.). (2013). Alkali activated materials: state-of-the-art report, RILEM TC224-AAM (Vol. 13). Springer Science & Business Media.
- [45]. Fernández-Jiménez, A., & Puertas, F. (2003). Effect of activator mix on the hydration and strength behaviour of alkali-activated slag cements. *Advances in cement research*, 15(3), 129-136.
- [46]. Wang, S. D., Scrivener, K. L., & Pratt, P. L. (1994). Factors affecting the strength of alkali-activated slag. *Cement and concrete research*, 24(6), 1033-1043.
- [47]. Dombrowski, K., Buchwald, A., & Weil, M. (2007). The influence of calcium content on the structure and thermal performance of fly ash based geopolymers. *Journal of Materials Science*, 42(9), 3033-3043.
- [48]. Robayo-Salazar, R. A., Valencia-Saavedra, W., & Mejía de Gutiérrez, R. (2020). Construction and Demolition Waste (CDW) Recycling—As Both Binder and Aggregates—In Alkali-Activated Materials: A Novel Re-Use Concept. *Sustainability*, 12(14), 5775.
- [49]. Puertas, A. Barba, M. Gazulla, M. Gómez, M. Palacios, S. Martínez, Residuoscerámicos para su posible uso como materia prima en la fabricación de Clinkerde cemento portland: caracterización y activación alcalina, *Mater. Constr.* 56(2006) 7–84
- [50]. Khater, H. M. (2012). Effect of calcium on geopolymerization of aluminosilicate wastes. *Journal of Materials in Civil Engineering*, 24(1), 92-101.
- [51]. Allahverdi, A., & Kani, E. N. (2013). Use of construction and demolition waste (CDW) for alkali-activated or geopolymer cements. In *Handbook of recycled concrete and demolition waste* (pp. 439-475). Woodhead Publishing.
- [52]. Vásquez, A., Cárdenas, V., Robayo, R. A., & de Gutiérrez, R. M. (2016). Geopolymer based on concrete demolition waste. *Advanced Powder Technology*, 27(4), 1173-1179.
- [53]. Mahmoodi, O., Siad, H., Lachemi, M., Dadsetan, S., & Sahmaran, M. (2021). Development of normal and very high strength geopolymer binders based on concrete waste at ambient environment. *Journal of Cleaner Production*, 279, 123436.

- [54]. Ulugöl, H., Kul, A., Yıldırım, G., Şahmaran, M., Aldemir, A., Figueira, D., & Ashour, A. (2021). Mechanical and microstructural characterization of geopolymers from assorted construction and demolition waste-based masonry and glass. *Journal of Cleaner Production*, 280, 124358.
- [55]. De Rossi, A., Ribeiro, M. J., Labrincha, J. A., Novais, R. M., Hotza, D., & Moreira, R. F. P. M. (2019). Effect of the particle size range of construction and demolition waste on the fresh and hardened-state properties of fly ash-based geopolymer mortars with total replacement of sand. *Process Safety and Environmental Protection*, 129, 130-137.
- [56]. Sumajouw, D. M. J., Hardjito, D., Wallah, S. E., & Rangan, B. V. (2005). Behaviour and strength of reinforced fly ash-based geopolymer concrete beams. In *Australian Structural Engineering Conference 2005* (p. 453). Engineers Australia.
- [57]. Kumar, P. U., & Kumar, B. S. C. (2016). Flexural behaviour of reinforced geopolymer concrete beams with GGBS and metakaoline. *International Journal of Civil Engineering and Technology*, 7(6).
- [58]. Jeyasehar, C. A., Saravanan, G., Salahuddin, M., & Thirugnanasambandam, S. (2013). Development of fly ash based geopolymer precast concrete elements.
- [59]. S. Kumaravel, Thirugnanasambandam, “Flexural Behaviour Of Geopolymer Concrete Beams”, research paper E-ISSN2249–8974 (2013)
- [60]. Badar, M.S.; Kupwade-Patil, K.; Bernal, S.A.; Provis, J.L.; Allouche, E.N. Corrosion of steel bars induced by accelerated carbonation in low and high calcium fly ash geopolymer concretes. *Construct. Build. Mater.* **2014**, 61, 79–89.
- [61]. Chindaprasirt, P.; Chareerat, T.; Hatanaka, S.; Cao, T. High-strength geopolymer using fine high calcium fly ash. *J. Mater. Civ. Eng.* **2010**, 23, 264–270.
- [62]. Zeng, S.; Wang, J. Characterization of mechanical and electric properties of geopolymers synthesized using four locally available fly ashes. *Construct. Build. Mater.* **2016**, 121, 386–399.
- [63]. P. Saravanakumar, “Strength and Durability Studies on Geopolymer Recycled Aggregate Concrete”, *IJET* 7 (2.24), 370-375, (2018).
- [64]. S. Kumaravel, Thirugnanasambandam, “Flexural Behaviour Of Geopolymer Concrete Beams”, research paper E-ISSN2249–8974 (2013).
- [65]. [65]. M. Rajendran, N. Soundarapandian, “An experimental investigation on the flexural behavior of geopolymer ferrocement slabs”, *J. Eng. Technol.* 3 (2) (2013).
- [66]. [66]. Sanjay R, Dr. M. U. Aswath, Smita Singh, “An Experimental Study on Flexural Behaviour of Reinforced Geopolymer Concrete Beams with Recycled Aggregate in Bending”, *Research Gate: Issue 2, Vol.6 ISSN 2249-6149.* (2012)
- [67]. Raj S. D, Ganesan N, Abraham R, Raju A, Behavior of geopolymer and conventional concrete beam column joints under reverse cyclic loading. *Advances in Concrete Construction*, Vol. 4, No. 3 (2016) 161-172.

- [68]. Sofi, M., Van Deventer, J. S. J., Mendis, P. A., & Lukey, G. C. (2007). Bond performance of reinforcing bars in inorganic polymer concrete (IPC). *Journal of Materials Science*, 42(9), 3107-3116.
- [69]. Hutagi, A., & Khadiranaikar, R. B. (2016, March). Flexural behavior of reinforced geopolymer concrete beams. In 2016 International Conference on Electrical, Electronics, and Optimization Techniques (ICEEOT) (pp. 3463-3467). IEEE.
- [70]. Visintin, P., Ali, M. M., Albitar, M., & Lucas, W. (2017). Shear behaviour of geopolymer concrete beams without stirrups. *Construction and Building Materials*, 148, 10-21.
- [71]. Yost, J. R., Radlińska, A., Ernst, S., Salera, M., & Martignetti, N. J. (2013). Structural behavior of alkali activated fly ash concrete. Part 2: Structural testing and experimental findings. *Materials and structures*, 46(3), 449-462.
- [72]. Darmawan, M. S., Bayuaji, R., Sugihardjo, H., Husin, N. A., & Anugraha Affandhie, R. B. (2019). Shear Strength of Geopolymer Concrete Beams Using High Calcium Content Fly Ash in a Marine Environment. *Buildings*, 9(4), 98.
- [73]. Ambily, P. S., Madheswaran, C. K., Sharmila, S., & Muthiah, S. (2011). Experimental and analytical investigations on shear behaviour of reinforced geopolymer concrete beams. *International Journal of Civil & Structural Engineering*, 2(2), 682-697.
- [74]. Madheswaran, C. K., Ambily, P. S., Dattatreya, J. K., & Ramesh, G. (2015). Experimental studies on behaviour of reinforced geopolymer concrete beams subjected to monotonic static loading. *Journal of the institution of engineers (India): Series A*, 96(2), 139-149.
- [75]. Umniati, B. S., & Risdanareni, P. (2017). Flexural Test of Fly Ash based Geopolimer Concrete Beams. In MATEC Web of Conferences (Vol. 97, p. 01030). EDP Sciences.
- [76]. Yacob, N. S., ElGawady, M. A., Sneed, L. H., & Said, A. (2019). Shear strength of fly ash-based geopolymer reinforced concrete beams. *Engineering Structures*, 196, 109298.
- [77]. Ahmed H. Q, Jaf D. K, Yaseen Ş. A, Flexural Capacity and Behaviour of Geopolymer Concrete Beams Reinforced with Glass Fibre-Reinforced Polymer Bars
- [78]. Sumajouw D. M. J, Hardjito D, Wallah S. E, Rangan B. V, Fly ash-based geopolymer concrete: Study of slender reinforced columns *Journal of Materials Science* May 2007. *International Journal of Concrete Structures and Materials*. (2020).
- [79]. Wu C, Hwang H, Shi C, Li N, Du Y, Shear tests on reinforced slag-based geopolymer concrete beams with transverse reinforcement. *Engineering Structures*. Volume 219, 15 September 2020, 110966.
- [80]. Mathew, G. and Joseph, B. (2020), Flexural Behaviour of Geopolymer Concrete Beams Exposed to Elevated Temperatures. *Journal of Building Engineering*. Volume 15.

- [81]. Turkish Earthquake Code (TEC2018). Specifications for the buildings to be constructed in disaster areas, Prime Ministry Disaster and Emergency Management Authority, **2018**; Ankara, Turkey.
- [82]. Azak TE, Ay BO, Akkar S. A statistical study on geometrical properties of turkish reinforced concrete building stock, 2nd European Conference on Earthquake Engineering and Sesimology, **2014**; Istanbul, Turkey.
- [83]. Kurt EG, Binici B, Kurc O, Canbay E, Akpınar U, Özcebe G. Seismic performance of a deficient reinforced concrete test frame with infill walls, *Earthquake Spectra*, **2011**; 27(3): 817-838.
- [84]. Sucuoğlu H, Lin W, Binici B, Ezzatfar P. Pseudo-dynamic testing, performance assessment, and modeling of deficient reinforced concrete frames, *ACI Structural Journal*, **2014**; 111(5): 1203-1212.
- [85]. Sipos TK, Sigmund V, Hadzima-Nyarko M. Earthquake performance of infilled frames using neural networks and experimental database, *Engineering Structures*, **2013**; 51(1): 113-127.
- [86]. Binici, B., Canbay, E., Aldemir, A., Demirel, I.O., Uzgan, U., Eryurtlu, Z., Bulbul, K. and Yakut, A. (2019). Seismic behavior and improvement of autoclaved aerated concrete infill walls. *Engineering Structures*. Volume 193.
- [87]. Federal Emergency Management Agency (FEMA356). *Prestandard and Commentary for the Seismic Rehabilitation of Buildings*, **2000**; Washington, DC.
- [88]. ASTM C39 (2015). "Compressive Strength of Cylindrical Concrete Specimens". American Society for Testing and Materials Standard, West Conshohocken, USA.
- [89]. ASTM C496 (2017). "Standard Test Method for Splitting Tensile Strength of Cylindrical Concrete Specimens". American Society for Testing and Materials Standard, West Conshohocken, USA.
- [90]. Akbarnezhad, A., Ong, K. C. G., Zhang, M. H., Tam, C. T., & Foo, T. W. J. (2011). Microwave assisted beneficiation of recycled concrete aggregates. *Construction and Building Materials*, 25(8), 3469-3479.
- [91]. Otsuki, N., Miyazato, S. I., & Yodsudjai, W. (2003). Influence of recycled aggregate on interfacial transition zone, strength, chloride penetration and carbonation of concrete. *Journal of materials in civil engineering*, 15(5), 443-451.
- [92]. American Concrete Institute (ACI), "Building Code Requirements, Structural Concrete and Commentary", ACI Committee 318, **2011**.
- [93]. Turkish Standards (TS500) (2000). *Design and Construction Rules of Reinforced Concrete Structures*. Turkish Standards Institute, Ankara, Turkey.